# Gauge and Yukawa Couplings in SUSY QCD

Dissertation
zur Erlangung des Doktorgrades
des Fachbereichs Physik
der Universität Hamburg

vorgelegt von
Markos Maniatis
aus Hamburg

Hamburg
2001

| | |
|---|---|
| Gutachter der Dissertation: | Prof. Dr. P. M. Zerwas<br>Prof. Dr. J. Bartels |
| Gutachter der Disputation: | Prof. Dr. P. M. Zerwas<br>Prof. Dr. B. A. Kniehl |
| Datum der Disputation: | 5.2.2002 |
| Dekan des Fachbereichs Physik und Vorsitzender des Promotionsausschusses: | Prof. Dr. F.-W. Büßer |

# Abstract

The calculation of the process $e^+e^- \to \tilde{q}\bar{\tilde{q}}g$ at next-to-leading order in $\alpha_s$ within the Minimal Supersymmetric Standard Model (MSSM) is presented. Supersymmetry requires the involved squark-squark-gluon gauge coupling $\alpha_s'$ to be equal to the Standard Model gauge coupling $\alpha_s$. Thus the calculation serves as a building block to establish supersymmetry at future colliders.



# Zusammenfassung

In dieser Arbeit wird die Berechnung des Prosesses $e^+e^- \to \tilde{q}\bar{\tilde{q}}g$ in nächstführender Ordnung in $\alpha_s$ im Minimalen Supersymmetrischen Standardmodell (MSSM) vorgestellt. Supersymmetrie erfordert, daß die in diesen Prozess eingehende starke Squark-Squark-Gluon Eichkopplung $\alpha_s'$ mit der Kopplung $\alpha_s$ im Standardmodell übereinstimmt. Dieser Prozess erlaubt somit einen Test von Supersymmetrie an zukünftigen Beschleunigern.

# Contents


**1 Introduction** **1**

**2 Supersymmetry** **5**
2.1 Hierarchy problem . . . . . 5
2.2 Supersymmetry algebra . . . . . 7
2.3 Chiral- and gauge-supermultiplets . . . . . 7
2.4 MSSM field content . . . . . 8
2.5 Interactions of the MSSM . . . . . 9
2.6 Matter-parity . . . . . 10
2.7 Soft supersymmetry breaking . . . . . 11
2.8 Unification of gauge couplings . . . . . 13
2.9 Gauge and Yukawa couplings in the SUSY QCD sector . . . . 14

**3 The process $e^+e^- \to \tilde{q}\bar{\tilde{q}}g$** **19**
3.1 Tree level calculation . . . . . 19
3.2 Next to leading order calculation . . . . . 22
3.2.1 *Virtual correction* . . . . . 29
3.2.2 *Renormalization* . . . . . 31
3.2.3 *Supersymmetry-restoring counterterm* . . . . . 35
3.2.4 *Real correction* . . . . . 35
3.3 LO and NLO results . . . . . 40
3.3.1 *MSSM $\beta$-function* . . . . . 40
3.3.2 *Cross sections* . . . . . 40
3.3.3 *Scale dependence of the cross section* . . . . . 41
3.3.4 *Gluon energy cut* . . . . . 43

**Conclusion** **45**

**A Feynman rules** **47**

**B Tensor reduction** **51**

**C Scalar integrals** **55**

**D Relation of $D_{00}$ and $D_0^6$** **61**

**E Renormalization constants** **65**

**F Final state infrared singularities** **67**

**G Phase space** **75**

**Bibliography** **79**

# Chapter 1

# Introduction

In gauge theories like the Standard Model space-time symmetries and internal symmetries are independent of each other, i.e. the Lorentz algebra and the algebra of the inner symmetries commute. It was proven by Coleman and Mandula [1] that this is the case in any four-dimensional quantum field theory with non-zero scattering amplitudes. The Coleman-Mandula theorem can be evaded by introducing fermionic supersymmetry generators $Q$ and $\bar{Q}$ that obey anticommutation rather than commutation relations. These supersymmetry generators carry spin 1/2 and transform fermions into bosons and vice versa. The anticommutator of these generators is a spin-1 vector and must be proportional to the momentum operator $P_\mu$. Thus supersymmetry is directly related to the Poincaré symmetry. Furthermore, local supersymmetry implies local Poincaré symmetry and thus gravity.

Since the supersymmetry generators carry spin 1/2, the representations of the supersymmetry algebra, the supermultiplets, must contain bosonic and fermionic components. The number of fermionic and bosonic degrees of freedom in every supermultiplet must be equal.

Supersymmetry links fermions with bosons and vice versa. As a consequence, boson and fermion loops appear always in parallel. Since they come with opposite sign, large corrections are suppressed. In particular, quadratic divergences are absent in supersymmetric quantum field theories [2].

In non-supersymmetric theories like the Standard Model this quadratic corrections are proportional to $\Lambda_{UV}^2$, where $\Lambda_{UV}$ is the scale, where new physics becomes effective. Typically it is assumed that this scale is the Planck scale $M_P \approx 10^{19}$ GeV, where quantum gravitational effects become important, or the grand unification scale $M_{GUT} \approx 10^{16}$ GeV, where the gauge couplings of the Standard Model extrapolated to high energies indicate a unification.

Thus, while the Higgs mass is of the order of the electroweak scale, radia-

tive corrections destabilize the hierarchy between this scale and the Planck respectively GUT scale. This is known as the naturalness problem [3],[4],[5]. Supersymmetry provides a solution to this problem, since the large quadratic corrections are naturally absent.

It turns out, that none of the Standard Model bosons can be a supersymmetric partner of one of the Standard Model fermions, because of the different quantum numbers. Therefore, one has to introduce a new superpartner for each degree of freedom of the Standard Model. Moreover the Higgs sector of the Standard Model has to be enlarged by including a second Higgs doublet. This is necessary in order to provide masses for up- and down-type fermions and to ensure anomaly cancellation. In this way one arrives at the *Minimal Supersymmetric Standard Model* (MSSM) [6],[7],[8].

The MSSM conserves $R$ parity. This is a multiplicative quantum number, which is related to baryon number $B$, lepton number $L$, and spin $s$ by

$$R = (-1)^{3(B-L)+2s}$$

The Standard Model particles have $R = 1$ and their superpartners have $R = -1$. The conservation of $R$ parity implies that the superpartner particles can only be produced *in pairs* and that the *lightest supersymmetric particle* (LSP) is stable.

Despite the fact that the MSSM predicts many new particles in addition to the Standard Model particles, the interaction strengths between the particles of the supermultiplets which contain the fermions and the multiplets which contain the gauge bosons as well as the quartic scalar interactions are given in terms of the $SU(3)_C \times SU(2)_L \times U(1)_Y$ gauge couplings. For example, the Yukawa interaction between a quark ($q$), its scalar partner, the so-called squark ($\tilde{q}$), and the fermionic partner of the gluon, a so-called gluino ($\tilde{g}$), is governed by the strong gauge coupling constant, $g_s$.

Moreover the MSSM has just the right particle content to ensure that the evolution of the three gauge couplings can unify at a scale $M_{GUT} \approx 2 \times 10^{16}$ GeV.

Because no supersymmetric particle has been experimentally discovered so far, supersymmetry must be broken. Supersymmetry breaking should introduce a splitting of the masses within supermultiplets but should not destroy crucial features of the supersymmetry concept, in particular the cancellation of the quadratic divergences in the radiative corrections of the Higgs-boson mass. This can be achieved by introducing only *soft* supersymmetry-breaking Lagrangian terms, i.e. mass terms or interactions with couplings of positive mass dimension [9].

In order to stabilize the weak scale, these masses should be below order 1 TeV. As a consequence, the superpartners of the known particles should be within reach of the ongoing and proposed collider experiments.

To establish supersymmetry there are two major steps necessary after the discovery of new particles:

- The quantum numbers must be measured to ensure that new discovered particles and Standard Model particles match the supermultiplets.
- The equality of gauge and Yukawa couplings have to be verified.

In this thesis we focus on the verification of the equality of the gauge and Yukawa couplings in the $SU(3)_C$ gauge sector of the MSSM. In particular supersymmetry predicts the coupling strengths of the gauge vertices $qqg$, $\tilde{q}\bar{\tilde{q}}g$, and the Yukawa vertex $\bar{q}\tilde{q}\tilde{g}$ to be equal.

These vertices can be investigated experimentally at electron positron colliders with signatures

$$\begin{array}{ll} (1) & e^+e^- \to q\bar{q}g, \\ (2) & e^+e^- \to \tilde{q}\bar{\tilde{q}}g, \\ (3) & e^+e^- \to q\bar{\tilde{q}}\tilde{g} \end{array} \tag{1.1}$$

with high accuracy. These processes involve the different vertices already at tree level. The discovery of the gluon in process (1) in 1979 established the $SU(3)_C$ gauge group in the Standard Model and allowed to measure the gauge coupling $g_s$ [10],[11],[12].

The comparison of the gauge and Yukawa interactions require not only to measure the cross sections of these 3 processes experimentally but also to predict the cross sections under the assumption of equal couplings. Thus the cross sections of these processes (1)-(3) must be calculated and since QCD corrections are in general large, *next-to-leading order* NLO calculations of these processes are desirable.

The NLO calculation to the process (1) within the Standard Model was performed [13],[14],[15],[16]. The additional MSSM corrections, i.e. gluinos in internal lines have not yet been implemented; they are suppressed strongly due to the large gluino mass. The process (3) has just been calculated at NLO [17]. In this thesis we present the calculation of process (2) which is the last missing building block in the comparison.

### Outline of the thesis

In chapter 2 we give a brief introduction to supersymmetry and the MSSM, which underlie the whole calculation. In particular the prediction of equal

gauge and Yukawa couplings is derived as an feature of supersymmetry. The chapter 3 is divided into the tree level and NLO calculation of the process $e^+e^- \to \tilde{q}\bar{\tilde{q}}g$. In the NLO calculation in section 3.2.1 we present the determination of the virtual corrections, in section 3.2.2 the renormalization formalism, and in 3.2.4 the real corrections. Since the usual regularization scheme like dimensional regularization violates supersymmetry, an extra finite counterterm has to be introduced, given in section 3.2.3. In section 3.3 we present the results of the calculation and compare them at LO and NLO.

The appendices finally give explicit details of the calculation as the Feynman rules in appendix A, the tensor reduction formalism in B, the emerging divergent scalar integrals are given in C, the relation between the tensor coefficient $D_{00}$ and the scalar integral $D_0^6$ is derived in appendix D, the renormalization constants can be found in E, the dipole functions in context with the real corrections in F, and the parameterization of the 3 and 4 particle phase space in G.

# Chapter 2

# Supersymmetry

The Standard Model provides a remarkably successful description of presently known phenomena. The experimental high-energy frontier has advanced into the hundreds of GeV range with no confirmed deviations from Standard Model predictions and few unambiguous hints of additional structure. Still, it seems quite clear that the Standard Model will have to be extended to describe physics at arbitrarily high energies. Certainly a new framework will be required at the Planck scale $M_P \approx 10^{19}$ GeV, where quantum gravitational effects become important.

Despite the great success of the Standard Model there are several reasons to extend this model. In this thesis we focus on the theory of supersymmetry introduced for field theory in four dimensions in 1973 by Wess and Zumino [18]. Beside hints like the unification of gauge symmetries [19],[20],[21],[22], directly related to the prediction of the weak mixing angle, and the dark matter problem one of the main motivations for supersymmetry is the hierarchy problem. Since the hierarchy problem is very useful to introduce many features of supersymmetry it is briefly described here followed by a glance at the unification of couplings.

## 2.1 Hierarchy problem

The electrically neutral part of the Standard Model Higgs field is a complex scalar $H$ with a classical potential given by

$$V = \mu|H|^2 + \lambda|H|^4. \tag{2.1}$$

The Standard Model requires a non-vanishing vacuum expectation value for $H$ at the minimum of the potential. This will occur if $\mu < 0$, resulting in

$\langle H \rangle = \sqrt{-\mu/2\lambda}$. The term involving $\mu$ is a mass term and determines the mass of the field $H$ as $m_H^2 = \mu$. Since we know experimentally that $\langle H \rangle = 174$ GeV from measurements of the properties of the weak interactions, it is clear that $m_H^2$ is very roughly of order $(100\ \text{GeV})^2$. However, $m_H^2$ receives enormous quantum corrections from the virtual effects of every particle which couples, directly or indirectly, to the Higgs field. For example, from a fermion $f$ with mass $m_f$ and a Lagrangian term $-\lambda_f H \overline{f} f$ the one loop correction gives

$$\Delta m_H^2 = \frac{|\lambda_f|^2}{16\pi^2}[-2\Lambda_{UV}^2 + 6m_f^2 \ln(\Lambda_{UV}/m_f) + \ldots]. \tag{2.2}$$

Here $\Lambda_{UV}$ is an ultraviolet momentum cutoff used to regulate the loop integral; it can be interpreted as the energy scale at which new physics enters to alter the high-energy behavior of the theory. The ellipses represent terms which do not get large as $\Lambda_{UV}$ does. In the Standard Model each of the leptons and quarks can play the role of $f$. The problem is that for $\lambda_f \approx 1$ and $\Lambda_{UV}$ of order $M_P$ this correction to $m_H^2$ is about 30 orders of magnitude larger than the value of $m_H^2 \approx (100\ \text{GeV})^2$! This large corrections only concern the Higgs scalar boson mass, because quantum corrections to fermion and gauge boson masses do not have the quadratic sensitivity to $\Lambda_{UV}^2$ found in (2.2). However the quarks and leptons and the electroweak gauge bosons of the Standard Model all owe their masses to $\langle H \rangle$, so that the entire mass spectrum of the Standard Model is sensitive to the cutoff $\Lambda_{UV}$. Furthermore, there is a contribution similar to (2.2) from the virtual effects of any arbitrarily heavy particles which might exist. For example a heavy complex scalar particle $S$ with mass $m_S$ which couples to the Higgs with a Lagrangian term $-\lambda_S |H|^2 |S|^2$ the boson gives a loop correction

$$\Delta m_H^2 = \frac{\lambda_S}{16\pi^2}[\Lambda_{UV}^2 - 2m_S^2 \ln(\Lambda_{UV}/m_S) + \ldots]. \tag{2.3}$$

The systematic cancellation of the large contributions to $\Delta m_H^2$ should be generated by a symmetry. From the different sign in the fermion loop and the boson loop (2.2),(2.3) it is obvious that this symmetry must relate fermions and bosons.

Supersymmetry is the invariance of the Lagrangian under transformations which mix fermionic and bosonic fields. Supersymmetry postulates for every fermionic degree of freedom in the Lagrangian a corresponding bosonic degree and vice versa. The contributions of a fermionic loop and two corresponding boson loops from (2.2), (2.3) give a radiative correction to the Higgs mass of the form

$$\Delta m_H^2 = \frac{1}{8\pi^2}(\lambda_S - |\lambda_f|^2)\Lambda_{UV}^2 + \ldots. \tag{2.4}$$

If the couplings $\lambda_S$ and $|\lambda_f|^2$ are equal the quadratically divergent corrections cancel.

## 2.2 Supersymmetry algebra

The operator $Q$ which generates supersymmetry transformations must be an anticommuting spinor with

$$Q\,|boson\rangle = |fermion\rangle, \qquad Q\,|fermion\rangle = |boson\rangle \tag{2.5}$$

The possible forms of such symmetries are highly restricted by the Haag-Lopuszanski-Sohnius extension of the Coleman-Mandula theorem [1],[23]. For realistic theories describing chiral fermions, i.e. fermions whose left- and right-handed pieces transform differently under the gauge group and thus the possibility of parity-violating interactions, this theorem implies that the generators $Q$ and its conjugate $\bar{Q}$ must satisfy the algebra

$$\begin{array}{lcl} \{Q_a, \bar{Q}_b\} & = & 2\,\gamma^\mu_{ab} P_\mu \\ [P^\mu, Q_a] & = & 0 \\ [M^{\mu\nu}, Q_a] & = & -\Sigma^{\mu\nu}_{ab}\, Q_b, \end{array} \tag{2.6}$$

where $a$ and $b$ are spinor indices, $P^\mu$ is the momentum generator of spacetime translations, $M^{\mu\nu}$ is the generator of Lorentz transformations and the spin tensor is defined by $\Sigma^{\mu\nu} = i/4[\gamma^\mu, \gamma^\nu]$. The first equation connects supersymmetry with spacetime transformations and the last equation says that supersymmetry transformation generators transform as spinors under Lorentz transformations.

The single particle states of a supersymmetric theory fall into irreducible representations of the supersymmetry algebra which are called *supermultiplets*. Each supermultiplet contains both fermion and boson states, called *superpartners*. The supersymmetry generators commute with the generators of gauge transformations. Therefore particles in the same supermultiplet must also be in the same representation of the gauge group, and so must have the same electric charge, weak isospin, and color degrees of freedom. Furthermore in each supermultiplet the number of bosonic and fermionic degrees of freedom must be equal.

## 2.3 Chiral- and gauge-supermultiplets

The matter fields in a low-energy supersymmetric model are part of so called *chiral multiplets* $\hat{\Phi} := (\Phi, \Psi_L, F)$, where the superfield is indicated by a

symbol with a caret. In this superfield, $\Phi$ and $F$ are complex scalars while $\Psi_L$ is a left handed fermion. $F$ is an auxiliary field with no kinetic energy term. Its equation of motion is purely algebraic; consequently the auxiliary fields can be expressed in terms of other dynamical fields. The massless gauge fields are components of a massless real *vector supermultiplet* $\hat{A}^a := (\lambda_L^a, A^{\mu a}, D^a)$, where $a$ labels the component of the adjoint representation of the gauge group. In this superfield, $\lambda_L$ is a complex left handed spinor, $A^\mu$ is the massless gauge field, and $D$ is a real auxiliary scalar field. The auxiliary fields $F$ and $D$ ensure that the chiral and matter supermultiplets respectively contain just equal numbers of bosonic and fermionic degrees of freedom. Off-shell, the degrees of freedom of the auxiliary fields have to be taken into account. The fermion field $\Psi_L$ has 4 degrees of freedom matching the 2 of each of the complex scalar fields $\Phi$ and $F$. In the vector supermultiplet the fermionic field $\lambda_L^a$ counts 4, the gauge field $A^{\mu a}$ 3, and the real scalar filed $D^a$ count 1 degree of freedom. On-shell the equation of motion remove the auxiliary fields. The complex fermion fields now each have 2 degrees of freedom matching the 2 bosonic ones of the complex scalar $\Phi$ and the massless vector field $A^{\mu a}$ on-shell.

## 2.4 MSSM field content

The *Minimal Supersymmetric extension of the Standard Model* (MSSM) [6],[7], [8] contains the particles of the Standard Model extended by the minimal number of superpartners:
The fermions (quarks and leptons) of the Standard Model are paired with scalar partners called *squarks* and *sleptons*. In order to give masses to up- and down-type fermions and to avoid triangle anomalies, the Standard Model Higgs doublet must be replaced by two Higgs doublets and the corresponding *higgsino* doublets. The upper part of table 2.1 shows the chiral supermultiplets of the MSSM classified according to their transformation properties under the Standard Model gauge group $SU(3)_C \times SU(2)_L \times U(1)_Y$. An extra symbol in the second column denotes the supermultiplets. For example $\hat{Q}$ stands for the $SU(2)_L$-doublet supermultiplet containing $u_L$, $d_L$ and $\tilde{u}_L$, $\tilde{d}_L$.

The gauge bosons (photon, $W^\pm$, $Z^0$ and gluon) have fermionic (spin 1/2) superpartners called *photino*, *wino*, *zino* and *gluino*. The gauge supermultiplets of the MSSM containing gauge bosons and their superpartners are summarized in the lower part of table 2.1.

| *Chiral supermultiplets* $\hat{\Phi}$ | | spin 1/2 | spin 0 | $SU(3)_C$ | $SU(2)_L$ | $U(1)_Y$ |
|---|---|---|---|---|---|---|
| quark ($q$), squark ($\tilde{q}$) | $\hat{Q}$ | $(u_L,d_L)$ | $(\tilde{u}_L,\tilde{d}_L)$ | **3** | **2** | $\frac{1}{6}$ |
| | $\hat{U}$ | $u_R$ | $\tilde{u}_R$ | $\bar{\mathbf{3}}$ | **1** | $-\frac{2}{3}$ |
| | $\hat{D}$ | $d_R$ | $\tilde{d}_R$ | $\bar{\mathbf{3}}$ | **1** | $\frac{1}{3}$ |
| lepton ($l$), slepton ($\tilde{l}$) | $\hat{L}$ | $(\nu,e_L)$ | $(\tilde{\nu},\tilde{e}_L)$ | **1** | **2** | $-\frac{1}{2}$ |
| | $\hat{E}$ | $e_R$ | $\tilde{e}_R$ | **1** | **1** | 1 |
| Higgsino ($\tilde{H}$), Higgs ($H$) | $\hat{H}_u$ | $(\tilde{H}_u^+,\tilde{H}_u^0)$ | $(H_u^+,H_u^0)$ | **1** | **2** | $+\frac{1}{2}$ |
| | $\hat{H}_d$ | $(\tilde{H}_d^0,\tilde{H}_d^-)$ | $(H_d^0,H_d^-)$ | **1** | **2** | $-\frac{1}{2}$ |
| *Gauge supermultiplets* $\hat{A}$ | | spin 1 | spin 1/2 | $SU(3)_C$ | $SU(2)_L$ | $U(1)_Y$ |
| gluon ($g$), gluino ($\tilde{g}$) | $\hat{G}$ | $g$ | $\tilde{g}$ | **8** | **1** | 0 |
| W boson, wino ($\tilde{W}$) | $\hat{W}$ | $W^{\pm}$, $W^0$ | $\tilde{W}^{\pm}$, $\tilde{W}^0$ | **1** | **3** | 0 |
| B boson, bino ($\tilde{B}$) | $\hat{B}$ | $B^0$ | $\tilde{B}^0$ | **1** | **1** | 0 |

Table 2.1: *Chiral and gauge supermultiplets of the MSSM*

## 2.5 Interactions of the MSSM

Having specified the superfields of the theory, the next step is to construct the supersymmetric Lagrangian [20],[21],[22]. The fields of the MSSM have canonical kinetic energy terms

$$\mathcal{L}_{ke} = (D_\mu \Phi^{*i})(D^\mu \Phi_i) + i\bar{\Psi}^i \not{D} \Psi_i - \frac{1}{4} F^A_{\mu\nu} F_A^{\mu\nu} + \frac{i}{2} \bar{\lambda}^A \not{D} \lambda_A, \qquad (2.7)$$

where $D$ is the $SU(3)_C \times SU(2)_L \times U(1)_Y$ gauge invariant derivative. The implicit sum over $i$ is over all the fermion fields of the Standard Model, $\Psi_i$, and their scalar partners, $\Phi_i$, and also over the 2 Higgs doublets with their fermionic partners. The implicit sum over $A$ is over the $SU(3)_C$, $SU(2)_L$ and $U(1)_Y$ gauge fields with their fermionic partners, the gauginos, $\lambda_A$.

The interactions between the chiral and the gauge superfields are completely specified by the gauge symmetries and by supersymmetry, as are the quartic interactions of the scalars,

$$\mathcal{L}_{int} = -\sqrt{2}\, g_A \Phi^{*i} T^A P_L \bar{\Psi}_i \lambda_A + h.c. - \frac{1}{2} \sum_A \left( g_A \Phi^{*i} T^A \Phi_i \right)^2, \qquad (2.8)$$

where the projectors are defined by $P_{R/L} = (1 \pm \gamma_5)/2$ and $g_A$ is the relevant gauge coupling constant. Obviously the interaction strengths are given in terms of the gauge couplings. For example, the Yukawa interaction between a quark, its scalar partner, the squark, and the gluino is governed by the strong coupling constant, $g_s$. As can be seen from the last term, the same coupling determines the quartic squark interaction.

The most general renormalizable non-gauge interactions for chiral supermultiplets are determined by a single analytic function of the complex scalar fields, the *superpotential* $W$. The Lagrangian of these interactions is

$$\mathcal{L}_W = -\frac{1}{2}W^{ij}\Psi_i\Psi_j + W^i F_i + h.c., \tag{2.9}$$

where $W^{ij}$ and $W^i$ are functions of the boson fields. The requirement of invariance under supersymmetry transformations of the Lagrangian $\mathcal{L}_W$ yields

$$W^{ij} = \frac{\delta^2}{\delta\Phi_i\delta\Phi_j}W = M^{ij} + y^{ijk}\Phi_k \tag{2.10}$$

$$W^i = \frac{\delta}{\delta\Phi_i}W = M^{ij}\Phi_j + y^{ijk}\Phi_j\Phi_k \tag{2.11}$$

with the superpotential

$$W = \frac{1}{2}M^{ij}\Phi_i\Phi_j + \frac{1}{6}y^{ijk}\Phi_i\Phi_j\Phi_k, \tag{2.12}$$

where $M^{ij}$ is a symmetric mass matrix for the fermion fields, and $y^{ijk}$ is a Yukawa coupling of a scalar $\Phi_k$ and two fermions $\Psi_i\Psi_j$, which must be totally symmetric under interchange of $i$, $j$, $k$.

## 2.6 Matter-parity

If one introduces the most general superpotential $W$ to describe the non-gauge interactions of the chiral supermultiplets (2.12) there arise also lepton and baryon number violating Lagrangian terms. On the other hand there are very severe experimental constraints on the violation of lepton and baryon numbers [24], but it is also known from non-perturbative electroweak effects that lepton and baryon number are violated even though those effects are negligible for experiments at ordinary energies. Therefore, in the MSSM [1] one adds a new symmetry which has the effect of eliminating the possibility of baryon and lepton number violating terms in the superpotential, called *matter parity* $P_M$ [21],[25]. Matter parity is a multiplicatively conserved quantum number defined as

$$P_M = (-1)^{3(B-L)}, \tag{2.13}$$

[1] In the Standard Model there are no possible renormalizable Lagrangian terms which violate the baryon number or the lepton number.

where B and L are the baryon and the lepton number. The symmetry principle is that a term in the Lagrangian is allowed only if the product of $P_M$ of all of the fields in it is +1. The advantage of matter parity is that it can in principle be an exact symmetry, which B and L themselves cannot. It is useful to recast matter parity in terms of *R-parity*, defined for each particle as

$$P_R = (-1)^{3(B-L)+2s} \tag{2.14}$$

where $s$ is the spin of the particle. Now, matter parity and $R$-parity conservation are equivalent, since the factor $(-1)^{2s}$ is equal to +1 for the particles involved in any interaction vertex in a theory that conserves angular momentum. All the Standard Model particles and the Higgs bosons have $R$-parity +1, while all the squark, sleptons, gauginos and higgsinos have $R$-parity −1. $R$-parity odd particles ($P_R = -1$) are called *supersymmetric particles* or *sparticles*, and they are distinguished by a tilde. If $R$-parity is exactly conserved, there are several direct consequences:

- The lightest sparticle, called the *lightest supersymmetric particle* or LSP, must be absolutely stable. If the LSP is electrically neutral, it interacts only weakly with ordinary matter, and so can be a candidate for dark matter. [26],[27].
- Each sparticle other than the LSP must eventually decay into an odd number of LSP's which can give signatures of missing transversal energy $E_T$ in detectors.
- In collider experiments, sparticles can only be produced in even numbers.

Without the matter-parity violating terms we arrive at the superpotential of the MSSM

$$\mathcal{L}_W^{MSSM} = \hat{U}\mathbf{y_u}\hat{Q}\hat{H}_u - \hat{D}\mathbf{y_d}\hat{Q}\hat{H}_d - \hat{E}\mathbf{y_e}\hat{L}\hat{H}_d + \mu\hat{H}_u\hat{H}_d, \tag{2.15}$$

where $\hat{Q}$, $\hat{L}$, $\hat{U}$, $\hat{D}$, $\hat{E}$, $\hat{H}_u$, $\hat{H}_d$ are chiral supermultiplets introduced in table 2.1 and the scalar and dimensionless Yukawa-coupling terms $\mathbf{y_u}$, $\mathbf{y_d}$, $\mathbf{y_e}$ are $3 \times 3$-matrices in family space.

## 2.7 Soft supersymmetry breaking

None of the supersymmetric particles has been discovered. If supersymmetry were unbroken, then there should be superpartners to every detected

Standard Model particle with exactly the same mass. From the experimental point of view this is excluded so supersymmetry must be a broken symmetry. However unbroken supersymmetry guarantees that the quadratic divergences in squared scalar masses vanish to all orders in perturbation theory. If broken supersymmetry is still to provide a solution to the hierarchy problem, then the relationship between dimensionless couplings (2.4) which hold in unbroken supersymmetry must be maintained.

In the MSSM the supersymmetry is *softly* broken. Soft means that no quadratic divergences to the corrections to the Higgs mass are reintroduced in order to maintain the hierarchy between the electroweak scale and the Planck mass scale. This can be done by introducing only soft supersymmetry breaking terms where the effective Lagrangian can be written in the form

$$L = L_{SUSY} + L_{soft} \tag{2.16}$$

where $L_{SUSY}$ preserves supersymmetry invariance, and $L_{soft}$ violates supersymmetry but contains only mass terms and couplings with positive mass dimension. If the largest scale associated with the soft terms is denoted $m_{soft}$, then the additional radiative corrections to the Higgs scalar mass are of the form

$$\Delta m_H^2 = m_{soft}^2[\frac{\lambda}{16\pi^2}\ln(\Lambda_{UV}/m_{soft}) + \ldots]. \tag{2.17}$$

Here $\lambda$ is a dimensionless coupling, and the ellipses stand for terms which are independent of $\Lambda_{UV}$ and for higher loop corrections which depend on $\Lambda_{UV}$ through powers of logarithms. Since the mass splittings between the known Standard Model particles and their superpartners are determined by the parameter $m_{soft}$, (2.17) gives a rough estimate of the masses of the superpartners in order not to introduce large corrections and thus not to destroy the hierarchy between the high and the low scale. Using $\Delta m_H^2 < (100\ \mathrm{GeV})^2$, $\Lambda_{UV} \approx M_P$ and $\lambda \approx 1$ in (2.17), one finds that roughly at least the lightest superpartners should not be heavier than about 1 TeV.

The most general soft supersymmetry breaking Lagrangian which is compatible with gauge invariance and matter parity conservation is [2]

$$\begin{aligned}
\mathcal{L}_{soft} \;=\; & \frac{1}{2}\left[M_3\tilde{g}\tilde{g} + M_2\tilde{W}\tilde{W} + M_1\tilde{B}\tilde{B}\right] + c.c. \\
& - \left[\bar{\tilde{u}}\mathbf{a_u}\tilde{Q}H_u - \bar{\tilde{d}}\mathbf{a_d}\tilde{Q}H_d - \bar{\tilde{e}}\mathbf{a_e}\tilde{L}H_d\right] + c.c \\
& - \tilde{Q}^\dagger\mathbf{m_Q^2}\tilde{Q} - \tilde{L}^\dagger\mathbf{m_L^2}\tilde{L} - \bar{\tilde{u}}\mathbf{m_{\bar{u}}}^2\bar{\tilde{u}}^\dagger - \bar{\tilde{d}}\mathbf{m_{\bar{d}}}^2\bar{\tilde{d}}^\dagger - \bar{\tilde{e}}\mathbf{m_{\bar{e}}}^2\bar{\tilde{e}}^\dagger \\
& - m_{H_u}^2 H_u^* H_u - m_{H_d}^2 H_d^* H_d - (bH_u H_d) + c.c),
\end{aligned} \tag{2.18}$$

[2] There could be additional terms of the form $-\frac{1}{2}c_i^{jk}\Phi^{*i}\Phi_j\Phi_k + c.c$ but they are in general negligibly small and so are not taken into account [28]

where $M_3$, $M_2$, and $M_1$ are the gluino, wino, and bino mass terms. Each of $\mathbf{a_u}$, $\mathbf{a_d}$, $\mathbf{a_e}$ is a complex $3 \times 3$ matrix in family space. The third line consists of squark and slepton mass terms. Each of $\mathbf{m_Q^2}$, $\mathbf{m_L^2}$, $\mathbf{m_{\bar{u}}}^2$, $\mathbf{m_{\bar{d}}}^2$, $\mathbf{m_{\bar{e}}}^2$ is also a complex $3 \times 3$ matrix. Finally, in the last line of (2.18) we have supersymmetry-breaking contributions to the Higgs potential with masses $m_{H_u}^2$, $m_{H_d}^2$ and $b$.

In contrast to the supersymmetry conserving terms, the soft-breaking terms in $\mathcal{L}_{soft}$ introduces many new parameters. In [29] they count 105 masses, phases and mixing angles in the MSSM Lagrangian.

A complete set of Feynman rules for the MSSM deduced from the Lagrangian is given in the review of Haber and Kane [30]. The Feynman rules needed in this thesis are summarized in appendix A.

## 2.8 Unification of gauge couplings

In unified field theories there is only one gauge group and hence only one coupling constant. The simplest example of such a gauge group, containing the standard model, is $SU(5)$ which is broken down into the standard model gauge group at the grand unification scale $m_{GUT}$ [31]:

$$SU(5) \longrightarrow SU(3)_C \times SU(2)_L \times U(1)_Y \tag{2.19}$$

In a gauge theory, coupling constants scale with energy according to the *renormalization group* (RG) equations. If at some scale all couplings meet this can be interpreted as a hint of unification at this scale.

The evolution of couplings is illustrated in figure 2.1. In this figure the RG evolution of the inverse couplings $\alpha_i^{-1}$ are compared, including two-loop effects, in the Standard Model and the MSSM. Unlike the Standard Model, the MSSM has just the right particle content to ensure that the gauge couplings can unify, at a scale $m_{GUT} \approx 2 \times 10^{16}$ GeV.

Vice versa one can predict the weak mixing angle $\sin^2\theta_W$ from the constraint of unification of the couplings and the known strong coupling and the electromagnetic fine structure constant. The resulting value at the $Z^0$-pole is $\sin^2\theta_W^{SM}(m_Z) \approx 0.207$ in the Standard Model and $\sin^2\theta_W^{MSSM}(m_Z) \approx 0.230$ in the MSSM. The experimental value is $\sin^2\theta_W^{exp}(m_Z) = 0.23117 \pm 0.00016$ [33] which is in good agreement with the MSSM.

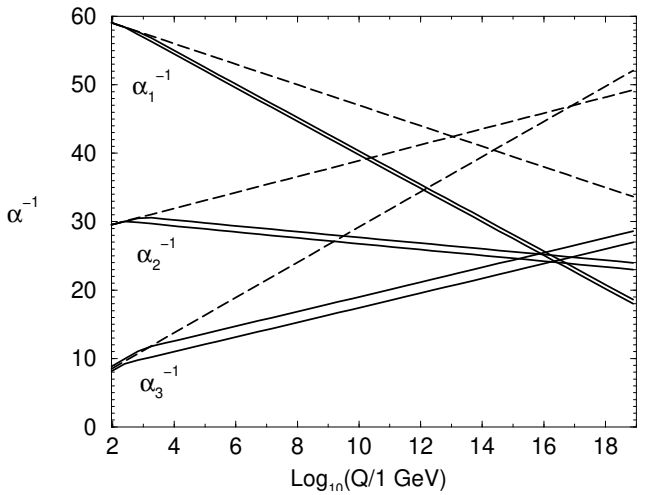


Figure 2.1: *Renormalization Group evolution of the inverse gauge couplings* $\alpha_i^{-1}(Q)$ *in the Standard Model (dashed lines) and the MSSM (solid lines). In the MSSM case,* $\alpha_3(m_Z)$ *is varied between 0.113 and 0.123, and the sparticle mass thresholds between 250 GeV and 1 TeV. Two-loop effects are included [32].*

## 2.9 Gauge and Yukawa couplings in the SUSY QCD sector

Supersymmetry breaking introduces many unknown parameters. However the gauge interactions and the Yukawa couplings are completely fixed by gauge invariance and supersymmetry as already indicated by (2.4). Especially within the QCD sector which is the subject of this thesis the gauge and Yukawa coupling constants in the interaction Lagrangian terms which couple quarks, gluons, squarks, and gluinos have to be equal: The strong gauge coupling $g_s$ determines on the one hand the gauge couplings emerging in the Lagrangian (2.7) and on the other hand the Yukawa and quartic squark couplings coming from the Lagrangian (2.8). The strong gauge interactions are obtained by turning derivatives into covariant derivatives, $\partial_\mu \to D_\mu = \partial_\mu + ig_s A_\mu^a t_a$ in the fermionic term and $\partial_\mu \to D_\mu = \partial_\mu + ig_s' A_\mu^a t_a$ in the bosonic term in (2.7) in a representation of the gauge group with hermitian matrices $t_a$ where $A_\mu$ denotes the gauge field. The Yukawa interaction between a quark and a squark and a gluino as well as the quartic squark coupling can directly be deduced from (2.8) when we substitute $T^A \to t^a$ and $g_A \to \hat{g}_s$. Gauge invariance and supersymmetry constraint this couplings

from different Lagrangian terms to be equal:

$$g_s = g_s' = \hat{g}_s \tag{2.20}$$

The equality of gauge and Yukawa couplings in softly broken SUSY is not restricted to the $SU(3)_C$ coupling $g_s$ but also must hold for the $SU(2)_L$ and $U(1)_Y$ couplings $g_2$ and $g_1$. These $SU(2)_L$ and $U(1)_Y$ couplings were investigated in [34] and [35]. Here we focus on the $SU(3)_C$ couplings.

When at future colliders new particles are discovered the first task is to measure masses and quantum numbers like the spin. Figure 2.2 shows the current status of experimental search for squarks and gluinos from the Tevatron detectors D0 and CDF. They are looking for signatures, where the squarks and gluinos decay and according to matter parity end up in form of the LSP plus additional jets and multileptons, where the LSP escapes the detector. Thus they expect squarks and gluinos in signatures of jets and leptons accompanied by missing transverse energy representing the LSP. The figure shows the excluded regions in the investigated squark-gluino mass spectrum. In this analysis it was assumed, motivated by supergravity models, all scalar particle masses to unify to one mass parameter $m_0$ as well as all gaugino masses to unify to the mass $m_{1/2}$ at the GUT scale and the neutralino to be the LSP.

After the discovery of new particles it will be essential to decide whether these particles belong to a supersymmetric theory and therefore to investigate the couplings. If the gauge and Yukawa couplings are equal this will give a direct indication of supersymmetry

In principle the gauge and Yukawa couplings could be analyzed in proton colliders like the TEVATRON or the LHC. The gauge coupling of the squark-squark-gluon vertex $g_s'$ for instance emerges in the process $pp(\bar{p}) \to \tilde{q}\bar{\tilde{q}}X$. The corresponding cross section was already calculated at NLO [36]. But it is preferable to investigate these couplings in lepton colliders like TESLA [37] or CLIC [38] because they allow for high precision experiments due to the well defined initial state. In electron-positron annihilation the processes involving the three complementary strong gauge and Yukawa couplings $g_s$, $g_s'$, and $\hat{g}_s$ at tree level are shown in figure 2.3.

The tree level calculation of the Standard Model process $e^+e^- \to q\bar{q}g$ was performed by [39],[40],[41]. The other two processes were performed in 1983 at tree level without taking into account the $Z^0$-Boson exchange and neglecting squark and gluino masses [42] and two years later without these simplifications [43]. The QCD NLO corrections of the Standard Model process were computed in [13],[14],[15],[16].

There are several reasons to compute the MSSM NLO corrections in the strong coupling to all three of these processes:

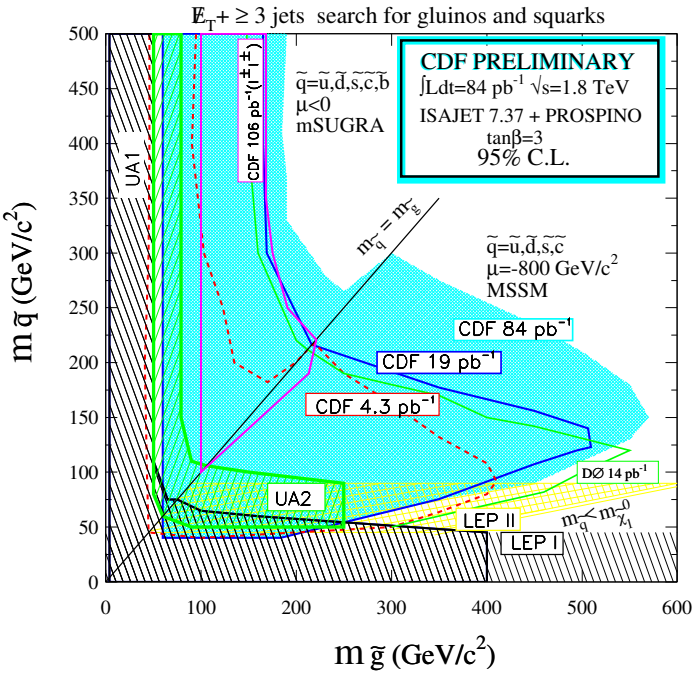


Figure 2.2: *Exclusion plot of gluino and squark masses. The filled area is the currently covered region of the CDF-detector at Tevatron.*

- Since the equality of the couplings is essential in a supersymmetric theory it is desirable to investigate this processes to as high accuracy as possible.
- At tree level there is a large dependence on the *renormalization scale*. In NLO a significant reduction of this unphysical scale dependence is expected.
- The computation of the process $e^+e^- \to q\bar{q}g$ yields large NLO QCD corrections. Presumably we have corrections of the same order also in the other two processes.

The MSSM QCD corrections to the process $e^+e^- \to q\bar{\tilde{q}}\tilde{g}$ have been finished in the thesis [17] and the MSSM QCD corrections to the remaining process $e^+e^- \to \tilde{q}\bar{\tilde{q}}g$ are presented in the next sections.

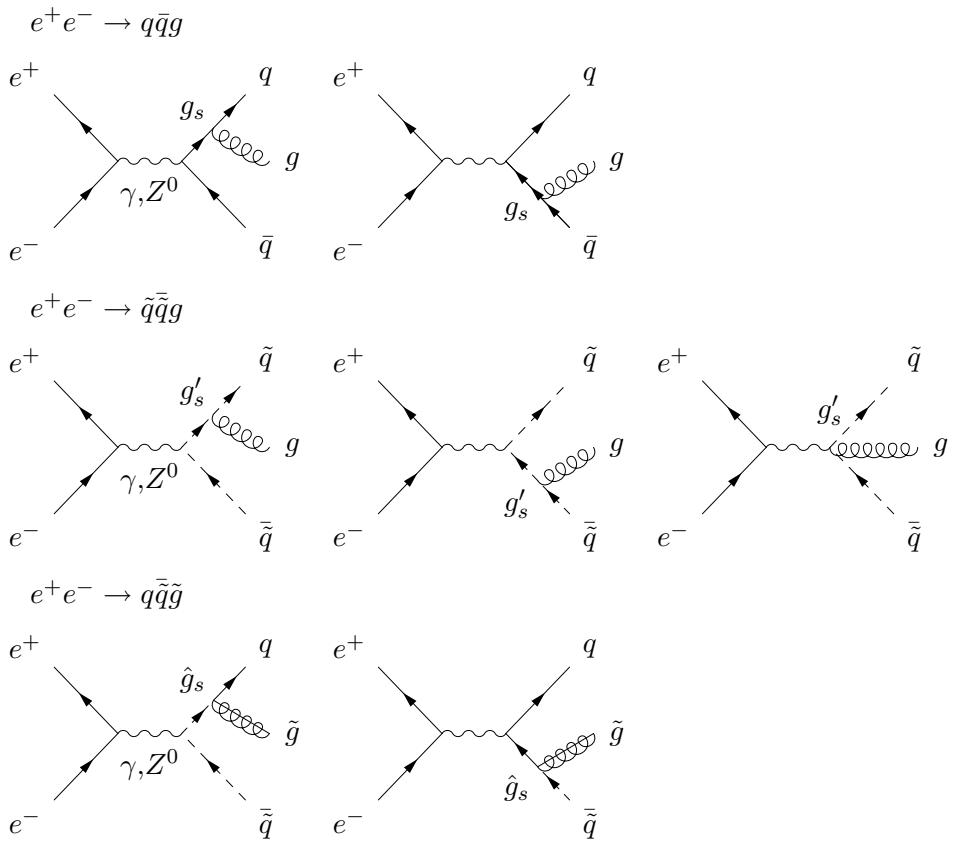


Figure 2.3: *Strong gauge and Yukawa couplings emerging in electron positron collisions.*

# Chapter 3

# The process $e^+e^- \longrightarrow \tilde{q}\bar{\tilde{q}}g$

Before performing the *next-to-leading order* (NLO) calculation, we confirmed the tree level calculation, first presented in [42] and [43]. The Feynman diagrams of this process $e^+e^- \to \tilde{q}\bar{\tilde{q}}g$ are also the real emission part of the NLO corrections in $\alpha_s$ to the process $e^+e^- \to \tilde{q}\bar{\tilde{q}}$ and thus the divergences in the *soft* gluon region of phase space belong to the $\tilde{q}\bar{\tilde{q}}$ final state [1]. As a consequence, we introduce a phase space cut in the minimal gluon energy $E_g^{cut}$.

The SUSY-breaking terms (2.18) allow for mixing of all left- and right-handed squarks and squarks of different flavor. The non-diagonal terms of the mass matrix are proportional to the corresponding quark mass and thus the squark mixing is suppressed for the 5 light flavors. In our calculation we assume no left/right mixing and no flavor mixing. Also we assume mass degeneracy of all squarks and neglect the masses of the 5 light quarks in internal loops. This assumptions simplify the calculation considerably. Since we consider centre-of-mass energies far above the $Z^0$-resonance we also neglect the width of the $Z^0$-boson.

## 3.1 Tree level calculation

Figure 3.1 shows the three tree level diagrams contributing to the process $e^+e^- \to \tilde{q}\bar{\tilde{q}}g$.

The matrix element can be written as a lepton current times a hadron current

$$M = j_\mu^{L/R}\Gamma_Z^\mu, \tag{3.1}$$

[1] Soft divergences are discussed in more detail in section 3.2.

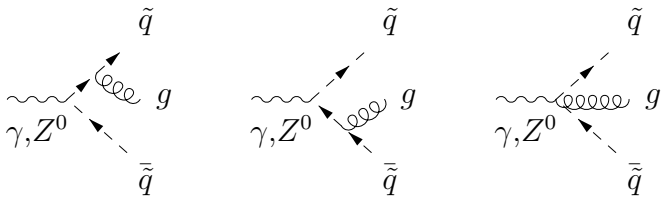


Figure 3.1: *Tree level diagrams in the process* $e^+e^- \longrightarrow \tilde{q}\bar{\tilde{q}}g$*. The annihilation of* $e^+e^-$ *into a virtual* $\gamma$ *respectively* $Z^0$ *is not drawn.*

where $L/R$ denote the helicity of the squarks [2] and the lepton current contains both, $\gamma$ and $Z$-boson exchange

$$\begin{aligned} j_\mu^{L/R} &= \left[-Q_{\tilde{q}}Q_e\frac{e}{s} - \frac{e}{s-M_Z^2}c_V^e(c_V^{\tilde{q}} \pm c_A^{\tilde{q}})\right]\bar{v}\gamma_\mu u + \left[\frac{e}{s-M_Z^2}c_A^e(c_V^{\tilde{q}} \pm c_A^{\tilde{q}})\right]\bar{v}\gamma_\mu\gamma^5 u \\ &= e\left(\bar{c}_V^{L/R}\,\bar{v}\gamma_\mu u + \bar{c}_A^{L/R}\,\bar{v}\gamma_\mu\gamma^5 u\right) \end{aligned} \tag{3.2}$$

and $\Gamma_Z^\mu$ represents the virtual $Z$-boson decay. In the lepton current $Q_f$ with $f = \tilde{q}, e$ denotes the charges of squark and electron in units of the positron charge ($e > 0$). $\bar{v}\gamma_\mu u$ and $\bar{v}\gamma_\mu\gamma^5 u$ are the vector respectively axial vector currents of the electron. The centre-of-mass energy is $\sqrt{s}$ and the vector respectively axial vector couplings for the particle $f$ are

$$c_V^f = \frac{I_3^f - 2Q_f\sin^2\theta_W}{2\cos\theta_W\sin\theta_W} \quad c_A^f = \frac{I_3^f}{2\cos\theta_W\sin\theta_W}, \tag{3.3}$$

where $I_3^f$ is the $z$-component of the weak isospin of particle $f$ and $\theta_W$ is the Weinberg angle.

With these abbreviations we can split the calculation into a lepton part $L_{\mu\nu}^{L/R}$ and a hadron part $H^{\mu\nu}$, thus the major part of the calculation is the decay of the $Z$-boson:

$$|M|^2 = j_\mu^{L/R*} j_\nu^{L/R}\,\Gamma_Z^{\mu*}\Gamma_Z^\nu = L_{\mu\nu}^{L/R}H^{\mu\nu} \tag{3.4}$$

We choose a system of coordinates in the centre-of-mass of the final state. With respect to this coordinates, the initial state is described by three Euler angles $\alpha$, $\beta$, and $\gamma$. With the 3-particle phase space factor written in form of this angles and the scaled energies ($x_1 = \frac{2\,E_{\tilde{q}}}{\sqrt{s}}$, $x_2 = \frac{2\,E_{\bar{\tilde{q}}}}{\sqrt{s}}$, $x_3 = \frac{2\,E_g}{\sqrt{s}}$) of two hadrons

$$dP^{(3)} = \frac{1}{2^3(2\pi)^5}\frac{d^3p_1}{p_{10}}\frac{d^3p_2}{p_{20}}\frac{d^3p_3}{p_{30}}\delta^4(q-p_1-p_2-p_3) = \frac{s}{32(2\pi)^5}d\alpha\,d\cos\beta\,d\gamma\,dx_1\,dx_2, \tag{3.5}$$

[2] The handedness here does not refer to the helicity of the squarks but to that of their superpartners.

we can integrate out the angular dependence of the lepton tensor

$$\int d\alpha\, d\cos\beta\, d\gamma\, L_{\mu\nu}^{L/R} = (\alpha_{em} 4\pi) s\pi^2\, \frac{8}{3} \left( (\bar{c}_V^{L/R})^2 + (\bar{c}_A^{L/R})^2 \right) \left[ \frac{q^\mu q^\nu}{q^2} - g^{\mu\nu} \right], \tag{3.6}$$

where $\alpha_{em} = e^2/4\pi$ is the QED fine structure constant. Inserting the flow factor $\frac{1}{2s}$, averaging over the lepton spins, and calculating the hadron tensor we get the differential cross section [44]

$$\begin{aligned} \frac{d\sigma_{Born}^{L/R}}{dx_1\, dx_2} &= \alpha_{em}^2\, \alpha_s\, \frac{4}{3}\, s \left( (\bar{c}_V^{L/R})^2 + (\bar{c}_A^{L/R})^2 \right) \\ &\quad \left\{ 3 - \frac{z^2(x_1^2 - z^2)}{4(1-x_1)^2} - \frac{z^2(x_2^2 - z^2)}{4(1-x_2)^2} \right. \\ &\quad \left. - \frac{(z^2-2)(x_1^2 + x_2^2 - x_3^2 - 2z^2)}{4(1-x_1)(1-x_2)} \right\}, \end{aligned} \tag{3.7}$$

where the scaled squark mass $z = \frac{2\, m_{\tilde{q}}}{\sqrt{s}}$ is scaled like the energies and $\alpha_s = \frac{g_s^2}{4\pi}$ is the SUSY QCD coupling constant. Expressed in scaled energies, energy conservation is simply $x_1 + x_2 + x_3 = 2$. The kinematic boundaries are given by the constraint $\cos\theta_{ij} = \pm 1$, where $\theta_{ij}$ is the angle between the particles $i$ and $j$ (appendix G). The *soft* divergence of the gluon is directly evident from the denominator of (3.7) in the limit $x_3 \to 0$ for which $x_{1/2} \to 1$.

Finally, the differential cross section (3.7) integrated analytically over the phase space of the scaled energies $x_1$ and $x_2$ with the constraint $x_3 > x_{cut}$ yields a total cross section:

$$\begin{aligned} &\sigma_{Born}^{tot}(e^+e^- \to \tilde{q}_{L/R}\, \bar{\tilde{q}}_{L/R}\, g) = \int_{x_3 > x_{cut}} d\sigma_{Born}^{L/R} \\ &= \alpha_{em}^2\, \alpha_s\, \frac{8}{3}\, s \left( (\bar{c}_V^{L/R})^2 + (\bar{c}_A^{L/R})^2 \right) \left\{ \left[ - Li_2\,(1 - \rho\,\omega) - Li_2 \left( 1 - \frac{\rho}{\omega} \right) \right.\right. \\ &\quad - \left( \omega^2 \ln(\omega) - \omega^2 + \ln(\omega) + 1 \right) \ln \left( \frac{1 - \rho\,\omega}{-\omega + \rho} \right) \left( 1 + \omega^2 \right)^{-1} \\ &\quad \left. -1/2\, \ln^2(\omega) - 1/2\, \ln^2(\rho) \right] \left( z^2 - 1 \right) \left( z^2/2 - 1 \right) \\ &\quad + \left( -x_{cut} + z^2/2 + z^2\, x_{cut} - z^4/8 \right) \ln(\rho) \\ &\quad \left. - \frac{1}{2}\, \frac{(-1 + x_{cut})\,(5 + x_{cut} - 7z^2/2)\,(1 - \rho)}{1 + \rho} \right\} \end{aligned} \tag{3.8}$$

where we used the abbreviations

$$\begin{aligned} x_{cut} &= \tfrac{2E_g^{cut}}{\sqrt{s}}, & \omega &= \tfrac{1-\beta}{1+\beta}, \\ \beta &= \sqrt{1-z^2}, & \rho &= \tfrac{1-\sqrt{1-\frac{z^2}{(1-x_{cut})}}}{1+\sqrt{1-\frac{z^2}{(1-x_{cut})}}}. \end{aligned} \tag{3.9}$$

## 3.2 Next to leading order calculation

Before explaining major parts of the calculation of the process $e^+e^- \to \tilde{q}\bar{\tilde{q}}g$ at NLO in the strong coupling $\alpha_s$ in more detail we give an outline of the calculation in this section.

The general structure of a QCD cross section at NLO is

$$\sigma = \sigma^{LO} + \sigma^{NLO}. \tag{3.10}$$

The leading order cross section $\sigma^{LO}$ is obtained by integrating the fully differential Born cross section $d\sigma^{Born}$ over the phase space of $m$ partons in the final state:

$$\sigma^{LO} = \int_m d\sigma^{Born} \tag{3.11}$$

where the Born cross section is

$$d\sigma^{Born} = d\Phi^{(m)}\ |M_m^{Born}|^2\ F_J^{(m)} \tag{3.12}$$

and $M_m^{Born}$ denotes the Born matrix element to produce $m$ final-state partons, $d\Phi^{(m)}$ denotes the phase space factor. In our calculation the number of final state particles is $m = 3$. The function $F_J^{(m)}$ defines the physical quantity that will be computed, possibly including the experimental cuts.

At NLO one has to consider the fully differential cross section $d\sigma^{real}$ with $m+1$ partons in the final state and the one-loop corrections $d\sigma^{virt}$ to the process with $m$ partons in the final state:

$$\sigma^{NLO} = \int_{m+1} d\sigma^{real} + \int_m d\sigma^{virt} \tag{3.13}$$

While the Born cross section requires to determine the squared Born matrix elements $|M_m^{Born}|^2$, the NLO corrections require on the one hand at the one-loop level to determine the interference term of the loop matrix elements with the hermitian conjugated Born amplitude $ReM_m^{Born\dagger}M_m^{virt}$ and on the other hand to determine the squared amplitude of the real corrections $|M_{m+1}^{real}|^2$. The Born cross section is of $\mathcal{O}(\alpha_s)$, the interference term $ReM_m^{Born\dagger}M_m^{virt}$ as well as the real corrections $|M_{m+1}^{real}|^2$ are of $\mathcal{O}(\alpha_s^2)$.

In the matrix elements of the virtual corrections $M_m^{virt}$ we encounter loops in form of self energies, vertex corrections and box diagrams. In loop diagrams we have to integrate over the loop momentum. Depending on the number of propagators and the masses of the particles these integrals are divergent. To handle these divergences we have to *regularize* these divergent integrations. We use the scheme of *dimensional regularization* [45], [46], where the number of space-time dimensions in the calculation is generalized to $D = 4 - 2\epsilon$, where $\epsilon$ is the regularization parameter.

In particular the integration over the loop momentum $q$ is done in D dimensions:

$$\int \frac{d^4q}{(2\pi)^4} \longrightarrow \mu^{4-D} \int \frac{d^Dq}{(2\pi)^D} \tag{3.14}$$

where $\mu$ is an arbitrary mass scale necessary to keep the coupling dimensionless in $D$ dimensions. For sufficiently small D, any loop-momentum integral will converge and in the limit $\epsilon \to 0$, i.e. $D \to 4$ we get poles $(1/\epsilon^n)$ representing the divergences.

In general care must be taken to treat the matrix $\gamma_5$ consistent in $D \neq 4$ dimensions. In our calculation we can simply use an anticommuting $\gamma_5$ [47]. The propagators for gauge bosons and fermions as well as the couplings that contain derivatives generate tensors of the integration momenta in the numerators of loop integrals. A systematic method to reduce these tensor integrals to a set of basic scalar integrals is applied here [48],[49],[50]. In appendix B the reduction formalism is described in detail.

The behavior of the scalar integrals with respect to their divergences can be summarized as follows: When the number of propagators in a scalar loop integral is one or two this integrals diverge for large momenta [3], called *ultraviolet* (UV) divergence. The 3-point, 4-point, and the derivatives of 2-point integrals are in general *soft* and *collinear* divergent. Soft poles emerge when a massless particle is exchanged between two on-shell external legs, provided that the emission of this massless particle does not change the masses of the emitting particles, collinear poles emerge when a massless particle splits into 2 massless collinear particles and double poles result from integrals containing soft and collinear singularities. Soft and collinear singularities together are referred to as *infrared* (IR) singularities in this thesis. The calculation of the loop integrals in $d\sigma^{virt}$ leads to ultraviolet, soft and collinear singularities.

The Lagrangian involves a certain number of free parameters which have to be determined experimentally. These are chosen such that they have an intuitive physical meaning at tree level (physical mass, couplings), i.e. they are

[3] The special case of a 2-point integral with vanishing outer momentum and vanishing masses in the loop particles gives both, infrared and ultraviolet divergences.

directly related to experimental quantities. This direct relation is destroyed through higher order corrections. Moreover the parameters of the original Lagrangian, the so-called *bare* parameters, differ from the corresponding physical quantities by UV divergent contributions. In renormalizable theories these divergences cancel exactly the UV divergences in the loop integrals.

In the *counterterm approach* the UV-divergent bare parameters are expressed by finite renormalized parameters and divergent renormalization constants, the counterterms. In addition the bare fields have to be replaced by renormalized fields and counterterms. The finite parts of the counterterms are fixed through *renormalization conditions*. These can be chosen arbitrarily, determining the relation between renormalized and physical parameters.

Except for the strong coupling $\alpha_s$ we use the *on-shell* renormalization scheme where the residue of the propagators are set to one and the fields are the physical fields. The strong coupling $\alpha_s$ is renormalized in the *modified minimal-subtraction scheme* ($\overline{MS}$) where in addition to the divergences remnants of the regularization procedure are subtracted [51],[52].

The soft and collinear singularities originating from the virtual corrections are accompanied by analogous singularities arising from the integration over the phase space of the real corrections. This is directly evident, when we consider a final-state particle in an arbitrary process. Supposed the final-state particle with momentum $p$ and mass $m$ emits a massless particle with momentum $k$ the corresponding propagator is proportional to

$$\frac{1}{(p+k)^2 - m^2} = \frac{1}{2k_0(p_0 - |\vec{p}|\cos\theta)} \tag{3.15}$$

where $\theta$ is the angle between the two particles. This propagator becomes singular in phase space regions $k_0 \to 0$ which is called a soft divergence and for $m = 0$ in the region $\theta \to 0$, called collinear divergence. To handle this soft and collinear divergences also the dimensional regularization scheme can be applied [45], [53]. Again in the procedure of regularization a mass scale $\mu$ has to be introduced to keep the number of mass dimensions constant in $D \neq 4$ dimensions.

The soft and collinear divergences of the real corrections cancel exactly the divergences coming from the loop integrations at any order of perturbation theory [54], [55], [56]. This cancellation is an important check of the calculation. From the experimental point of view soft and collinear emissions of additional particles can not be separated from the investigated process: Every detector has a limited energy resolution to detect additional soft particles and a limited angular resolution to distinguish between a single particle

and a collinear pair of particles. Thus the theoretical requirement of including real soft and collinear particles is consistent with the experimental situation.

On the one hand analytic calculations of the real cross sections are impossible for all but the simplest quantities because of the involved kinematics for multi-parton configurations. On the other hand, the use of numerical methods is far from trivial because real and collinear contributions have to be integrated separately over different phase-space regions and because of the analytic continuation in the arbitrary number of space-time dimensions $D$.

One solution to this problem is to somehow simplify and extract the singular parts of the cross section and treat them analytically, the remainder can then be treated numerically.

In principle there are two general methods: The *phase-space slicing* method [14] and the *subtraction* method [13]. Both methods can be generalized in a process-independent manner. The key to this process-independence is that the singular parts of the QCD matrix elements for real emission can be singled out in a general way by using the factorization properties of soft and collinear radiation [57]. Owing to this universality, the two methods have led to general algorithms for NLO QCD calculations.

In the phase space slicing approach the phase space region of the NLO real process is sliced into soft regions, collinear regions and the remaining *hard* region. The diagrams have to be separated in different color structures. A parameter $x_{cut}$ must be introduced to define the slice regions in phase space. This parameter is directly related to the threshold soft energy and the threshold collinear angle separating the regions. In the soft and collinear regions the divergences can be regularized via dimensional regularization. The remaining hard phase space region is convergent and may be integrated in $D = 4$ dimensions numerically. The independence of the phase space integration on the slicing parameter $x_{cut}$ has to be checked.

The results obtained this way are correct up to $\mathcal{O}(x_{cut})$, so precise predictions require small values of $x_{cut}$. For $x_{cut} \to 0$ parts of the numerical integration grow like $\ln(x_{cut})$. Consequently, much CPU time is needed to calculate the singular terms that cancel in the final result anyhow.

These large numerical cancellations are absent in subtraction methods. In contrast to the slicing method we have a cancellation of soft and collinear singularities before performing the numerical phase-space integration and no dependence on any variable $x_{cut}$. The subtraction method, applied in our

calculation is the so-called *dipole formalism* first derived for massless partons [58] and recently generalized to massive partons [59].

The general idea is to subtract and add the same quantity $d\sigma^A$:

$$\sigma^{NLO} = \int_{m+1} \left[ d\sigma^{real} - d\sigma^A \right] + \int_{m+1} d\sigma^A + \int_m d\sigma^{virt} \tag{3.16}$$

The cross section contribution $d\sigma^A$ has to fulfill the properties

- The contribution $d\sigma^A$ must be a proper approximation of $d\sigma^{real}$ such as to have the same *point-wise* singular behavior as $d\sigma^{real}$ itself. Thus $d\sigma^A$ acts as a local counterterm for $d\sigma^{real}$ and one can safely perform the limit $\epsilon \to 0$ under the integral sign:

$$\sigma^{NLO\{m+1\}} = \int_{m+1} \left[ d\sigma^{real} - d\sigma^A \right] = \int_{m+1} \left[ (d\sigma^{real})_{\epsilon=0} - (d\sigma^A)_{\epsilon=0} \right] \tag{3.17}$$

- $d\sigma^A$ has to be analytically integrable (in $D$ dimensions) over the one-parton subspace leading to the soft and collinear divergences. In this case the last two terms of (3.16) can be written as

$$\sigma^{NLO\{m\}} = \int_{m+1} d\sigma^A + \int_m d\sigma^{virt} = \int_m \left[ d\sigma^{virt} + \int_1 d\sigma^A \right]_{\epsilon=0}. \tag{3.18}$$

Performing the analytical integration $\int_1 d\sigma^A$, one obtains $\epsilon$-pole contributions canceling the divergences in $d\sigma^{virt}$. The remainder is finite in the limit $\epsilon \to 0$ and thus defines the integrand of a cross section contribution with $m$-parton kinematics that can be integrated numerically in four dimensions. We arrive at the final NLO cross section adding the two terms in (3.18) and (3.17)

$$\sigma^{NLO} = \sigma^{NLO\{m\}} + \sigma^{NLO\{m+1\}}. \tag{3.19}$$

In the dipole formalism the subtraction matrix element $d\sigma^A$ is derived from the soft and collinear factorization theorems for QCD matrix elements. According to this factorization theorems, the singular behavior of a generic tree-level matrix element with $m+1$ final-state partons has the structure:

$$|M_{m+1}(p_1, ..., p_j, ..., p_{m+1})|^2 \overset{soft}{\to} |M_m(p_1, ..., p_{m+1}|^2 \otimes_C \mathbf{J}^2(p_j) \tag{3.20}$$

$$|M_{m+1}(p_1, ..., p_j, p_i, ..., p_{m+1})|^2 \overset{collinear}{\to} |M_m(p_1, ...p_j + p_i, ..., p_{m+1}|^2 \otimes_h \mathbf{P_{ij}} \tag{3.21}$$

In the soft limit the momentum $p_j$ vanishes and in the collinear limit the momenta $p_i$ and $p_j$ become parallel. The contribution $M_m$ on the right-hand sides denote the tree-level matrix elements to produce $m$ partons and are obtained from the original $m+1$ parton matrix element by removing the soft parton $p_j$ or combining the two collinear partons $p_i$ and $p_j$ into a single-parton momentum, respectively. The other contributions on the right hand sides are the soft and collinear singular contributions. The factor $\mathbf{J}^2(p_j)$ is the eikonal current for the emission of the soft gluon with momentum $p_j$, and $\mathbf{P_{ij}}$ is the Altarelli-Parisi splitting function. These factors are universal in the sense that they do not depend on the process but only on the momenta and quantum numbers of the QCD partons in $M_m$. In particular, $\mathbf{J}^2(p_j)$ depends on the color charges of the partons in $M_m$, and $\mathbf{P_{ij}}$ depends on their helicities. Because of these color and helicity correlations (3.20) and (3.21) are not real factorizations and are denoted symbolically by $\otimes_C$ and $\otimes_h$.

Owing to their universality, the limiting formulae (3.20), (3.21) can be used to approximate the matrix element $|M_{m+1}|^2$ and thus to find a subtracted cross section $d\sigma^A$ that matches the real cross section $d\sigma^{real}$ in all the singular regions of phase space.

The dipole formalism introduces universal dipole splitting functions $\mathbf{V}_{ij}$ which coincide with the eikonal current and with the Altarelli-Parisi splitting functions in the soft and collinear limits. Thus the subtraction matrix element is given by a single formula that approximates the real matrix element $|M_{m+1}|$ for an arbitrary process in all of its singular limits.

$$d\sigma^A = d\Phi^{(m+1)} \sum_{ij} |M_m(\{\tilde{p}_k\})|^2 \otimes \mathbf{V}_{ij} \times F_J^m(\{\tilde{p}_k\}). \tag{3.22}$$

The set $\tilde{p}_1, ..., \tilde{p}_m$ of modified momenta is defined starting from the original $m+1$ parton momenta in such a way that the m partons in $|M_m|^2$ are physical, that is, they are on-shell and energy-momentum conservation is implemented exactly. Color and helicity correlations are denoted by the symbol $\otimes$. The $m+1$ particle phase space is denoted by $d\Phi^{(m+1)}$. The detailed expressions for the modified parton momenta $\tilde{p}_k$ and for the dipole splitting functions $\mathbf{V}_{ij}$ are given in appendix F.

The function $F_J^m(\{\tilde{p}_k\})$ defines the physical quantity that will be computed. This quantity has to be a jet observable, that is, it has to be soft and collinear safe. Thus, in any case where the $m+1$-parton configuration is obtained from the $m$-parton configuration by adding a soft parton or replacing a parton with a pair of collinear partons carrying the total momentum we should have

$$F_J^{(m+1)} \to F_J^{(m)}. \tag{3.23}$$

The second part of the subtraction formalism is to determine the re-added part $\int_1 d\sigma^A$ in (3.18). This part requires the integration over the dipole phase space in $D$ dimensions. Having introduced the modified momenta $\tilde{p}_1, ..., \tilde{p}_m$, for each dipole term in (3.22), the phase space factorizes exactly

$$d\Phi^{(m+1)}(p_1, ..., p_{m+1}) = d\Phi^{(m)}(\tilde{p}_1, ..., \tilde{p}_m)\, d\phi(p_i + p_j), \tag{3.24}$$

where $d\phi$ is a single-particle subspace. With help of this phase space factorization the integration of the singular dipole contribution can be completely factorized except for the color and helicity correlations:

$$\begin{aligned} \int_{m+1} d\sigma^A &= \int_m d\Phi^{(m)}(\{\tilde{p}_k\}) |M_m(\{\tilde{p}_k\})|^2\, F_J^{(m)}(\{\tilde{p}_k\}) \otimes \sum_{ij} \int_1 d\phi(p_i + p_j) \mathbf{V}_{ij} \\ &= \int_m d\sigma^{Born} \otimes \mathbf{I}(\{\tilde{p}_k\}). \end{aligned} \tag{3.25}$$

The integrated dipole function $\mathbf{I}(\{\tilde{p}_k\})$ is defined by the sum

$$\mathbf{I}(\{\tilde{p}_k\}) = \sum_{ij} \int_1 d\phi(p_i + p_j) \mathbf{V}_{ij} \tag{3.26}$$

containing all the soft and collinear singularities that are necessary to compensate those in the virtual cross section $d\sigma^{virt}$. It is possible to integrate analytically the dipole splitting functions $\mathbf{V}_{ij}$ over the dipole phase space in $D$ dimensions. This leads to explicit and universal expressions for the factors $\mathbf{I}$, whose $\epsilon$-poles cancel those in the one-loop matrix element. The explicit expressions for the here investigated process are given in appendix F.

The renormalized virtual corrections together with the real contributions yield finite NLO corrections. The renormalization scale $\mu$ dependence comes into play through the $\beta$ function of QCD in the MSSM and the regularization of virtual and real divergences. The dependence on this scale $\mu$ can be compared between LO and NLO calculation which is expected to decrease with increasing order.

The algebraic computation from the generation of the matrix elements via Feynman rules to the tensor reduction is performed with help of the FORM program [60]. The FORM output is then transformed into C code in which the whole numerical computation is performed. UV or IR divergent scalar integrals have to be calculated analytically. The remaining convergent scalar integrals can be evaluated numerically from the general solutions of these integrals. They are available in form of a package which can be called from C-routines [61]. The multi-dimensional integration over the phase space is

done via the adaptive VEGAS [62] routine which also can be included into the C-code.

In the next sections the different steps to perform the NLO calculation are explained in more detail.

### 3.2.1 *Virtual correction*

One of the main parts of the NLO calculation is to determine the virtual corrections, i.e. calculating the interference term between the Born matrix element and the one-loop matrix elements $ReM^{Born\dagger}M^{virt}$. The calculation of the Born matrix element is already presented in section 3.1. The one-loop diagrams are organized in contributions with loops in the different vertices and propagators. Since we use the *on-shell renormalization* scheme no corrections to external lines have to be taken into account. In figure 3.2 all loop contributions are shown. The blobs represent the different corrections within the vertices and propagators. The explicit diagrams contained in the blobs are shown for two examples in figure 3.3.

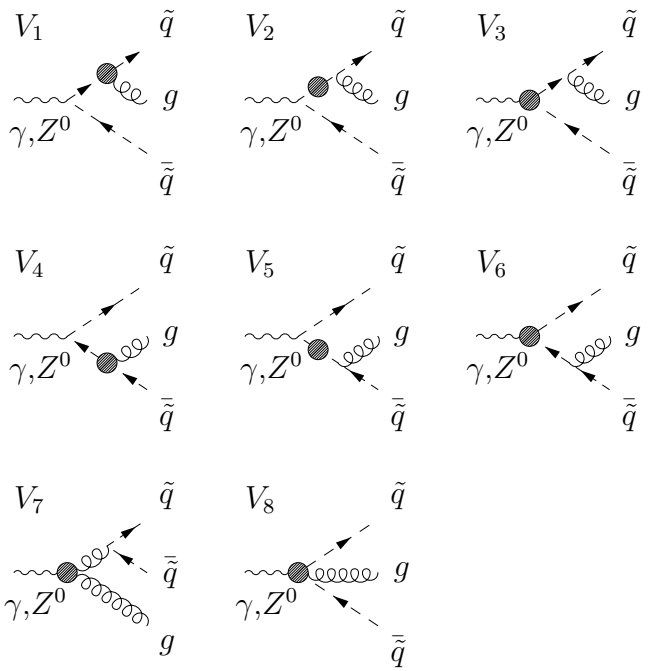


Figure 3.2: *Virtual corrections, where the blobs represent loops. The diagrams $V_1$-$V_7$ represent 2-point and 3-point contributions, $V_8$ contains 4-point contributions. The annihilation of $e^+e^-$ into a virtual $\gamma$ respectively $Z^0$ is not drawn.*

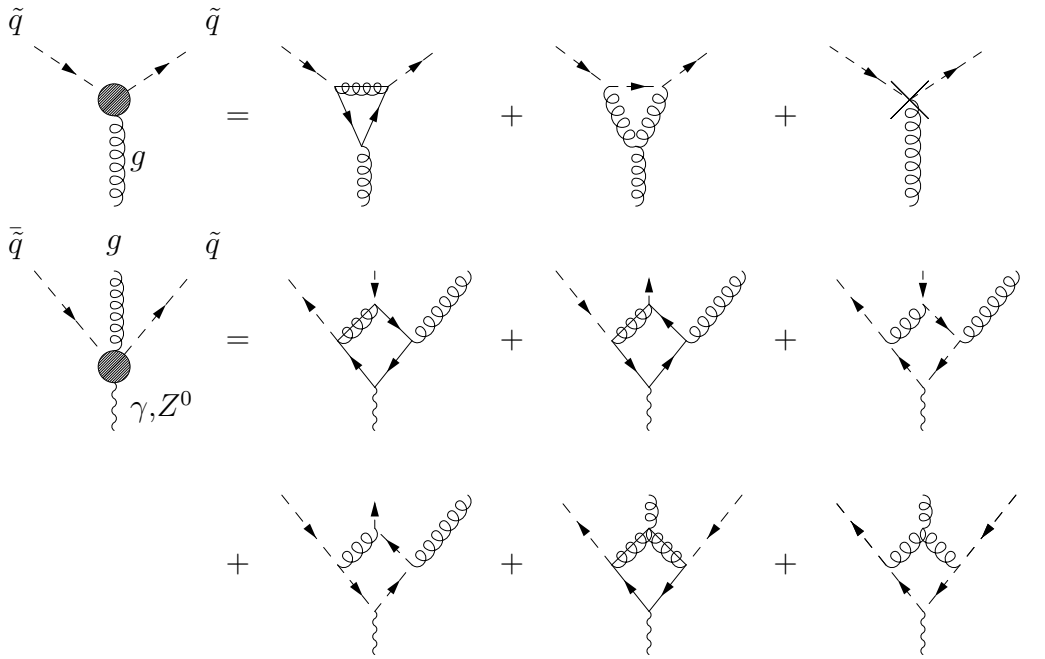


Figure 3.3: *Examples of the loop-diagrams contained in the blobs in figure 3.2. The last diagram in the top row is the counterterm of this squark-squark-gluon loop correction. The second and third row show scalar four-point integrals contained in the blob. There are additional diagrams not shown here.*

Just like in the calculation of the Born matrix element we can decompose the one-loop matrix element into a lepton tensor and a hadron tensor (3.1). This allows to focus on the calculation of the $Z$-boson decay into the final state particles.

The propagators for gauge bosons and fermions as well as vertices coming from Lagrangian terms containing derivatives generate tensors of the integration momenta in the numerator of the loop integrals. Thus we encounter one-, two-, three-, and four-point integrals up to rank two caused by the $Z$-boson and the external gluon. The tensor integrals can systematically be reduced to basic scalar integrals [48],[49],[50]. The definition of the tensor integrals as well as the tensor reduction formalism are given in appendix B.

The algebraic computation of all Feynman diagrams as well as the tensor reduction is performed with help of the algebraic program FORM [60]. After applying the tensor reduction we get an expression for the loop matrix element which contains up to four-point scalar integrals ($A_0$, $B_0$, $C_0$, $D_0$, see appendix C):

$$M^{virt} = \sum_i a_i A_0^i + \sum_i b_i B_0^i + \sum_i c_i C_0^i + \sum_i d_i D_0^i \tag{3.27}$$

Since the coefficients $a_i$-$d_i$ are rather lengthy they are not given here.

All IR respectively UV divergent scalar integrals have to be calculated analytically to provide the cancellation of divergences. This cancellation occurs on the one hand through renormalization and on the other hand when the real corrections are taken into account. The calculation of the scalar integrals are accomplished via Feynman parametrization of the integrand and Wick rotation of the integration contour from Minkowski space to Euclidian space. From the virtual correction term $ReM^{Born\dagger}M^{virt}$ it is evident that in the one-loop approximation only the real parts of the scalar integrals have to be calculated.

The four-point integrals $D_0$ usually can be calculated in $D = 4 - 2\epsilon$ dimensions in dimensional regularization. Alternatively one can use the tensor reduction formalism to write $D_0$ in form of a linear combination of three-point integrals $C_0$ and the coefficient $D_{00}$ of the $g_{\mu\nu}$ term in the Lorentz tensor decomposition (B.5). Since this coefficient $D_{00}$ is directly related to the infrared finite four-point scalar integral $D_0^6$ in $D = 6$ dimensions [63]

$$D_{00} = -\frac{1}{2\pi} D_0^6, \tag{3.28}$$

one can express every $D_0$ in a sum of $C_0$, reflecting the singularities of the $D_0$, and the finite six dimensional scalar integral $D_0^6$. Formula (3.28) is derived explicitly in appendix D.

In the loop calculation we encounter six different scalar box integrals. One of these integrals is infrared convergent and can be evaluated numerically. The remainder consists of three integrals which can not be obtained from each other by substituting kinematics in the outer momenta. Two of these integrals can be found in the literature [64] and the remaining unknown box integral has to be calculated analytically. All divergent scalar integrals used in this calculation are listed in appendix C.

All remaining UV and IR convergent scalar integrals are not needed in analytical form and are taken from the LoopTools package [61].

### 3.2.2 *Renormalization*

#### Renormalization constants

In the renormalization procedure we first have to choose a set of fields and independent parameters: We use the wave functions of the gluon $A_\mu^a$, where $\mu$ and $a$ are the polarization and the color indices, the gluino wave function $\tilde{A}^a$, the quark and squark wave functions $\Psi$ and $\tilde{\Psi}$, the masses of squark and gluino $m_{\tilde{q}}$, $m_{\tilde{g}}$ and the strong coupling constant $g_s$. In the counterterm

approach we separate the bare parameters and fields in the Lagrangian into renormalized parameters and fields and renormalization constants:

$$\begin{array}{lcll} A_\mu^{a\,0} & = & Z_A^{1/2}\, A_\mu^a & = (1 + 1/2\;\delta Z_A)\, A_\mu^a \\ \tilde{A}^{a\,0} & = & Z_{\tilde{A}}^{1/2}\, \tilde{A}_\mu^a & = (1 + 1/2\;\delta Z_{\tilde{A}})\, \tilde{A}_\mu^a \\ \Psi^0 & = & Z_q^{1/2}\, \Psi & = (1 + 1/2\;\delta Z_\Psi)\, \Psi \\ \tilde{\Psi}^0 & = & Z_{\tilde{q}}^{1/2}\, \tilde{\Psi} & = (1 + 1/2\;\delta Z_{\tilde{\Psi}})\, \tilde{\Psi} \\ m_{\tilde{q}}^0 & = & Z_{m_{\tilde{q}}}\, m_{\tilde{q}} & = m_{\tilde{q}} + \delta m_{\tilde{q}} \\ m_{\tilde{g}}^0 & = & Z_{m_{\tilde{g}}}\, m_{\tilde{g}} & = m_{\tilde{g}} + \delta m_{\tilde{g}} \\ g_s^0 & = & Z_{g_s}\, g_s & = (1 + \delta g_s) g_s \end{array} \tag{3.29}$$

The bare parameters, originally emerging in the bare Lagrangian ($\mathcal{L}^0$) are denoted by an index 0. The quantities $Z_A$, $Z_{\tilde{A}}$, $Z_q$ and $Z_{\tilde{q}}$ are called the gluon, the gluino, the quark, and the squark-field renormalization constants, while $Z_{m_{\tilde{q}}}$, $Z_{m_{\tilde{g}}}$, and $Z_{g_s}$ are called mass and coupling renormalization constants. In writing $Z = 1 + \delta Z$ for the multiplicative renormalization constants we can split the bare Lagrangian $\mathcal{L}^0$ into the renormalized Lagrangian $\mathcal{L}$ and the counterterm Lagrangian $\delta\mathcal{L}$. $\mathcal{L}$ has the same form as $\mathcal{L}^0$ but depends on renormalized parameters and fields instead of unrenormalized ones. $\delta\mathcal{L}$ contains the counterterms. The corresponding Feynman rules are listed in Appendix A. The counterterm diagrams have to be added to the loop graphs. Since we are only interested in one-loop corrections, we neglect terms of order $(\delta Z)^2$.

**Renormalization conditions**

The finite parts of the renormalization constants introduced in the last section are fixed by imposing renormalization conditions. The renormalization conditions which define the renormalized parameters affect physical predictions to finite orders of perturbation theory, while the conditions which define the renormalized fields are only relevant for Green functions and drop out in the calculation of S-matrix elements. Nevertheless their use is very convenient in the *on-shell* scheme. They not only allow to eliminate the explicit wave function renormalization of the external particles, but also simplify the explicit form of the renormalization conditions for the physical parameters. In the on-shell scheme all renormalization conditions are formulated for on mass shell external fields. The field and mass renormalization constants are fixed using the *one-particle irreducible* (1PI) two-point functions. For the coupling renormalization one three-point vertex function involving the strong coupling is needed. We choose the quark-quark-gluon vertex function. To formulate the renormalization conditions we need the 1PI two-point

functions defined in figure 3.4 and the three-point function defined in figure 3.5.

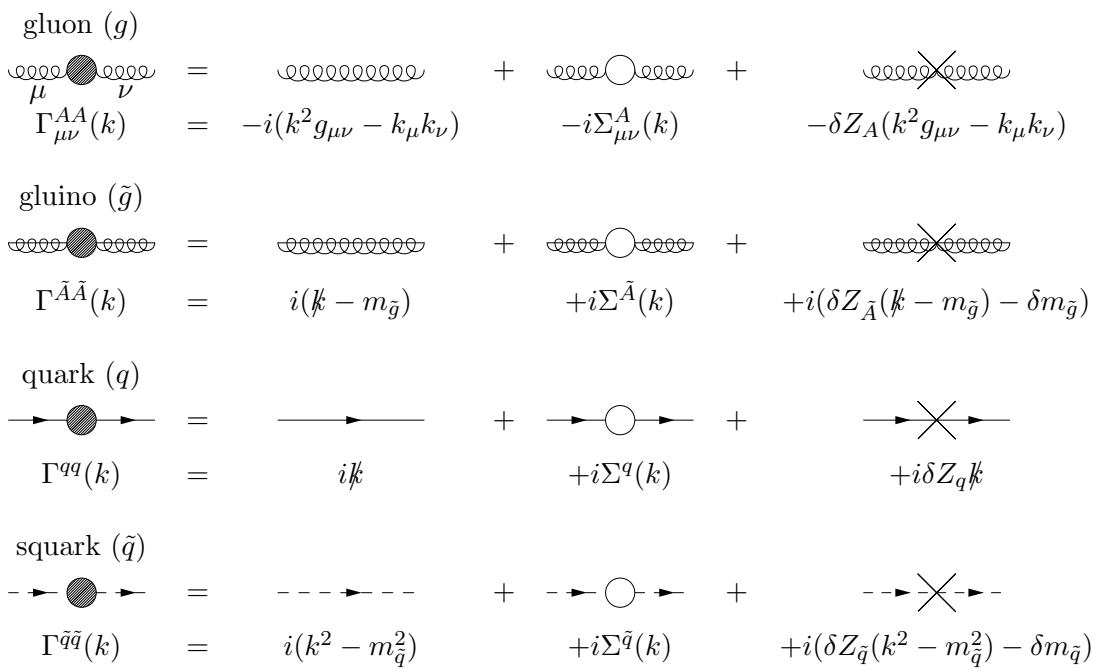


Figure 3.4: *1PI two-point functions to formulate the renormalization conditions. The particle momentum is denoted by $k$ and the polarization index of the gluon by $\mu$ and $\nu$. The selfenergies are denoted by the $\Sigma$-terms and the counterterm diagrams by a cross.*

The corresponding propagators are obtained as the inverse of these two-point functions. In the on-shell scheme the renormalized mass parameters of the particles are fixed by the requirement that they are equal to the physical masses, i.e. to the real parts of the poles of the corresponding propagators which are equivalent to the zeros of the one-particle irreducible two-point functions. Thus the on-shell renormalization conditions are

$$\begin{array}{ll} Re\,(\Gamma^{AA}_{\mu\nu})\,\epsilon^\nu(k)|_{k^2=0} = 0 & \lim_{k^2\to 0} \frac{1}{k^2}\Gamma^A_{\mu\nu}\,\epsilon^\nu(k) = -i\epsilon^\nu(k) \\ Re\,(\Gamma^{qq}(k))\,u(k)|_{k^2=0} = 0 & \lim_{k^2\to 0} \frac{1}{\not{k}} Re\,(\Gamma^{qq}_{\mu\nu})u(k) = iu(k) \\ Re\,(\Gamma^{\tilde{A}\tilde{A}}(k))\,u(k)|_{k^2=m_{\tilde{g}}} = 0 & \lim_{k^2\to m^2_{\tilde{g}}} \frac{1}{\not{k}-m_{\tilde{g}}} Re\,(\Gamma^{\tilde{A}\tilde{A}})u(k) = iu(k) \\ Re\,(\Gamma^{\tilde{q}\tilde{q}}(k))\,|_{k^2=m_{\tilde{q}}} = 0 & \lim_{k^2\to m^2_{\tilde{q}}} \frac{1}{k^2-m^2_{\tilde{q}}} Re\,(\Gamma^{\tilde{q}\tilde{q}}) = i, \end{array} \tag{3.30}$$

where $\epsilon^\nu(k)$ and $u(k)$ are the usual polarization vectors and Dirac-spinors.

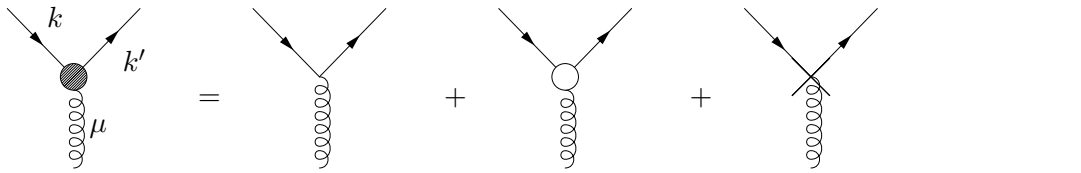


Figure 3.5: *Three-point function to formulate the renormalization condition for the strong coupling.*

Since in non-abelian gauge theories there exist no Thomson limit to fix the coupling the on-shell scheme is not valid to fix the strong coupling $g_s$. Commonly used renormalization schemes are the *minimal-subtraction scheme* ($MS$ scheme), where just the divergences are subtracted, or the *modified minimal-subtraction scheme* ($\overline{MS}$ scheme), where in addition remnants of the regularization procedure are subtracted. In one-loop calculations these remnants consist of $\ln(4\pi) - \gamma$, where $\gamma$ is the Euler constant.

Using the 3-point function $\Gamma_\mu^{Aqq}(k,k')$ in figure 3.5, the renormalization constant of the strong coupling $\delta g_s$ is fixed in the $\overline{MS}$-scheme by the condition just to compensate all UV singularities and corresponding $\ln(4\pi) - \gamma$ terms.

### Explicit renormalization constants

When we decompose the quark and gluino self-energy $\Sigma^q(k)$, $\Sigma^{\tilde{A}}(k)$ into a vector and a scalar part, develop the self energy of the squark $\Sigma^{\tilde{q}}(k)$ around $k^2 = m_{\tilde{q}}^2$, and decompose the self-energy of the gluon $\Sigma_{\mu\nu}^A(k)$ due to transversality:

$$\begin{aligned}
\Sigma^q(k) &= \not{k}\Sigma_V^q(k^2) \\
\Sigma^{\tilde{A}}(k) &= \not{k}\Sigma_V^{\tilde{A}}(k^2) + m_{\tilde{g}}\Sigma_S^{\tilde{A}}(k^2) \\
\Sigma^{\tilde{q}}(k) &= \Sigma^{\tilde{q}}(m_{\tilde{q}}^2) + (k^2 - m_{\tilde{q}}^2)\Sigma'^{\tilde{q}}(m_{\tilde{q}}^2) \\
\Sigma_{\mu\nu}^A(k) &= (g_{\mu\nu} - k_\mu k_\nu/k^2)\ \Sigma_T^A(k^2)
\end{aligned} \tag{3.31}$$

we arrive at the renormalization constants

$$\begin{aligned}
\delta Z_q &= -\Sigma_V^q(0) \\
\delta m_{\tilde{g}} &= m_{\tilde{g}}\left[\Sigma_V^{\tilde{A}}(m_{\tilde{g}}^2) + \Sigma_S^{\tilde{A}}(m_{\tilde{g}}^2)\right] \\
\delta Z_{\tilde{A}} &= -\Sigma_V^{\tilde{A}}(m_{\tilde{g}}^2) - 2m_{\tilde{g}}^2\left[\Sigma_V'^{\tilde{A}}(m_{\tilde{g}}^2) + \Sigma_S'^{\tilde{A}}(m_{\tilde{g}}^2)\right] \\
\delta m_{\tilde{q}}^2 &= \Sigma^{\tilde{q}}(m_{\tilde{q}}) \\
\delta Z_A &= -\Sigma_T'^A(0).
\end{aligned} \tag{3.32}$$

From the calculation of the self-energies we find the explicit renormalization constants given in appendix E. The mass and wave function renormalization

constants directly determine the coupling renormalization constants in the $\overline{MS}$ scheme, where we compensate just the divergences and $\ln(4\pi) - \gamma$ terms in $\delta g_s$ to keep $\hat{\Gamma}^{Aqq}_{\mu}(k, k')$ in figure 3.5 finite as $\epsilon \to 0$.

From the renormalization constants we get counterterms in form of additional Feynman diagrams listed also in appendix E.

As discussed in section 3.2.1 we organized the one-loop diagrams in contributions with loops in the different vertices and propagators including the counterterms. This allows to check on cancellation of UV divergences in each of these 1PI vertex functions separately. Thus we arrive at virtual corrections of the form 2 $ReM^{Born\dagger}M^{virt}$ which are free of ultraviolet divergences but still contain soft and collinear singularities.

### 3.2.3 *Supersymmetry-restoring counterterm*

As described in the last section, we applied the dimensional regularization scheme to regularize ultraviolet, soft, and collinear divergences.

Since gluons have $D-2$ and gluinos 2 polarization degrees of freedom, dimensional regularization introduces a mismatch between the number of gauge-bosons and gaugino degrees of freedom in $D \neq 4$ dimensions, i.e. violates supersymmetry explicitly. In particular, the $q\tilde{q}\tilde{g}$ Yukawa coupling $\hat{g}_s$, which by supersymmetry should coincide with the $qqg$ and $\tilde{q}\tilde{q}g$ gauge couplings $g_s$ and $g'_s$, deviates by a finite amount at the one-loop order. Requiring the physical amplitudes to be independent of the regularization scheme, a shift between the bare Yukawa and gauge coupling must be introduced in this scheme [65],

$$\hat{g}_s = g_s[1 + \frac{\alpha_s}{4\pi}(\frac{2}{3}N_C - \frac{1}{2}C_f)] = g_s[1 + \frac{\alpha_s}{3\pi}], \tag{3.33}$$

which effectively subtracts the contributions of the false, non-supersymmetric degrees of freedom; $N_C$ and $C_f$ are the Casimir invariants of the $SU(3)_C$ gauge group.

Alternatively one could use the *dimensional reduction scheme* to avoid the shift in the Yukawa coupling (3.33) [66],[67]. Dimensional reduction preserves supersymmetry at least to one-loop order but is mathematically inconsistent [68]. A consistent regularization scheme with the assumed symmetry properties is not known.

### 3.2.4 *Real correction*

In this section we present the calculation of real cross section $d\sigma^{real}$ in (3.16).

In figure 3.6 the diagrams for the NLO real emission part are drawn. This are contributions to two processes, namely the process (a) with an additional final state gluon $e^+e^- \to \tilde{q}\bar{\tilde{q}}gg$ and the process (b) $e^+e^- \to \tilde{q}\bar{\tilde{q}}q\bar{q}$ from the splitting of a gluon into a quark-antiquark pair. Also diagrams with the same final state but without any divergences are drawn and have in general to be taken into account. In analogy to the Born and virtual calculation we split the real matrix elements into a lepton current and a hadron current $M = j_\mu \Gamma_Z^\mu$.

Only the diagrams 4 and 5 in process (b) in figure 3.6 contain diagrams, where the virtual $Z^0$ boson couples to the quark. In all other diagrams we find a coupling of the virtual $Z^0$ to the squark which results in a coupling structure proportional to $c_V^{\tilde{q}} \pm c_A^{\tilde{q}}$ for left respectively right handed squarks, defined in (3.3). This coupling structure is exactly what we find in the Born and one-loop diagrams. In the diagrams 4 and 5 in process (b) where the $Z^0$-boson couples to a quark, the matrix elements are not proportional to this vector plus/minus axial vector part. Furthermore this couplings are independent of the helicity of the outer squarks which do not couple to the $Z^0$-boson directly.

To take this into account we split the real matrix element for process (b) $M_{(b)}^{real}$ into parts which couple to squarks and into the diagrams 4 and 5 which couple to quarks. The latter are further decomposed in vector and axial-vector parts:

$$M_{(b)}^{real} = j_\mu^{L/R} \Gamma_{\tilde{q}}^{\mu\, V+A} + j_\mu^V \Gamma_q^{\mu\, V} + j_\mu^A \Gamma_q^{\mu\, A}, \tag{3.34}$$

where the lepton current $j_\mu^{L/R}$ is given by (3.2) and the additional currents are defined by

$$j_\mu^V = \left[ -Q_{\tilde{q}} Q_e \frac{e}{s} - \frac{e}{s - M_Z^2} c_V^e (c_V^{\tilde{q}}) \right] \bar{v} \gamma_\mu u + \left[ \frac{e}{s - M_Z^2} c_A^e (c_V^{\tilde{q}}) \right] \bar{v} \gamma_\mu \gamma^5 u \tag{3.35}$$

$$j_\mu^A = \left[ -\frac{e}{s - M_Z^2} c_V^e (c_A^{\tilde{q}}) \right] \bar{v} \gamma_\mu u + \left[ \frac{e}{s - M_Z^2} c_A^e (c_A^{\tilde{q}}) \right] \bar{v} \gamma_\mu \gamma^5 u \tag{3.36}$$

where all quantities are introduced in section 3.1. Only the lepton current $j_\mu^{L/R}$ in (3.34) depends on the helicity of the final state squark pair.

When we square the matrix element (3.34) several interference terms vanish: The interference terms proportional to $\Gamma_{\tilde{q}}^{\mu\, V+A} \Gamma_q^{\nu\, A*}$ as well as $\Gamma_q^{\mu\, V} \Gamma_q^{\nu\, A*}$ vanish algebraically. The interference term proportional to $\Gamma_{\tilde{q}}^{\mu\, V+A} \Gamma_q^{\nu\, V*}$ is odd under exchange of the momenta of the quarks while the phase space is even and thus will yield a vanishing phase space integration.

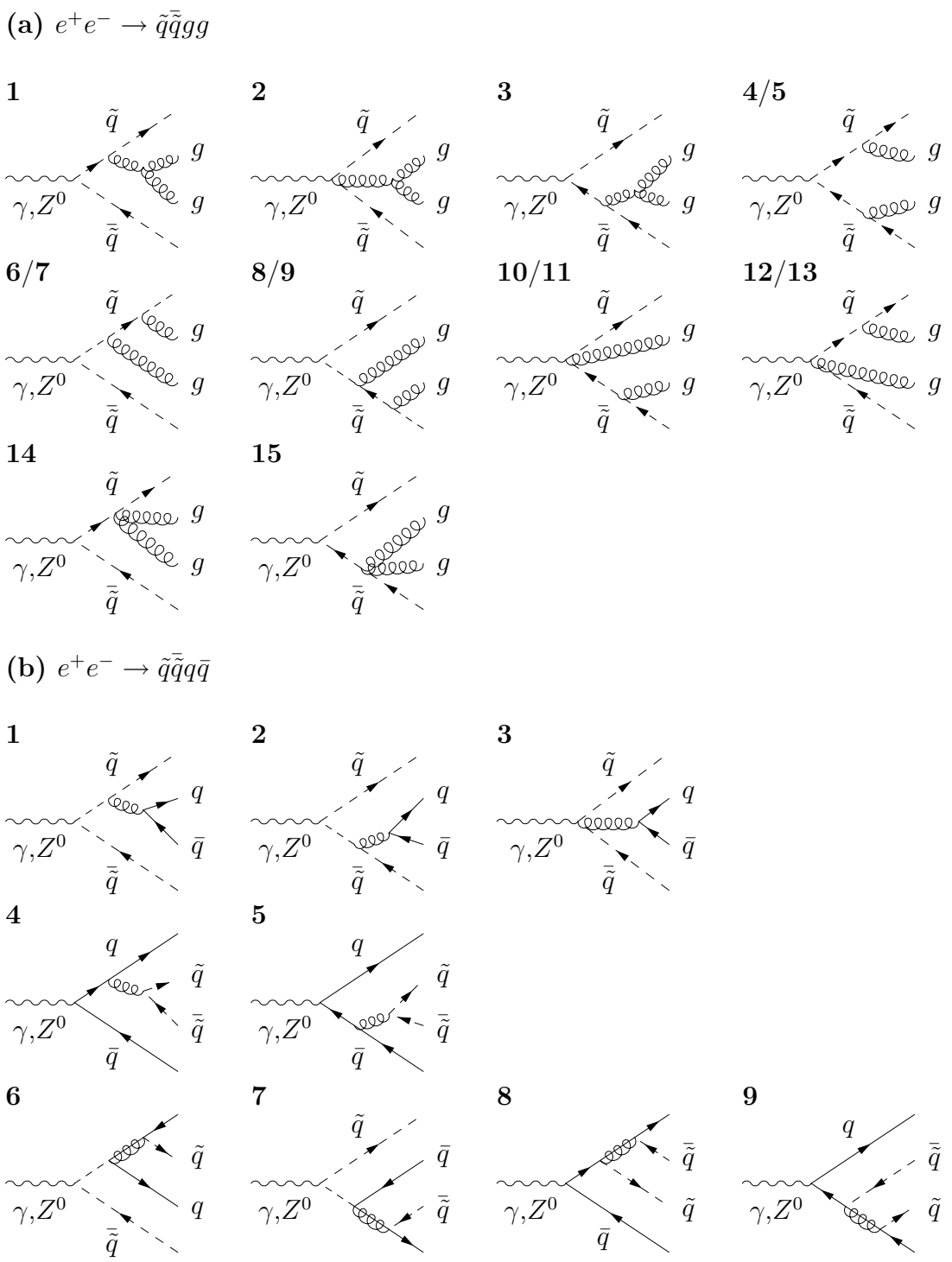


Figure 3.6: *Feynman diagrams for the real emission of an additional gluon and the splitting of a gluon into a (massless) quark-antiquark pair and the corresponding diagrams with the same final state. Diagrams where also the crossed outer gluons have to be taken into account are double counted.*

In the case where the gluino is heavier than the squark the real correction diagrams 6-9 of process (b) contain phase space regions where the gluino becomes resonant. Actually this resonant gluino production with subsequent decay of this gluino into a quark squark pair belongs to the complementary process $e^+e^- \to q\bar{\tilde{q}}\tilde{g}$ and should not be considered in the real corrections. From this point of view one should avoid resonant gluino production and thus could take into account the total width of the gluino $\Gamma(\tilde{g})$ in these gluino diagrams and subtract the resonant gluino production cross section. A disadvantage of this procedure is that the remaining part will depend on the unknown total width $\Gamma(\tilde{g})$. To avoid this dependence on an additional parameter (apart from the masses of the superpartners squark and gluino) we could also neglect this diagrams which are suppressed outside the resonant phase space regions anyway. We implemented both, an explicit width of the gluino, where we used the partial width for the decay into a quark squark pair at tree level [6],[7],[8]

$$\Gamma_0(\tilde{g} \to q + \bar{\tilde{q}}, \bar{q} + \tilde{q}) = \alpha_s \frac{n_f}{2} m_{\tilde{g}} \left(1 - \frac{m_{\tilde{q}}^2}{m_{\tilde{g}}^2}\right)^2 \tag{3.37}$$

and alternatively we neglect the diagrams containing the gluino propagator. Comparing these two approaches we find deviations at the per mil level. Thus we decide to neglect this gluino diagrams in the further investigations. With this reflections we arrive at the following squared amplitudes for the processes (a) and (b):

$$\begin{aligned} |M_{(a)}^{real}|^2 &= j_\mu^{L/R} j_\nu^{L/R*} \Gamma_{\tilde{q}}^{\mu V+A} \Gamma_{\tilde{q}}^{\nu V+A*} \\ |M_{(b)}^{real}|^2 &= j_\mu^{L/R} j_\nu^{L/R*} \Gamma_{\tilde{q}}^{\mu V+A} \Gamma_{\tilde{q}}^{\nu V+A*} + j_\mu^V j_\nu^{V*} \Gamma_q^{\mu V} \Gamma_q^{\nu V*} + j_\mu^A j_\nu^{A*} \Gamma_q^{\mu A} \Gamma_q^{\nu A*} \end{aligned} \tag{3.38}$$

As mentioned in the context of the Born calculation we require a minimal gluon energy. Thus we require a minimal gluon energy in the 3 particle phase space integration $E_g > E_g^{cut}$. This cut has also to be implemented properly in the $m+1$ final-state of the real corrections. In order to respect the constraint (3.23) we require the centre-of-mass energy reduced by the energies of the two squarks to be greater than the minimal energy of the remnant $E_X^{cut}$

$$\sqrt{s} - E_{\tilde{q}} - E_{\bar{\tilde{q}}} > E_X^{cut} \tag{3.39}$$

This definition is infrared safe. This remnant $X$ consists of a gluon pair in process (a) and of a quark pair in process (b).

Experimentally, the cut condition (3.39) requires to tag the final state squarks. The final-state squarks decay dominantly into a quark plus a superpartner which escapes the detector, leaving behind missing transversal

energy. Since we have in the final state two squarks it will be very difficult to tag the squarks and thus to implement the cut condition properly. To evade this difficulty one should apply a more general cut. For instance with help of a jet algorithm one could impose the cut condition $\sqrt{s} - E_{jet_i} - E_{jet_j} > E_X^{cut}$ for all jet combinations, which implies the infrared safe condition (3.39) and is experimentally feasible.

However this experimental aspects are beyond the scope of this thesis and will in addition depend on the technical design of the detector. Thus we simply apply the theoretically motivated condition (3.39).

The construction of the subtraction cross sections, denoted by $d\sigma_a^A$ and $d\sigma_b^A$ for both processes (a) and (b) according to the formula (3.16) is performed explicitly in terms of the dipole subtraction formalism in appendix F.

The implementation of the subtraction parts within the real corrections yields point-wise compensating singular parts and thus the numerical integration over the 4-particle phase space can be performed. The integration variables together with its boundaries of the 4-particle phase space are given in appendix G. Thus we get a finite real correction contribution in the VEGAS integration.

According to (3.16) also the integrated cross section $\int_{m+1} d\sigma^A$ has to be generated. This integrated cross section reveals the analytic infrared singularities to cancel the singularities in the virtual corrections. The deduction of the integrated cross section is given in appendix F.

The integrated subtraction cross section factorizes in the Born cross section and a remnant containing the infrared divergent part. Since we expect these divergences to cancel the virtual corrections also the virtual corrections have to factorize in the Born cross section and a remnant. This infrared divergent remnant factor is also listed in appendix F. The resulting finite sum of virtual corrections and integrated subtraction cross section can be integrated numerically over the 3-particle phase space with VEGAS.

In the subtraction procedure there is introduced an arbitrary parameter $\kappa$ redistributing non-singular terms between the subtracted and the added integrated cross section. This parameter $\kappa$ emerges on the one hand in the subtraction splitting functions (F.10) and (F.11) and on the other hand in the integrated subtraction term (F.35). The independence of the sum of virtual and real corrections on this parameter $\kappa$ was checked and serves as a consistency check of the implementation of the dipole formalism.

## 3.3 LO and NLO results

After discussing the scale dependence of the strong coupling $\alpha_s$ in the MSSM and the expected scale dependence of the LO and NLO cross sections we present numerical results of the calculation. Here we present an example of a general analysis without going into further detail. However the program code is available to perform a more detailed analysis.

### 3.3.1 *MSSM $\beta$-function*

The coupling renormalization constant as derived in section 3.2.2 reads

$$\delta g_s = -\frac{\alpha_s}{8\pi}\,\beta_0\,\left(\frac{1}{\epsilon_{UV}} - \gamma + \ln(4\pi)\right), \tag{3.40}$$

where $\beta_0 = 3N_C - n_f$ in the MSSM. This allows to calculate the Renormalization Group (RG) $\beta$-function [69], [70]

$$\beta = \mu\frac{\partial g_s}{\partial \mu} = -\frac{g_s^3}{16\pi^2}\,\beta_0, \tag{3.41}$$

determining the leading order running of $\alpha_s$

$$\alpha_s(\mu) = \frac{\alpha_s(\mu_0)}{1 + 2\frac{\alpha_s(\mu_0)}{4\pi}\beta_0 \ln\frac{\mu}{\mu_0}} \tag{3.42}$$

from one scale $\mu_0$ to another scale $\mu$. The experimental value of $\alpha_s^{QCD}$ is given in a scheme with 5 light quark flavors. In the MSSM we take into account also the heavy particles like the squarks, gluinos, and the top quark. Thus the experimental value of $\alpha_s^{QCD}$ corresponds to a MSSM scheme with all heavy particles decoupled. The translation from the light quark scheme to our scheme is

$$\alpha_s = \alpha_s^{QCD}\left[1 + \frac{\alpha_s^{QCD}}{4\pi}\left(-\frac{1}{3}\ln\frac{m_t^2}{m_Z^2} - n_f\frac{1}{6}\ln\frac{m_{\tilde{q}}^2}{m_Z^2} - N_C\frac{1}{3}\ln\frac{m_{\tilde{g}}^2}{m_Z^2}\right)\right]^2. \tag{3.43}$$

### 3.3.2 *Cross sections*

Figure 3.7 shows a comparison of the total cross section

$$\sum_{\tilde{q}_{L/R}} \sigma(e^+e^- \to \tilde{q}\bar{\tilde{q}}X)$$

at $\mathcal{O}(\alpha_s)$ and $\mathcal{O}(\alpha_s^2)$ plotted against the centre-of-mass energy $\sqrt{s}$, where, as indicated before, we require $\sqrt{s} - E_{\tilde{q}} - E_{\bar{\tilde{q}}} > E_X^{cut}$ with a minimal remnant

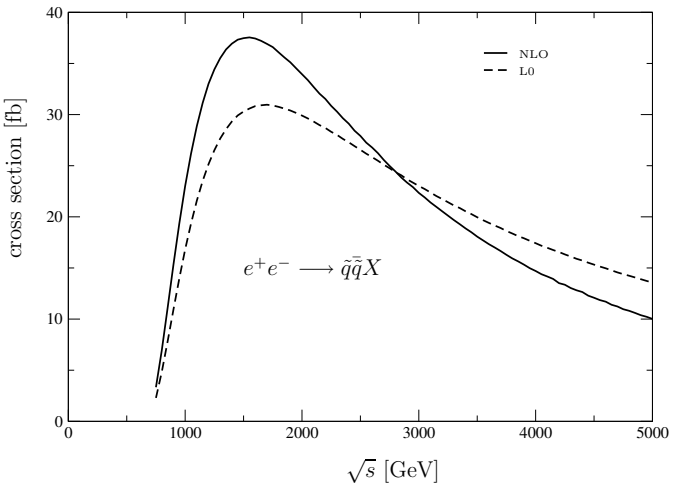


Figure 3.7: *Cross section of the LO and NLO result depending on the centre-of-mass energy $\sqrt{s}$. The masses of squark and gluino are $m_{\tilde{q}} = 300$ GeV and $m_{\tilde{g}} = 400$ GeV.*

energy of $E_X^{cut} = 50$ GeV. At $\mathcal{O}(\alpha_s)$ this is the LO contribution to the process $e^+e^- \to \tilde{q}\bar{\tilde{q}}g$. We assume a squark mass of $m_{\tilde{q}} = 300$ GeV and a gluino mass of $m_{\tilde{g}} = 400$ GeV. These mass values are chosen outside the CDF exclusion limits. We choose a scale of $\mu = 1000$ GeV. In all cross sections shown in this section we sum over 5 external flavors and both helicities of the squark. With respect to the Born cross section we find an enhancement of the cross section in the peak region of about 22 % with a slightly shifted peak down to a lower centre-of-mass energy. Above the threshold energy of two squark masses we get a very large gradient of the NLO cross section caused by the Coulomb singularity. At very high energies above 2.8 TeV we find negative corrections.

### 3.3.3 *Scale dependence of the cross section*

The cross section can be written

$$\sigma = A\ \alpha_s(\mu) + B(\mu)\ \alpha_s^2(\mu) + \mathcal{O}(\alpha_s^3), \tag{3.44}$$

where the scale dependence of the coupling $\alpha_s(\mu)$ and the NLO coefficient $B(\mu)$ are indicated. Obviously the scale dependence of the Born cross section

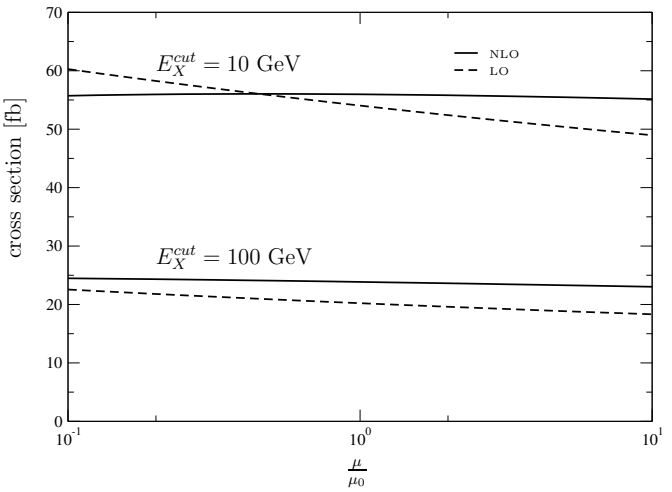


Figure 3.8: *Scale dependence of the cross section at LO and NLO for two different minimal remnant energies* $E_X^{cut}$.

is determined by the scaling of $\alpha_s(\mu)$. Summed to all orders the cross section is scale independent. The RG equation for the cross section reads $\mu\frac{d}{d\mu}\sigma = 0$ and with help of the $\beta$-function of the MSSM the solution of this equation is

$$B(\mu) = B(\mu_0) + \frac{2}{4\pi}\,\beta_0\,A\,\ln\frac{\mu}{\mu_0}. \tag{3.45}$$

This equation determines the scale dependence of the coefficient $B(\mu)$ in (3.44) and thus together with the scale dependence of the coupling $\alpha_s(\mu)$ the scale dependence of the whole cross section $\sigma(\mu)$ at NLO. The scale dependence of the NLO calculation was checked and fulfills this expected scale dependence serving as a further important check of the calculation.

In figure 3.8 the scale dependence of the cross section is drawn for masses of $m_{\tilde{q}} = 300$ GeV, $m_{\tilde{g}} = 400$ GeV, a centre-of-mass energy of $\sqrt{s} = 2000$ GeV, and a reference scale of $\mu_0 = 1000$ GeV. The figure shows the scale dependence for two different values of the minimal remnant energy $E_X^{cut}$.

The scale dependence of the Born cross section is fully determined by the running coupling and proportional to the Born coefficient $A$ in (3.44). When we change the scale $\mu$ from one tenth respectively to a factor of 10 we get deviations of the running coupling of +11.6 % respectively −9.38 %. Since the Born cross section and thus the coefficient $A$ increases strongly with decreasing $E_X^{cut}$ due to the soft divergence in the limit $E_X^{cut} \to 0$ we get

large scale dependences of the absolute value of the cross section with small $E_X^{cut}$. This scale dependence reduces significantly at NLO to deviations of about 1 % (3 %) for cut values of $E_X^{cut} = 10$ GeV (100 GeV) when we change the scale ratio $\mu/\mu_0$ over two orders of magnitude. Thus the NLO calculation yields a more reliable result with a reduced theoretical error.

### 3.3.4 *Gluon energy cut*

Apart from the masses of squark and gluino an important parameter is the minimal energy of the remnant $E_X^{cut}$. Figure 3.9 shows the cross section depending on the cut $E_X^{cut}$ with a fixed centre-of-mass energy of $\sqrt{s} = 2000$ GeV and masses of $m_{\tilde{q}} = 300$ GeV and $m_{\tilde{g}} = 400$ GeV. The LO (NLO) cross section increases from 20.22 fb (23.86 fb) to 89.61 fb (80.81 fb) when we decrease the value of $E_X^{cut}$ from 100 GeV down to 1 GeV. For small values of $E_X^{cut}$ this

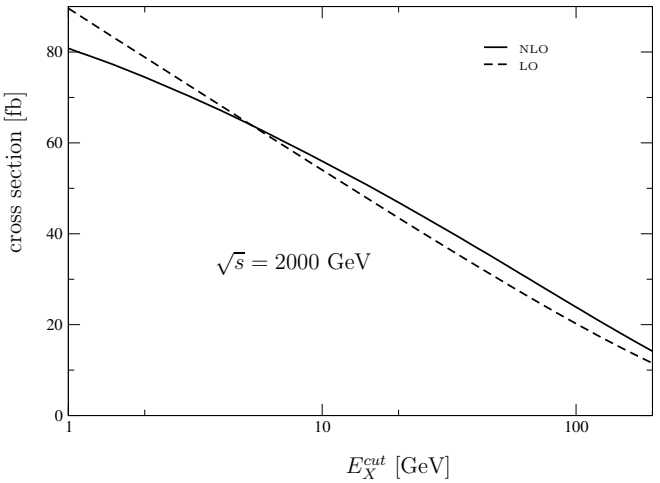


Figure 3.9: *Dependence of the cross section at LO and NLO on the chosen minimal remnant energy* $E_X^{cut}$.

is caused by the dominant contribution proportional to $\ln(E_X^{cut}/\sqrt{s})$ in the total Born cross section, obvious in the logarithmic plot. The NLO cross section shows a still higher dependence on $E_X^{cut}/\sqrt{s}$ with negative corrections for very small values of $E_X^{cut}$. The dependence on the ratio $E_X^{cut}/\sqrt{s}$ determines the behavior for small values of $E_X^{cut}$ corresponding to high values of $\sqrt{s}$. Thus negative corrections for small values $E_X^{cut}$ coincide with negative

corrections for high centre-of-mass energies $\sqrt{s}$ as shown in figure 3.7. In a comparison with experimentally measured cross sections at future colliders the applied cut $E_X^{cut}$ will depend on the experimental resolution.

# Conclusion

In supersymmetric theories the gauge and Yukawa couplings have to be equal. In this thesis we focus on the QCD sector of the MSSM. The three complementary processes

$$e^+e^- \to \begin{cases} q\bar{q}g \\ \tilde{q}\bar{\tilde{q}}g \\ q\bar{\tilde{q}}\tilde{g} \end{cases}$$

serve as a framework to investigate this sector. Supposed the superpartners of quarks and gluon have masses below the TeV scale, future colliders will detect these complementary processes.

From the theoretical point of view it is necessary to predict the corresponding cross sections under the constraint of equal gauge and Yukawa couplings, thus to be able to verify the equality of the couplings phenomenologically. Since QCD corrections are relatively large a calculation beyond the tree approximation is desirable.

After confirming the calculation of the process $e^+e^- \to \tilde{q}\bar{\tilde{q}}g$ at tree level we present a NLO calculation at $\mathcal{O}(\alpha_s^2)$ in the MSSM. This NLO calculation divides into major parts: The renormalization procedure of the QCD sector in the MSSM was discussed in detail yielding a UV finite virtual correction. Soft and collinear singularities were compensated by the real corrections in the framework of the dipole subtraction formalism. The problem of dimensional regularization in the context of supersymmetry was accounted for by introducing an additional finite counterterm.

The cross sections of the LO and NLO calculation were presented as a function of the centre-of-mass energy. For a squark mass of 300 GeV and a gluino mass of 400 GeV we find cross sections of the order of several tens of femtobarn. The absolute value depends strongly on the applied minimal gluon energy cut, which must be imposed already at tree level to avoid soft gluons. The NLO calculation gives predictions of the cross section, which are enhanced in the peak region of roughly 20 % with respect to the LO calculation. The scale dependence was investigated. We found that for realistic cut

conditions the scale dependence at NLO is reduced to 3 % in contrast to 20 % at LO when the scale is varied over two orders of magnitude. Thus the NLO calculation yields a more reliable result. Together with the complementary processes these NLO predictions allow for a phenomenological investigation of the QCD sector of the MSSM at future colliders.

# Appendix A

# Feynman rules

The Feynman rules of the QCD sector in Feynman gauge of the MSSM are given in this appendix. Also the vertices which couple the photon or the $Z^0$ boson to the QCD sector are written. Note, in particular the mixed quartic $SU(3)_C/SU(2)_L \times U(1)_Y$ $\tilde{q}\tilde{q}VV$ vertex.

To take into account the majorana character of the gluinos, there is drawn an additional fermion flow in the Feynman diagrams [71]. The Dirac algebra has to be calculated along the fermion flow. In this way of handling fermion violating Lagrangian's it is not necessary to find the correct sign of a diagram via Wick's theorem.

Additional Feynman rules:

- Over every loop has to be integrated with the measure $d^D q/(2\pi)^D$ where $q$ is the loop momentum and $D$ is the number of space-time dimensions.
- Closed Loops of anticommuting fields get an additional factor $-1$.
- A symmetry factor $1/S$ has to be inserted, where $S$ is the number of possibilities of mapping the graph onto itself by permutation of lines and vertices (gluon and gluino loops get a factor 1/2).

Remarks on the Feynman diagrams: The indices of the adjoint representation of the color gauge group $SU(N)_C$ are denoted by the letters $a$-$e$, the indices of the fundamental representation by the letters $i$-$l$. $t_a$ are the generators and $f^{abc}$ the structure constants of the color group. Lorentz indices are labeled with Greek letters.

The momenta ($p$ and $q$) are always outgoing. In cases where the Feynman rules depend on the chirality of the squarks this is labeled by L(eft) and R(ight). The vector and axial-vector couplings are $c_v = \frac{I_3 - 2Q\sin^2\theta_W}{2\cos\theta_W \sin\theta_W}$ and $c_a = \frac{I_3}{2\cos\theta_W \sin\theta_W}$, where $I_3$ is the $z$-component of the isospin and $Q$ the charge of the particle in units of the positron charge. In the quartic squark

vertex $f$ and $f'$ denote the flavor and $h$, $h'$ denote the chirality of the squarks. To get the Feynman rules for the vertices with a photon line instead of a $Z^0$ boson line replace $c_a = 0$ and $c_v = Q \sin\theta_W$.

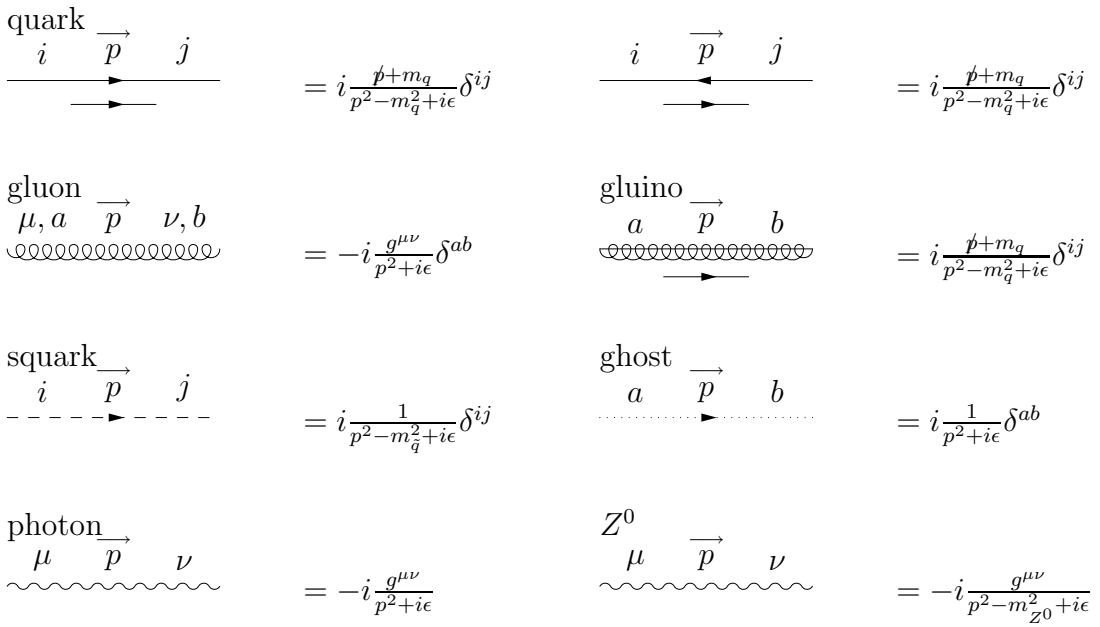


Figure A.1: *Propagators of SUSY QCD particles, photon and $Z^0$ boson*

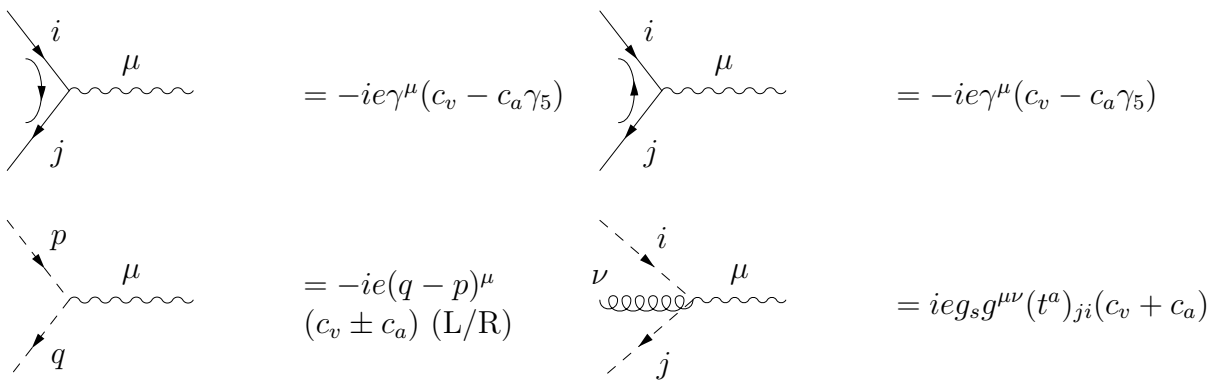


Figure A.2: *Vertices of the $Z^0$ boson coupled to the SUSY QCD sector.*

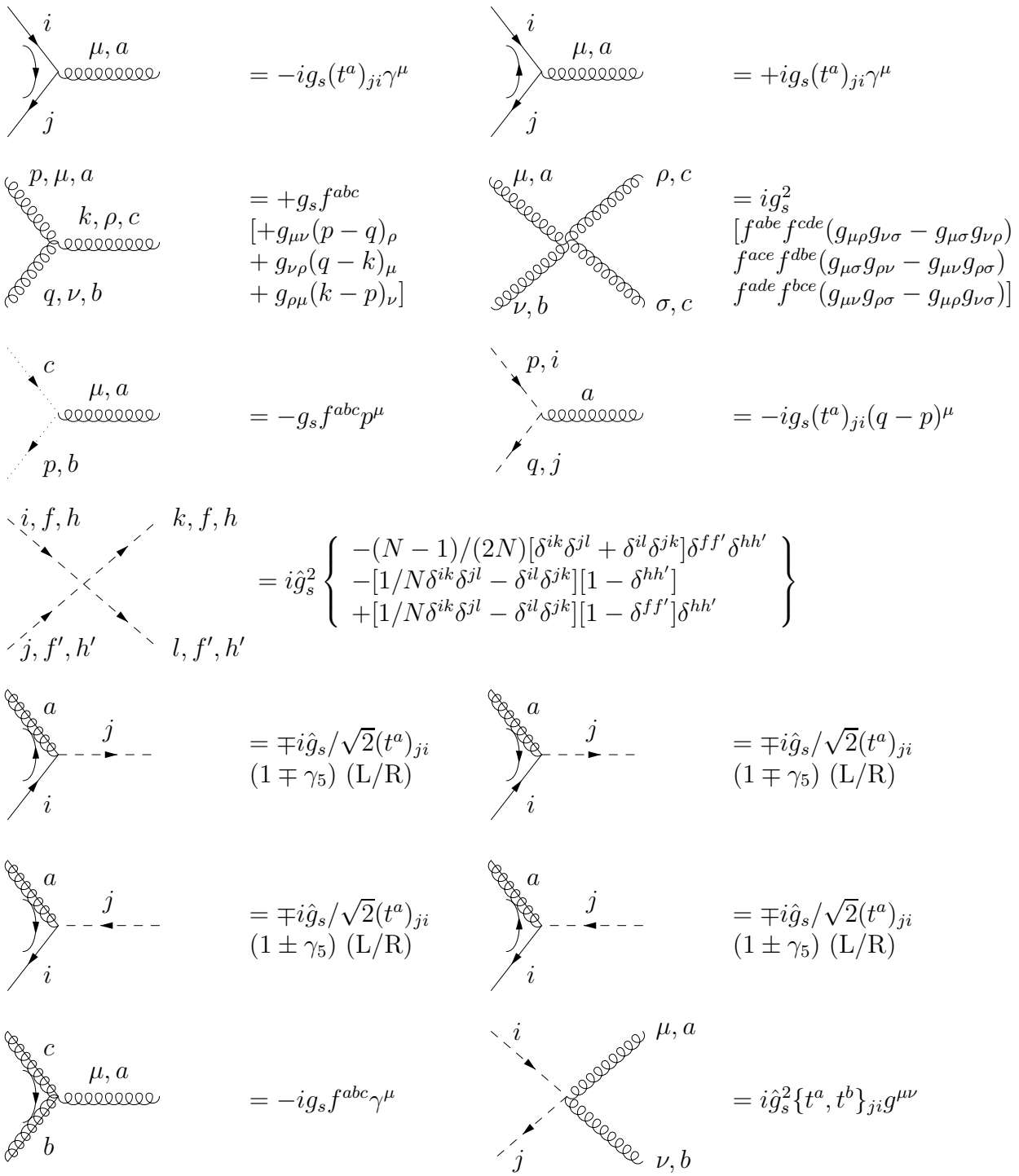


Figure A.3: *Vertices of the SUSY QCD sector.*

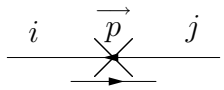


$= i\,\delta Z_q\,\not{p}\,\delta^{ij}$

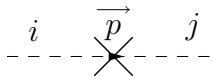


$= i\,(\delta Z_{\tilde{q}}(k^2 - m_{\tilde{q}}^2) - \delta m_{\tilde{q}})\,\delta^{ij}$

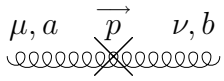


$= -\delta Z_A\,(p^2 g_{\mu\nu} - p_\mu p_\nu)\,\delta^{ab}$

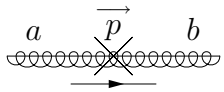


$= i\,(\delta Z_{\tilde{A}}(\not{k} - m_{\tilde{g}}) - \delta m_{\tilde{g}})\,\delta^{ab}$

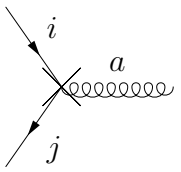


$= -ig_s(t^a)_{ji}\gamma^\mu(\delta g_s + \delta Z_q + \frac{1}{2}\delta Z_A)$

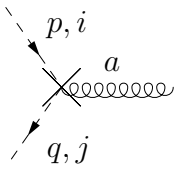


$= -ig_s(t^a)_{ji}(q-p)^\mu(\delta g_s + \delta Z_{\tilde{q}} + \frac{1}{2}\delta Z_A)$

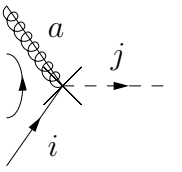


$= \mp i\hat{g}_s/\sqrt{2}(t^a)_{ji}$
$(1 \mp \gamma_5)(\delta g_s + \frac{1}{2}\delta Z_q + \frac{1}{2}\delta Z_{\tilde{q}} + \frac{1}{2}\delta Z_{\tilde{A}})$ (L/R)

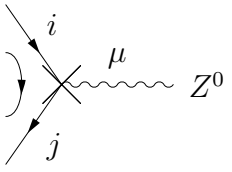


$= -ie\gamma^\mu(c_V - c_A\gamma_5)\,\delta Z_q$

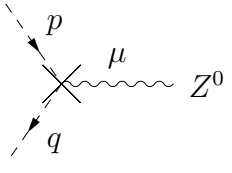


$= -ie(q-p)^\mu(c_V \pm c_A)\,\delta Z_{\tilde{q}}$ (L/R)

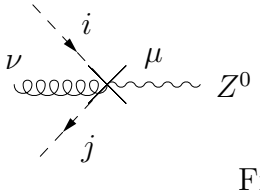


$= ieg_s g^{\mu\nu}(t^a)_{ji}(c_V + c_A)(\delta g_s + \delta Z_{\tilde{q}} + \frac{1}{2}\delta Z_A)$

Figure A.4: *counterterms of SUSY QCD*

# Appendix B

# Tensor reduction

The propagators for gauge bosons and fermions as well as vertices coming form Lagrangian terms containing derivatives generate tensors of the integration momenta in the numerator of the loop integrals. This tensor integrals can be systematically reduced to basic scalar integrals [48],[49],[50]. Here we follow closely [50].

The one-loop integrals in $D$ dimensions are classified according to the number $N$ of propagator factors in the denominator and the number $P$ of integration momenta in the numerator. For $P + D - 2N \geq 0$ these integrals are UV-divergent.

These divergencies are regularized in dimensional regularization by calculating the integrals in general dimensions $D \neq 4$. For renormalizable theories we have $P \leq N$ and thus a finite number of divergent integrals.

The general one-loop tensor integral is defined as

$$T^N_{\mu_1 \ldots \mu_P}(p_1, \ldots, p_{N-1}, m_0, \ldots, m_{N-1}) = \frac{(2\pi\mu)^{4-D}}{i\pi^2} \int d^D q \frac{q_{\mu_1} \ldots q_{\mu_P}}{D_0 D_1 \ldots D_{N-1}} \tag{B.1}$$

with the denominator factors

$$D_0 = q^2 - m_0^2 + i\epsilon, \qquad D_i = (q + p_i)^2 - m_i^2 + i\epsilon, \qquad i = 1, \ldots, N-1, \tag{B.2}$$

originating from the propagators in the Feynman diagrams. Furthermore we introduce $p_{i0} = p_i$ and $p_{ij} = p_i - p_j$. Obviously the tensor integrals are invariant under arbitrary permutations of the propagators $D_i$, $i \neq 0$ and totally symmetric in the Lorentz indices $\mu_k$. $i\epsilon$ is an infinitesimal imaginary part needed to regulate singularities of the integrand. Its specific choice ensures causality. After integration it determines the correct imaginary parts of the logarithms and dilogarithms. The parameter $\mu$ has mass dimension

and serves to keep the dimension of the integrals fixed for varying $D$. Conventionally $T^N$ is denoted by the $N$th character of the alphabet, i.e. $T^1 = A$, $T^2 = B$, ..., and the scalar integrals carry an index 0.

Lorentz covariance of the integral allows to decompose the tensor integrals into tensors constructed from the external momenta $p_i$, and the metric tensor $g_{\mu\nu}$ with totally symmetric coefficient functions $T^N_{i_1\ldots i_P}$. Formally an artificial momentum $p_0$ is introduced in order to write the terms containing $g_{\mu\nu}$ in a compact way

$$T^N_{\mu_1\ldots\mu_P}(p_1,\ldots,p_{N-1},m_0,\ldots,m_{N-1}) = \sum_{i_1,\ldots,i_P=0}^{N-1} T^N_{i_1\ldots i_P} p_{i_1\mu_1}\ldots p_{i_P\mu_P}. \quad \text{(B.3)}$$

From this formula the correct $g_{\mu\nu}$ terms are recovered by omitting all terms containing an odd number of $p_0$'s and replacing products of even numbers of $p_0$'s by the corresponding totally symmetric tensor constructed from the $g_{\mu\nu}$, e.g.

$$\begin{array}{lcl} p_{0\mu_1}p_{0\mu_2} & \to & g_{\mu_1\mu_2} \\ p_{0\mu_1}p_{0\mu_2}p_{0\mu_3}p_{0\mu_4} & \to & g_{\mu_1\mu_2}g_{\mu_3\mu_4} + g_{\mu_1\mu_3}g_{\mu_2\mu_4} + g_{\mu_1\mu_4}g_{\mu_2\mu_3} \end{array} \quad \text{(B.4)}$$

The explicit Lorentz decompositions for the lowest order integrals needed in this calculation read

$$\begin{array}{lcl} B_\mu & = & p_{1\mu}B_1, \\ B_{\mu\nu} & = & g_{\mu\nu}B_{00} + p_{1\mu}p_{1\nu}B_{11}, \\ C_\mu & = & p_{1\mu}C_1 + p_{2\mu}C_2, \\ C_{\mu\nu} & = & g_{\mu\nu}C_{00} + p_{1\mu}p_{1\nu}C_{11} + p_{2\mu}p_{2\nu}C_{11} + (p_{1\mu}p_{2\nu} + p_{2\mu}p_{1\nu})C_{12}, \\ D_\mu & = & p_{1\mu}D_1 + p_{2\mu}D_2 + p_{3\mu}D_3, \\ D_{\mu\nu} & = & g_{\mu\nu}D_{00} + \sum_{i,j=1}^3 p_{i\mu}p_{j\nu}D_{ij}. \end{array} \quad \text{(B.5)}$$

Using the Lorentz decomposition of the tensor integrals (B.5) the invariant functions $T^N_{i_1\ldots i_P}$ can be iteratively reduced to the scalar integrals $T^N_0$. The product of the integration momentum $q_\mu$ with an external momentum can be expressed in terms of the denominators

$$qk = \frac{1}{2}[D_k - D_0 - f_k], \qquad f_k = p_k^2 - m_k^2 + m_0^2. \quad \text{(B.6)}$$

Multiplying (B.1) with $p_k$ and substituting ($B$.6) yields

$$\begin{array}{lcl} R^{N,k}_{\mu_i\ldots\mu_{P-1}} & = & T^N_{\mu_1\ldots\mu_P} p_k^{\mu_P} \\ & = & \dfrac{1}{2}\dfrac{(2\pi\mu)^{4-D}}{i\pi^2}\displaystyle\int d^Dq \left[\frac{q_{\mu_1}\ldots q_{mu_{P-1}}}{D_0\ldots D_{k-1}D_{k+1}\ldots D_{N-1}}\right. \end{array}$$

$$
\begin{aligned}
& -\frac{q_{\mu_1}\dots q_{\mu_{P-1}}}{D_1\dots D_{N-1}} - f_k \frac{q_{\mu_1}\dots q_{\mu_{P-1}}}{D_1\dots D_{N-1}}\Bigg] \\
&= \frac{1}{2}\left[T^{N-1}_{\mu_1\dots\mu_{P-1}}(k) - T^{N-1}_{\mu_1\dots\mu_{P-1}}(0) - f_k T^{N}_{\mu_1\dots\mu_{P-1}}\right], \qquad \text{(B.7)}
\end{aligned}
$$

where the argument $k$ of the tensor integrals in the last line indicates that the propagator $D_k$ was canceled. Note that $T^{N-1}_{\mu_1\dots\mu_{P-1}}(0)$ has an external momentum in its first propagator. Therefore a shift of the integration momentum has to be performed in this integral in order to bring it to the form (B.1). All tensor integrals on the right-hand side of (B.7) have one Lorentz index less than the original tensor integral. In two of them also one propagator is eliminated. For $P \geq 2$ we obtain one more relation by contracting (B.1) with $g^{\mu\nu}$ and using $g^{\mu\nu}q_\mu q_\nu = q^2 = D_0 + m_0^2$. This yields

$$
\begin{aligned}
R^{N,00}_{\mu_i\dots\mu_{P-2}} &= T^{N}_{\mu_1\dots\mu_P} g^{\mu_{P-1}\mu_P} \\
&= \frac{1}{2}\frac{(2\pi\mu)^{4-D}}{i\pi^2}\int d^Dq \left[\frac{q_{\mu_1}\dots q_{mu_{P-2}}}{D_1\dots D_N} + m_0^2\frac{q_{\mu_1}\dots q_{\mu_{P-}}}{D_0\dots D_N}\right] \\
&= \left[T^{N-1}_{\mu_1\dots\mu_{P-2}}(0) + m_0^2\, T^{N}_{\mu_1\dots\mu_{P-2}}\right]. \qquad \text{(B.8)}
\end{aligned}
$$

Inserting the Lorentz decomposition (B.5) for the tensor integrals $T$ into (B.7) and (B.8) we obtain a set of linear equations for the corresponding coefficient functions. This set decomposes naturally into disjoint sets of $N-1$ equations for each tensor integral. If the inverse of the coefficient matrix

$$
X_{N-1} = \begin{pmatrix} p_1^2 & p_1p_2 & \dots & p_1p_{N-1} \\ p_2p_1 & p_2^2 & \dots & p_2p_{N-1} \\ \vdots & \vdots & \ddots & \vdots \\ p_{N-1}p_1 & p_{N-1}p_2 & \dots & p_{N-1}^2 \end{pmatrix} \qquad \text{(B.9)}
$$

exists, these can be solved for the invariant functions $T^N_{i_1\dots i_P}$ yielding them in terms of invariant functions of tensor integrals with fewer indices. In this way all tensor integrals are expressed iteratively in terms of scalar integrals $T_0^L$ with $L \leq N$. If the matrix $X_{N-1}$ becomes singular, the reduction algorithm breaks down. In our case we have not to deal with a singular matrix $X_{N-1}$.

The result for the reduction of arbitrary $N$-point integrals depending on $M \leq N-1$ linear independent Lorentz vectors in $D$ dimensions for nonsingular $X_M$ is given here. Inserting the Lorentz decomposition of $T_N$ and $R^{Nk}$ as well as $R^{N,00}$

$$
\begin{aligned}
R^{N,k}_{\mu_1\dots\mu_{P-1}} &= T^N_{\mu_1\dots\mu_P}\, p_k^{\mu_P} &&= \textstyle\sum_{i_1\dots i_{P-1}=0}^{M} R^{N,k}_{i_1\dots i_{P-1}} p_{i_1\mu_1}\cdots p_{i_{P-1}\mu_{P-1}}, \\
R^{N,00}_{\mu_1\dots\mu_{P-2}} &= T^N_{\mu_1\dots\mu_P}\, g^{\mu_{P-1}\mu_P} &&= \textstyle\sum_{i_1\dots i_{P-2}=0}^{M} R^{N,00}_{i_1\dots i_{P-2}} p_{i_1\mu_1}\cdots p_{i_{P-2}\mu_{P-2}}, \qquad \text{(B.10)}
\end{aligned}
$$

into the first lines of (B.7) and (B.8) these equations can be solved for the $T^N_{i_1\dots i_P}$:

$$\begin{aligned} T^N_{00i_1\cdots i_{P-2}} &= \tfrac{1}{D+P-2-M}\Big[R^{N,00}_{i_1\dots i_{P-2}} - \textstyle\sum_{k=1}^{M} R^{N,k}_{ki_1\dots i_{P-2}}\Big], \\ T^N_{ki_1\dots i_{P-1}} &= \Big(X^{-1}_M\Big)_{kk'}\Big[R^{N,k'}_{i_1\dots i_{P-1}} - \textstyle\sum_{r=1}^{P-1}\delta^{k'}_{i_r} T^N_{00i_1\dots i_{r-1}i_{r+1}\dots i_{P-1}}\Big]. \end{aligned} \tag{B.11}$$

# Appendix C

# Scalar integrals

In this appendix the infrared and ultraviolet divergent scalar integrals are given. For one loop calculation in the interference term of Born and loop matrix elements only the real part of the scalar integrals is needed and is given here. The dimensionally regularized divergent part of this integrals results in a pole which is defined by $\epsilon = \frac{4-D}{2}$ where $D$ is the number of space-time dimensions. To distinguish between infrared divergent and ultraviolet divergent poles an index denotes the origin of this divergences ($\epsilon_{UR}$ and $\epsilon_{IR}$). The dilogarithm $Li_2$ emerging in some of these integrals has a cut along the positive real axis starting at point $x = 1$ and is numerically evaluated with help of the series expansion in [72]. In the definitions of the different scalar integrals the $i\epsilon$ terms coming from the propagators are suppressed. The factor $C$ emerging in singular scalar integrals is given by

$$C = (4\pi)^{\epsilon}\,\Gamma(1+\epsilon). \tag{C.1}$$

The scale $\mu$ in the scalar integrals is introduced by the dimensional regularization scheme. The convergent scalar integrals are taken from [61] and are available in form of a C-library.

**Scalar one-point integral**

$$A_0(m) \;=\; \frac{(2\pi\mu)^{4-D}}{i\pi^2}\int d^Dq \frac{1}{q^2-m^2} = Cm^2\left[\frac{1}{\epsilon_{UV}} + 1 - \ln\frac{m^2}{\mu^2}\right] \tag{C.2}$$

**Scalar two-point integral**

$$B_0(p^2; m_0, m_1) \;=\; \frac{(2\pi\mu)^{4-D}}{i\pi^2}\int d^Dq \frac{1}{[q^2-m_0^2][(q+p)^2-m_1^2]} \tag{C.3}$$

$$B_0(0;0,0) = \frac{1}{\epsilon_{UV}} - \frac{1}{\epsilon_{IR}} \tag{C.4}$$

$$B_0(0;m,m) = C\left[\frac{1}{\epsilon_{UV}} - \ln\frac{m^2}{\mu^2}\right] \tag{C.5}$$

$$B_0(0;m_0,m_1) = C\left[\frac{1}{\epsilon_{UV}} + 1 - \frac{m_0^2}{m_0^2-m_1^2}\ln\frac{m_0^2}{\mu^2} - \frac{m_1^2}{m_1^2-m_0^2}\ln\frac{m_1^2}{\mu^2}\right] \tag{C.6}$$

$$B_0(q^2;0,0) = C\left[\frac{1}{\epsilon_{UV}} + 2 - \ln\frac{q^2}{\mu^2}\right] \tag{C.7}$$

$$B_0(m^2;m,0) = C\left[\frac{1}{\epsilon_{UV}} + 2 - \ln\frac{m^2}{\mu^2}\right] \tag{C.8}$$

$$B_0(q^2;m,0) = C\left[\frac{1}{\epsilon_{UV}} + 2 - \frac{q^2-m^2}{q^2}\ln\frac{m^2-q^2}{m^2} - \ln\frac{m^2}{\mu^2}\right] \tag{C.9}$$

$$\begin{aligned} B_0(q^2;m_0,m_1) = C\Big[&\frac{1}{\epsilon_{UV}} + 2 + x_2\ln(1-\frac{1}{x_2}) \\ &+x_1\ln(1-\frac{1}{x_1}) - \ln\frac{m_0^2}{\mu^2}\Big] \end{aligned} \tag{C.10}$$

$$x_{1/2} = \frac{q^2+m_1^2-m_0^2}{2(q^2+i\epsilon)} \pm \sqrt{\left(\frac{q^2+m_1^2-m_0^2}{2(q^2+i\epsilon)}\right)^2 - \frac{m_1^2}{q^2+i\epsilon}}$$

**Derivatives of scalar 2-point integrals**

$$B_0'(p^2;m_0,m_1) = \frac{\partial}{\partial q^2}\, B_0(q^2;m_0,m_1)\Big|_{q^2=p^2} \tag{C.11}$$

$$B_0'(0;0,0) = 0 \tag{C.12}$$

$$B_0'(0;m,m) = \frac{1}{6m^2} \tag{C.13}$$

$$B_0'(0;m_0,m_1) = \frac{1}{(m_0^2-m_1^2)^2}\left[\frac{m_0^2+m_1^2}{2} - \frac{m_0^2m_1^2}{m_0^2-m_1^2}\ln\frac{m_0^2}{m_1^2}\right] \tag{C.14}$$

$$B_0'(m^2;m,0) = C\,\frac{1}{m^2}\left[\frac{1}{2\epsilon_{IR}} - 1 + \frac{1}{2}\ln\frac{m^2}{\mu^2}\right] \tag{C.15}$$

$$B_0'(m^2;m_0,0) = \frac{1}{m^2}\left[-1 - \frac{m_0^2}{m^2}\ln\frac{m_0^2-m^2}{m_0^2}\right] \tag{C.16}$$

$$B_0'(q^2;m_0,m_1) = \frac{-1}{q^2} + \frac{(x_2-x_2^2)\ln(1-\frac{1}{x_2}) - (x_1-x_1^2)\ln(1-\frac{1}{x_1})}{q^2(x_2-x_1)} \tag{C.17}$$

$$x_{1/2} = \frac{q^2+m_1^2-m_0^2}{2(q^2+i\epsilon)} \pm \sqrt{\left(\frac{q^2+m_1^2-m_0^2}{2(q^2+i\epsilon)}\right)^2 - \frac{m_1^2}{q^2+i\epsilon}}$$

**Scalar 3-point integrals**

$$C_0(p_1^2,(p_2-p_1)^2,p_2^2;m_0,m_1,m_2) \tag{C.18}$$
$$= \frac{(2\pi\mu)^{4-D}}{i\pi^2}\int d^Dq \frac{1}{[q^2-m_0^2][(q+p_1)^2-m_1^2][(q+p_2)^2-m_2^2]}$$

$$C_0(0,m_1^2,v;m_2,0,0) \tag{C.19}$$
$$= C\,\frac{1}{v-m_1^2}\left[-\frac{1}{\epsilon_{IR}}\ln\frac{v-m_2^2}{m_1^2-m_2^2}+Li_2\frac{v}{m_2^2}-Li_2\frac{m_1^2}{m_2^2}+\ln^2(1-\frac{v}{m_2^2})\right.$$
$$\left.-\ln^2(1-\frac{m_1^2}{m_2^2})+\ln\frac{v-m_2^2}{m_1^2-m_2^2}\ln\frac{m_2^2}{m_1^2}\right]$$

$$C_0(v,s,0;0,0,0) \tag{C.20}$$
$$= C\,\frac{1}{v-s}\,\ln\frac{s}{v}\left[\frac{1}{\epsilon_{IR}}\ln\frac{s}{v}-\frac{1}{2}\ln\frac{v}{\mu^2}-\frac{1}{2}\ln\frac{s}{\mu^2}\right]$$

$$C_0(m^2,v,m^2;0,m,m) \tag{C.21}$$
$$= C\,\frac{1}{v\beta}\left[\frac{1}{\epsilon_{IR}}\ln x+\ln\frac{\mu^2}{m^2}\ln x+\frac{1}{2}\ln^2 x-2\ln x\ln(1-x)-2Li_2x-\frac{2}{3}\pi^2\right]$$
$$\beta = \sqrt{1-4\frac{m^2}{v}} \qquad x=\frac{1-\beta}{1+\beta}$$

$$C_0(v,m^2,0;m,0,0) \tag{C.22}$$
$$= C\,\frac{1}{v-m^2}\left[\frac{1}{\epsilon_{IR}^2}\frac{1}{2}+\frac{1}{\epsilon_{IR}}\left(-\ln\frac{m^2-v}{\mu^2}+\frac{1}{2}\ln\frac{m^2}{\mu^2}\right)\right.$$
$$\left.+\frac{1}{2}\ln^2\frac{m^2-v}{\mu^2}-\frac{1}{4}\ln^2\frac{m^2}{\mu^2}-Li_2\frac{v}{v-m^2}\right]$$

**Scalar 4-point integrals**

$$D_0\,(p_1^2,(p_2-p_1)^2,(p_3-p_2)^2,p_3^2,p_2^2,(p_3-p_1)^2;m_0,m_1,m_2,m_3)$$
$$= \frac{(2\pi\mu)^{4-D}}{i\pi^2}\int d^Dq \frac{1}{[q^2-m_0^2][(q+p_1)^2-m_1^2][(q+p_2)^2-m_2^2][(q+p_3)^2-m_3^2]}$$

and the definition of the infrared convergent 6-dimensional scalar integrals (see section 3.2.1)

$$D_0^6\,(p_1^2,(p_2-p_1)^2,(p_3-p_2)^2,p_3^2,p_2^2,(p_3-p_1)^2;m_0,m_1,m_2,m_3)$$
$$= \frac{1}{i\pi^2}\int d^6q \frac{1}{[q^2-m_0^2][(q+p_1)^2-m_1^2][(q+p_2)^2-m_2^2][(q+p_3)^2-m_3^2]}$$

$$
\begin{aligned}
& D_0(0,q_1^2,m_1^2,q_2^2,m_1^2,s;0,0,m_2,0) \qquad \text{(C.23)}\\
&= \pi\Bigg\{+\frac{q_1-m_1^2+m_2^2}{m_1^2(q_2-m_1^2-s+q_1)}\\
&\quad\left[\frac{c_1-d_0}{(c_1-c_2)(c_1-n_0)}\right.\\
&\quad\left(\frac{\pi^2}{6}-Li_2\frac{c_1-1}{c_1}+Li_2\frac{c_1}{c_1-x_{ab}}-Li_2\frac{c_1-1}{c_1-x_{ab}}-Li_2\frac{c_1}{c_1-d_0}+Li_2\frac{c_1-1}{c_1-d_0}\right)\\
&\quad\frac{c_2-d_0}{(c_2-c_1)(c_2-n_0)}\\
&\quad\left(\frac{\pi^2}{6}-Li_2\frac{c_2-1}{c_2}+Li_2\frac{c_2}{c_2-x_{ab}}-Li_2\frac{c_2-1}{c_2-x_{ab}}-Li_2\frac{c_2}{c_2-d_0}+Li_2\frac{c_2-1}{c_2-d_0}\right)\\
&\quad\frac{n_0-d_0}{(n_0-c_1)(n_0-c_2)}\\
&\quad\left(\frac{\pi^2}{6}-Li_2\frac{n_0-1}{n_0}+Li_2\frac{n_0}{n_0-x_{ab}}-Li_2\frac{n_0-1}{n_0-x_{ab}}-Li_2\frac{n_0}{n_0-d_0}+Li_2\frac{n_0-1}{n_0-d_0}\right.\\
&\quad\left.\left.+\ln\frac{n_0-1}{n_0}\left(\ln\frac{m_1^2}{q_1-m_1^2+m_2^2}+\ln\frac{n_0}{n_0-d_0}+\ln(n_0-x_{ab})\right)\right)\right]\\
&\quad-\frac{s-q_2+m_2^2}{(m_1^2)(q_2-m_1^2-s+q_1)}\\
&\quad\left[\frac{a_1-b_0}{(a_1-a_2)(a_1-n_0)}\right.\\
&\quad\left(\frac{\pi^2}{6}-Li_2\frac{a_1-1}{a_1}+Li_2\frac{a_1}{a_1-x_{ab}}-Li_2\frac{a_1-1}{a_1-x_{ab}}-Li_2\frac{a_1}{a_1-b_0}+Li_2\frac{a_1-1}{a_1-b_0}\right)\\
&\quad\frac{a_2-b_0}{(a_2-a_1)(a_2-n_0)}\\
&\quad\left(\frac{\pi^2}{6}-Li_2\frac{a_2-1}{a_2}+Li_2\frac{a_2}{a_2-x_{ab}}-Li_2\frac{a_2-1}{a_2-x_{ab}}-Li_2\frac{a_2}{a_2-b_0}+Li_2\frac{a_2-1}{a_2-b_0}\right)\\
&\quad\frac{n_0-b_0}{(n_0-a_1)(n_0-a_2)}\\
&\quad\left(\frac{\pi^2}{6}-Li_2\frac{n_0-1}{n_0}+Li_2\frac{n_0}{n_0-x_{ab}}-Li_2\frac{n_0-1}{n_0-x_{ab}}-Li_2\frac{n_0}{n_0-b_0}+Li_2\frac{n_0-1}{n_0-b_0}\right.\\
&\quad\left.\left.+\ln\frac{n_0-1}{n_0}\left(\ln\frac{m_1^2}{s+m_2^2-q_2}+\ln\frac{n_0}{n_0-b_0}+\ln(n_0-x_{ab})\right)\right)\right]\Bigg\}\\
a_{1/2} &= \frac{m_1^2-q_2+s}{2m_1^2}\pm\sqrt{\frac{(m_1^2-q_2+s)^2}{4m_1^4}-\frac{s}{m_1^2}}
\end{aligned}
$$

$$
\begin{aligned}
c_{1/2} &= \frac{q_1}{2m_1^2} \pm \sqrt{\frac{q_1^2}{4m_1^4} - \frac{q_1}{m_1^2}} \\
n_0 &= \frac{q_1 - s}{q_2 - m_1^2 - s + q_1} \\
b_0 &= \frac{s}{s + m_2^2 - q_2} + i\epsilon \\
d_0 &= \frac{q_1}{q_1 - m_1^2 + m_2^2} + i\epsilon \\
x_{ab} &= \frac{m_1^2 - m_2^2}{m_1^2} + i\epsilon
\end{aligned}
$$

The following two box integrals can be found in the literature [64].

$$
\begin{aligned}
&D_0^6(m^2, q_3^2, m^2, q_2^2, 0, s; 0, m, 0, m) \qquad \text{(C.24)} \\
&= \frac{\pi}{q^2 x_3} \Bigg\{ \frac{(1-x_2)\alpha}{(\alpha - x_+^s)(\alpha - x_-^s)} \left[ -\frac{\pi^2}{6} + Li_2\left(\frac{\alpha - 1}{\alpha}\right) \right] \\
&\quad + \frac{(1-x_2)x_+^s}{(\alpha - x_+^s)(x_+^s - x_-^s)} \left[ \frac{\pi^2}{6} - Li_2\left(\frac{x_+^s - 1}{x_+^s}\right) + Li_2\left(\frac{x_+^s - 1}{x_+^s - \rho}\right) \right. \\
&\quad + Li_2\left(\frac{x_+^s - \rho}{x_+^s}\right) - Li_2\left(\frac{1 - \rho - x_+^s}{1 - x_+^s}\right) - Li_2\left(\frac{-x_+^s}{1 - x_+^s - \rho}\right) \\
&\quad \left. + \frac{1}{2}\ln^2\left(\frac{x_+^s}{x_+^s - \rho}\right) - \frac{1}{2}\ln^2\left(\frac{1 - x_+^s}{1 - \rho - x_+^s}\right) \right] \\
&\quad + \frac{(1-x_2)x_-^s}{(\alpha - x_-^s)(x_-^s - x_+^s)} \left[ \frac{\pi^2}{6} - Li_2\left(\frac{x_-^s - 1}{x_-^s}\right) + Li_2\left(\frac{x_-^s - 1}{x_-^s - \rho}\right) \right. \\
&\quad + Li_2\left(\frac{x_-^s - \rho}{x_-^s}\right) - Li_2\left(\frac{1 - \rho - x_-^s}{1 - x_-^s}\right) - Li_2\left(\frac{-x_-^s}{1 - x_-^s - \rho}\right) \\
&\quad \left. + \frac{1}{2}\ln^2\left(\frac{x_-^s}{x_-^s - \rho}\right) - \frac{1}{2}\ln^2\left(\frac{1 - x_-^s}{1 - \rho - x_-^s}\right) \right] \Bigg\} \\
&+ \quad (x_1 \leftrightarrow x_2)
\end{aligned}
$$

$$
\begin{aligned}
&D_0^6(m^2, q_1^2, 0, q_2^2, m^2, s; 0, m, m, m) \qquad \text{(C.25)} \\
&= \frac{\pi}{2[(1-x_3)(1-x_1)(1-x_2) - z x_3^2]} \\
&\quad \Big\{ (1-x_2)(1-x_3)(1-x_3-4z) \\
&\quad \times \Big[ -s(1-x_2)\, D_0(m^2, q_1^2, 0, q_2^2, m^2, s; 0, m, m, m) + C_0(m^2, q_1^2, m^2; 0, m, m) \Big] \\
&\quad + [(1-x_2)(1-x_3) - 2z x_3]
\end{aligned}
$$

$$\times \Big[(1-x_2)\, C_0(m^2,0,q_2^2;0,m,m) - x_3\, C_0(0,s,q_1^2;m,m,m)\Big]$$
$$+(1-x_2)\,[-x_2(1-x_3)+2z(x_1+x_2)]\; C_0(q_2^2,s,m^2;0,m,m)\Big\},$$

where the divergent $C_0(m^2,q_1^2,m^2;0,m,m)$ is given by (C.21), all others are convergent and

$$\begin{aligned}
&D_0(m^2,q_1^2,0,q_2^2,m^2,s;0,m,m,m) \qquad (C.26)\\
&= C\,\frac{1}{q^4}\,\frac{1}{1-x_2}\,\frac{1}{1-x_3}\,\frac{1}{1-2\eta}\\
&\quad \Bigg\{\left[\frac{1}{\epsilon_{IR}} - \ln\left(\frac{zs(\zeta-1)^2}{\mu^2}\right)\right]\ln\left(\frac{\eta}{1-\eta}\right) - \pi^2\\
&\quad -2\,Li_2\left(1-\frac{\eta}{1-\eta}\frac{\rho}{1-\rho}\right) - 2\,Li_2\left(1-\frac{\eta}{1-\eta}\frac{1-\rho}{\rho}\right)\\
&\quad +Li_2\left(1-\frac{\eta^2}{(1-\eta)^2}\right) - \ln^2\left(\frac{\rho}{1-\rho}\right)\Bigg\}.\\
x_1 &= 1-(q_3^2-m^2)/s\\
x_2 &= 1-(q_2^2-m^2)/s\\
x_3 &= 1-q_1^2/s\\
z &= \frac{m^2}{s},\\
\alpha &= \frac{1-x_1}{x_3},\\
\zeta &= \frac{1-x_2+z}{z},\\
\rho &= \frac{1}{2}(1-\sqrt{1-4z}),\\
x_\pm^s &= \frac{1}{2}(x_2 \pm \sqrt{x_2^2-4z}),\\
\eta &= \frac{1}{2}\left(1-\sqrt{1-\frac{4z}{1-x_3}}\right).
\end{aligned}$$

# Appendix D

# Relation of $D_{00}$ and $D_0^6$

Usually, all tensor integrals $T^N_{\mu_1\dots\mu_P}$, defined in (B.1), are reduced to scalar integrals. In particular the tensor integral $D_{\mu\nu}$ is decomposed into the Lorentz coefficients $D_{00}$ and $D_{ij}$ (B.5) which are subsequently reduced to scalar integrals $D_0$, $C_0$, $B_0$, and $A_0$. Thus the tensor reduction yields an equation which expresses $D_{00}$ in form of scalar integrals. This equation can be rearranged to express $D_0$ in form of $D_{00}$ and additional scalar integrals of lower rank.

In this appendix the relation of the scalar four-point integral $D_{00}$ and $D_0^6$ in 6 dimensions

$$D_{00} = -\frac{1}{2\pi}\, D_0^6, \tag{D.1}$$

is derived. With help of this equation we can write every $D_0$ in terms of $D_0^6$ and further scalar integrals of lower rank. Due to the 6-dimensional momentum integration the $D_0^6$ scalar integral is IR and UV finite. Furthermore it is in some special cases much easier to perform the analytical computation of $D_0^6$ in $D = 6$ rather than the corresponding $D_0$ in $D = 4 - 2\epsilon$ dimensions.

To derive (D.1) we start with the definition of $D_0$:

$$\begin{aligned} D_0 \;=\; & \frac{C}{i\pi^2}\int d^Dq \Big\{ \frac{1}{[q^2 - m_0^2 + i\epsilon][(q+p_1)^2 - m_1^2 + i\epsilon]} \\ & \frac{1}{[(q+p_2)^2 - m_2^2 + i\epsilon][(q+p_3)^2 - m_3^2 + i\epsilon]} \Big\}, \end{aligned} \tag{D.2}$$

where we defined $C = (2\pi\mu)^{4-D}$. Via the Feynman parametrization

$$\frac{1}{a\,b\,c\,d} = \int_0^1 dx_1 \int_0^{1-x_1} dx_2 \int_0^{1-x_1-x_2} dx_3 \frac{3!}{[x_1 a + x_2 b + x_3 c + (1 - x_1 - x_2 - x_3)d]^4}, \tag{D.3}$$

we get with the abbreviation $\int_F dx_i = \int_0^1 dx_1 \int_0^{1-x_1} dx_2 \int_0^{1-x_1-x_2} dx_3$

$$D_0 = \frac{C}{i\pi^2} 3! \int d^D q \int_F dx_i \frac{1}{\left[(q+p)^2 - p^2 + r\right]^4}, \tag{D.4}$$

where

$p = p_1\, x_1 + p_2\, x_2 + p_3\, x_3$
$r = -m_0^2\,(1 - x_1 - x_2 - x_3) + (p_1^2 - m_1^2)\, x_1 + (p_2^2 - m_2^2)\, x_3 + (p_3^2 - m_3^2)\, x_3 + i\epsilon.$

Applying a Wick rotation with $q_{E,0} = -iq_0$ and $q_{E,i} = q_i$ we arrive at

$$D_0 = i\,\frac{C}{i\pi^2} 3! \int d^D q_E \int_F dx_i \frac{1}{\left[-q_E^2 - p^2 + r\right]^4}. \tag{D.5}$$

In analogy to (D.4) we can write $D_{\mu\nu}$ as

$$D_{\mu\nu} = \frac{C}{i\pi^2} 3! \int d^D q \int_F dx_i \frac{q_\mu q_\nu}{\left[(q+p)^2 - p^2 + r\right]^4} \tag{D.6}$$

and with the substitution $q \to q + p$

$$D_{\mu\nu} = \frac{C}{i\pi^2} 3! \int d^D q \int_F dx_i \frac{q_\mu q_\nu - p_\mu q_\nu - p_\nu q_\mu + p_\mu p_\nu}{\left[(q+p)^2 - p^2 + r\right]^4}. \tag{D.7}$$

The Lorentz decomposition of $D_{\mu\nu}$ reads (B.5)

$$D_{\mu\nu} = g_{\mu\nu} D_{00} + \sum_{i,j=1}^{3} p_{i\mu} p_{j\nu} D_{ij}. \tag{D.8}$$

Comparison of the coefficients in (D.7) and (D.8) and contraction with $g_{\mu\nu}$ yield

$$D \cdot D_{00} = \frac{C}{i\pi^2} 3! \int d^D q \int_F dx_i \frac{q^2}{\left[q^2 - p^2 + r\right]^4} \tag{D.9}$$

and applying a Wick rotation gives

$$D \cdot D_{00} = -i\,\frac{C}{i\pi^2} 3! \int d^D q_E \int_F dx_i \frac{q_E^2}{\left[-q_E^2 - p^2 + r\right]^4}. \tag{D.10}$$

Since the integrand depends only on $q_E^2$ we get with $\int d^D q_E = d\Omega_D dq_E q_E^{D-1} = 1/2 d\Omega_D dq_E^2 (q_E^2)^{D/2-1}$

$$\begin{aligned} D \cdot D_{00} &= -i\,\frac{\int d\Omega_D}{\int d\Omega_{D+2}} \frac{C}{i\pi^2} 3! \int d\Omega_{D+2} \int dq_E \int_F dx_i \frac{k_E^{D+1}}{\left[-q_E^2 - p^2 + r\right]^4} \\ &= -i\,\frac{\int d\Omega_D}{\int d\Omega_{D+2}} \frac{C}{i\pi^2} 3! \int d^{D+2} q_E \int_F dx_i \frac{1}{\left[-q_E^2 - p^2 + r\right]^4}, \end{aligned} \tag{D.11}$$

where $d\Omega_D$ is the differential solid angle in $D$ dimensions. With $\int d\Omega_D = \frac{2\,\pi^{D/2}}{\Gamma(D/2)}$ we get

$$D_{00} = -i\,\frac{1}{2\pi}\frac{C}{i\pi^2}3!\int d^{D+2}q_E \int_F dx_i \frac{1}{[-q_E^2 - p^2 + r]^4}. \tag{D.12}$$

Finally the comparison of (D.12) with (D.5) results in

$$D_{00} = -\frac{1}{2\pi}\,D_0^6. \tag{D.13}$$

# Appendix E

# Renormalization constants

The renormalization constants are defined in section 3.2.2. The strong coupling constant is renormalized in the $\overline{MS}$-scheme and all other constants in the on-shell scheme. We assume massless quarks. The definitions of the scalar integrals are listed in appendix C.

$$\begin{aligned}
\delta Z_q &= \frac{\alpha_s}{8\pi} C_f \frac{1}{(m_{\tilde{g}}^2 - m_{\tilde{q}}^2)} \Big\{ -m_{\tilde{q}}^2 - m_{\tilde{g}}^2 + 2A_0(m_{\tilde{q}}) - 2m_{\tilde{g}}^2\, B_0(0, m_{\tilde{g}}, m_{\tilde{q}}) \\
&\quad + 2(m_{\tilde{q}}^2 - m_{\tilde{g}}^2) B_0(0,0,0) \Big\} && \text{(E.1)} \\
\delta Z_{\tilde{q}} &= \frac{\alpha_s}{2\pi} C_f \Big\{ (m_{\tilde{g}}^2 - m_{\tilde{q}}^2) B_0'(m_{\tilde{q}}^2, m_{\tilde{g}}, 0) - B_0(m_{\tilde{q}}^2, m_{\tilde{g}}, 0) \Big\} && \text{(E.2)} \\
\delta m_{\tilde{q}} &= \frac{\alpha_s}{2\pi} C_f \Big\{ A_0(m_{\tilde{q}}) - A_0(m_{\tilde{g}}) - 2m_{\tilde{q}}^2 B_0(m_{\tilde{q}}^2, m_{\tilde{q}}, 0) + (m_{\tilde{q}}^2 - m_{\tilde{g}}^2) B_0(m_{\tilde{q}}^2, m_{\tilde{g}}, 0) \Big\} && \text{(E.3)} \\
\delta Z_A &= \frac{\alpha_s}{12\pi} \Big\{ -n_f B_0(0, m_{\tilde{q}}, m_{\tilde{q}}) - 2N_C B_0(0, m_{\tilde{g}}, m_{\tilde{g}}) - 2B_0(0, m_t, m_t) \\
&\quad + (5N_C - 2n_f + 2) B_0(0,0,0) \Big\} && \text{(E.4)} \\
\delta Z_{\tilde{A}} &= \frac{\alpha_s}{4\pi} \frac{1}{m_{\tilde{g}}^2} \Big\{ N_C m_{\tilde{g}}^2 + 2(n_f - 1)(m_{\tilde{g}}^2 m_{\tilde{q}}^2 - m_{\tilde{g}}^4) B_0'(m_{\tilde{g}}^2, m_{\tilde{q}}, 0) \\
&\quad + 2(m_{\tilde{g}}^2 m_{\tilde{q}}^2 - m_{\tilde{g}}^4 - m_{\tilde{g}}^2 m_t^2) B_0'(m_{\tilde{g}}^2, m_t, m_{\tilde{q}}) + n_f A_0(m_{\tilde{q}}) - N_C A_0(m_{\tilde{g}}) - A_0(m_t) \\
&\quad - (n_f - 1)(m_{\tilde{g}}^2 + m_{\tilde{q}}^2) B_0(m_{\tilde{g}}^2, m_{\tilde{q}}, 0) - 2N_C m_{\tilde{g}}^2 B_0(m_{\tilde{g}}^2, m_{\tilde{g}}, 0) \\
&\quad + (m_t^2 - m_{\tilde{g}}^2 - m_{\tilde{q}}^2) B_0(m_{\tilde{g}}^2, m_t, m_{\tilde{q}}) \Big\} && \text{(E.5)} \\
\delta m_{\tilde{g}} &= \frac{\alpha_s}{4\pi} \frac{1}{m_{\tilde{g}}} \Big\{ n_f A_0(m_{\tilde{q}}) - N_C A_0(m_{\tilde{g}}) - A_0(m_t) + (n_f - 1)(m_{\tilde{g}}^2 - m_{\tilde{q}}^2) B_0(m_{\tilde{g}}^2, m_{\tilde{q}}, 0) \\
&\quad - 2N_C m_{\tilde{g}}^2 B_0(m_{\tilde{g}}^2, m_{\tilde{g}}, 0) + (m_t^2 - m_{\tilde{q}}^2 + m_{\tilde{g}}^2) B_0(m_{\tilde{g}}^2, m_t, m_{\tilde{q}}) + N_C m_{\tilde{g}}^2 \Big\} && \text{(E.6)} \\
\delta g_s^{\overline{MS}} &= -\frac{\alpha_s}{8\pi} \Big\{ \Big[ \frac{1}{\epsilon_{UV}} - \gamma + \ln(4\pi) \Big] [3N_C - n_f] \Big\} && \text{(E.7)}
\end{aligned}$$

# Appendix F

# Final state infrared singularities

### Final state singularities

The explicit formulae for processes with final state real emissions in the general case of massive partons are given in this section. This formulae are directly taken from [59].

The different real emission diagrams are organized in dipoles $D_{ij,k}$ which denote the splitting of a particle $\tilde{ij}$ into the particles $i$ and $j$ where $k$ is a spectator particle as shown in figure F.1.

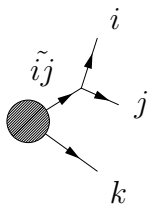


Figure F.1: *Dipole splitting function $D_{ij,k}$ for a final state real emission. The splitting particle is denoted with $\tilde{ij}$ and the spectator particle with $k$.*

### Dipole splitting functions

From the dipole functions $D_{ij,k}$ we can construct the subtraction cross section

$$d\sigma^A = d\Phi^{(m+1)} \sum_{ij} \sum_{k \neq i,j} D_{ij,k}(p_1, ..., p_{m+1}), \tag{F.1}$$

where the dipoles $D_{ij,k}$ are defined by by the factorization formula

$$D_{ij,k}(p_1, ..., p_{m+1}) = -\frac{1}{(p_i + p_j)^2 - m_{ij}^2} \left\langle ..., \tilde{ij}, ..., \tilde{k} \left| \frac{\mathbf{T}_k \, \mathbf{T}_{ij}}{\mathbf{T}_{ij}^2} \mathbf{V}_{ij,k} \right| ..., \tilde{ij}, ..., \tilde{k} \right\rangle_m . \tag{F.2}$$

The operators $\mathbf{T}_i$ describes the emission of a gluon (or gluino) from a parton $i$. For a parton $i$ its action onto the color space is defined by

$$\langle c_1, ..., c_i, ..., c_m \left| \mathbf{T}_i^n \right| b_1, ..., b_i, ..., b_m \rangle = \delta_{c_1\, b_1} ... T^n_{c_i\, b_i} ... \delta_{c_m\, b_m}, \tag{F.3}$$

where $T^n_{c_i\, b_i}$ is the color representation of the final-state particle, i.e. $T^n_{cb} = if_{cnb}$ if $i$ is a gluon (or gluino), $T^n_{cb} = t^n_{cb}$ if $i$ is a quark or squark and $T^n_{cb} = t^n_{cb}$ if $i$ is an antiquark or antisquark.

In (F.2) the color structure is split off the remaining *spin functions* $\mathbf{V}_{ij,k}$ defined in (F.8-F.11).

The partons $i$, $j$, and $k$ are on-shell and the sum of this triplet is defined by

$$p_i^2 = m_i^2, \qquad p_j^2 = m_j^2, \qquad p_k^2 = m_k^2, \qquad Q = p_i + p_j + p_k. \tag{F.4}$$

The $m$-parton matrix elements in (F.2) are obtained from the original $m+1$-parton matrix element by replacing $i$ and $j$ with the parent parton $\tilde{ij}$ in the splitting $\tilde{ij} \to i + j$ and by rescaling the momentum of the spectator parton $k$. These auxiliary momenta $\tilde{p}_{ij}$ and $\tilde{p_k}$ fulfill the on-shell and momentum conservation conditions

$$\tilde{p}_{ij}^2 = m_{ij}^2, \qquad \tilde{p}_k^2 = m_k^2, \qquad Q^\mu = \tilde{p}_{ij}^\mu + \tilde{p}_k^\mu \tag{F.5}$$

and are defined by

$$\begin{aligned} \tilde{p}_k^\mu &= \frac{\sqrt{\lambda(Q^2, m_{ij}^2, m_k^2, )}}{\sqrt{\lambda(Q^2, (p_i + p_j)^2, m_k^2, )}} \left( p_k^\mu - \frac{Qp_k}{Q^2} Q^\mu \right) + \frac{Q^2 + m_k^2 - m_{ij}^2}{2Q^2}\, Q^\mu, \\ \tilde{p}_{ij}^\mu &= Q^\mu - \tilde{p_k}^\mu, \end{aligned} \tag{F.6}$$

where the triangular function

$$\lambda(x, y, z) = x^2 + y^2 + z^2 - 2xy - 2yz - 2xz \tag{F.7}$$

is used.

The splitting functions $\mathbf{V}_{ij,k}$ in formula (F.2) are

$$\langle s \left| \mathbf{V}_{g\tilde{q},k} \right| s' \rangle = 8\pi\alpha_s C_f \left\{ \frac{2}{1 - \tilde{z}_j(1 - y_{ij,k})} - \frac{\tilde{v}_{ij,k}}{v_{ij,k}} \left( 2 + \frac{m_{\tilde{q}}^2}{p_i p_j} \right) \right\} \delta_{s,s'}, \tag{F.8}$$

$$\langle s \left| \mathbf{V}_{g\bar{\tilde{q}},k} \right| s' \rangle = \langle s \left| \mathbf{V}_{g\tilde{q},k} \right| s' \rangle \tag{F.9}$$

$$\langle \mu \left| \mathbf{V}_{q\bar{q},k} \right| \nu \rangle = 8\pi\alpha_s T_R \frac{1}{v_{ij,k}} \left\{ -g^{\mu\nu} \left[ 1 - 2\kappa \left( z_+ z_- - \frac{m_q^2}{(p_i + p_j)^2} \right) \right] \right.$$

$$-\frac{4}{(p_i+p_j)^2}\left[\tilde{z}_i^m p_i^\mu - \tilde{z}_j^m p_j^\mu\right]\left[\tilde{z}_i^m p_i^\nu - \tilde{z}_j^m p_j^\nu\right]\Bigg\} \tag{F.10}$$

$$\begin{aligned}\langle\mu\,|\mathbf{V}_{gg,k}|\,\nu\rangle &= 16\pi\alpha_s N_C\left\{-g^{\mu\nu}\left[\frac{1}{1-\tilde{z}_i(1-y_{ij,k})}+\frac{1}{1-\tilde{z}_j(1-y_{ij,k})}-\frac{2-\kappa z_+ z_-}{v_{ij,k}}\right]\right.\\ &\left.+\frac{1}{v_{ij,k}}\frac{1}{p_i p_j}\left[\tilde{z}_i^m p_i^\mu - \tilde{z}_j^m p_j^\mu\right]\left[\tilde{z}_i^m p_i^\nu - \tilde{z}_j^m p_j^\nu\right]\right\}\end{aligned} \tag{F.11}$$

where $s$, $s'$ and $\mu$, $\nu$ denote the helicities of $\tilde{ij}$ in $\left\langle ...\tilde{ij}...|...\tilde{ij}...\right\rangle$. There are several abbreviations used in the splitting functions: The velocity $\tilde{v}_{ij,k}$ between $\tilde{p}_{ij}$ and $\tilde{p}_k$

$$\tilde{v}_{ij,k} = \frac{\sqrt{\lambda(1,\mu_{ij}^2,\mu_k^2)}}{1-\mu_{ij}^2-\mu_k^2}, \tag{F.12}$$

where $\mu_n = \frac{m_n}{\sqrt{Q^2}}$ $(n = i,j,k,ij)$ are scaled masses introduced here. The variables $\tilde{z}_i$, $\tilde{z}_j$ and $y_{ij,k}$ are defined by

$$\tilde{z}_i = 1-\tilde{z}_j = \frac{p_i p_k}{p_i p_k + p_j p_k}, \qquad y_{ij,k} = \frac{p_i p_j}{p_i p_j + p_j p_k + p_i p_k}. \tag{F.13}$$

Also we have the definition of $z_\pm$

$$z_\pm = \frac{2\mu_i^2 + (1-\mu_i^2-\mu_j^2-\mu_k^2)\,y_{ij,k}}{2\mu_i^2+\mu_j^2+(1-\mu_i^2-\mu_j^2-\mu_k^2)\,y_{ij,k}}\,(1\pm v_{ij,i}\,v_{ij,k}) \tag{F.14}$$

with $v_{ij,k}$ and $v_{ij,i}$ the relative velocities between $p_i+p_j$ and $p_k$ respectively $p_i$:

$$v_{ij,k} = \frac{\sqrt{[2\mu_k^2+(1-\mu_i^2-\mu_j^2-\mu_k^2)(1-y_{ij,k})]^2-4\mu_k^2}}{(1-\mu_i^2-\mu_j^2-\mu_k^2)(1-y_{ij,k})} \tag{F.15}$$

$$v_{ij,i} = \frac{\sqrt{(1-\mu_i^2-\mu_j^2-\mu_k^2)y_{ij,k}^2-4\mu_i^2\mu_j^2}}{(1-\mu_i^2-\mu_j^2-\mu_k^2)y_{ij,k}+2\mu_i^2} \tag{F.16}$$

and $\tilde{z}_i^m$ and $\tilde{z}_j^m$ are defined by

$$\tilde{z}_i^m = \tilde{z}_i - \frac{1}{2}(1-v_{ij,k}) \qquad \tilde{z}_j^m = \tilde{z}_j - \frac{1}{2}(1-v_{ij,k}). \tag{F.17}$$

The parameter $\kappa$ in (F.11) can be chosen freely and only redistributes non-singular terms between the subtracted and the added cross section in (3.16). The $\kappa$ independence of the NLO cross section can serve as a consistency check of the calculation.

**Integrated insertion operator**

The cross section $\int_{m+1} d\sigma_A$ in (3.16) of the subtraction term integrated over the factorized one-parton phase space can be written as

$$\int_{m+1} d\sigma_A = \int_m \left[ d\sigma^{Born} \otimes \mathbf{I}_m \right], \tag{F.18}$$

where the notation $d\sigma^{Born} \otimes \mathbf{I}_m$ means that one has to write down the expression $d\sigma^{Born}$ and then replace the corresponding matrix element squared at the Born level

$$|M_m|^2 = \langle 1,...,m|1,...,m\rangle_m \to \langle 1,...,m|\mathbf{I}_m|1,...,m\rangle_m \tag{F.19}$$

where the insertion operator $\mathbf{I}_m$ depends on the color charges, momenta and masses of the $m$ final-state partons in $d\sigma^{Born}$

$$\mathbf{I}_m = -\frac{\alpha_s}{2\pi}\frac{(4\pi)^\epsilon}{\Gamma(1-\epsilon)}\sum_j \frac{1}{\mathbf{T}_j^2}\sum_{k\neq j}\mathbf{T}_j\mathbf{T}_k \times \left[\mathbf{T}_j^2\left(\frac{\mu^2}{2p_jp_k}\right)^\epsilon \mathcal{V}_j + \Gamma_j + \gamma_j + K_j\right]. \tag{F.20}$$

The color constants $\gamma_j$, $K_j$ are defined as

$$\gamma_q = \frac{3}{2}C_f, \quad K_q = \left(\frac{7}{2} - \frac{\pi^2}{6}\right) C_f \tag{F.21}$$

$$\gamma_g = \frac{11}{6}N_C - \frac{2}{3}T_R\, n_f, \quad K_g = \left(\frac{67}{18} - \frac{\pi^2}{6}\right) C_f - \frac{10}{9}T_R\, n_f \tag{F.22}$$

$$\gamma_{\tilde{q}} = 2C_f, \quad K_{\tilde{q}} = \left(4 - \frac{\pi^2}{6}\right) C_f \tag{F.23}$$

$$\gamma_{\tilde{g}} = \frac{3}{2}N_C, \quad K_{\tilde{g}} = \left(\frac{7}{2} - \frac{\pi^2}{6}\right) N_C. \tag{F.24}$$

The functions $\Gamma_j$ depend on the flavor of the parton $j$ and on the parton mass:

$$\Gamma_g = \frac{1}{\epsilon}\,\gamma_g \tag{F.25}$$

$$\Gamma_{\tilde{q}} = C_f\,[\frac{1}{\epsilon} + \ln\frac{m_{\tilde{q}}^2}{\mu^2} - 2] \tag{F.26}$$

The $\mathcal{V}_j$ kernels depend on the flavor of parton $j$ and on the momenta and masses of both partons $j$ and $k$. This functions $\mathcal{V}_j$ can be decomposed into a symmetric part with respect to the interchange of the indices $j$ and $k$ which

is also singular in four dimensions, or for vanishing masses, $\mathcal{V}^{(S)}$, and a part which is neither symmetric nor singular $\mathcal{V}_j^{(NS)}$

$$\left(\frac{\mu^2}{s_{jk}}\right)^{\epsilon}\mathcal{V}_j = \left(\frac{\mu^2}{s_{jk}}\right)^{\epsilon}\mathcal{V}_j^{(S)} + \mathcal{V}_j^{(NS)} + \mathcal{O}(\epsilon), \tag{F.27}$$

where $s_{jk} = 2\,p_j p_k$. With the abbreviations $Q_{jk}^2 = s_{jk} + m_j^2 + m_k^2$, $\bar{\mu}_{j/k} = m_{j/k}^2/Q_{jk}^2$, the relative velocity function

$$v_{p,q} = \frac{\sqrt{\lambda((p+q)^2, p^2, q^2)}}{(p+q)^2 - p^2 - q^2} \tag{F.28}$$

and

$$\rho = \sqrt{\frac{1-v_{jk}}{1+v_{jk}}} \qquad \rho_{j/k} = \sqrt{\frac{1-v_{jk}+2\bar{\mu}_{j/k}^2/(1-\bar{\mu}_j^2-\bar{\mu}_k^2)}{1+v_{jk}+2\bar{\mu}_{j/k}^2/(1-\bar{\mu}_j^2-\bar{\mu}_k^2)}} \tag{F.29}$$

the expanded kernels are:

$$\begin{aligned}\mathcal{V}^{(S)}(m_j>0, m_k>0) &= \frac{1}{v_{jk}}\left[\frac{1}{\epsilon}\ln\rho - \frac{1}{4}\ln^2\rho_j^2 - \frac{1}{4}\ln^2\rho_k^2 - \frac{\pi^2}{6}\right.\\ &\quad \left. + \ln\rho\ln\frac{Q_{jk}^2}{s_{jk}}\right] \qquad \text{(F.30)}\\ \mathcal{V}^{(S)}(m_j>0, m_k=0) &= \frac{1}{2\epsilon^2} + + \frac{1}{2\epsilon}\ln\frac{m_j^2}{s_{jk}} - \frac{1}{4}\ln^2\frac{m_j^2}{s_{jk}} - \frac{\pi^2}{12}\\ &\quad -\frac{1}{2}\ln\frac{m_j^2}{s_{jk}}\,ln\frac{s_{jk}}{Q_{jk}^2} - \frac{1}{2}\ln\frac{m_j^2}{Q_{jk}^2}\,ln\frac{s_{jk}}{Q_{jk}^2} \qquad \text{(F.31)}\\ \mathcal{V}^{(S)}(m_j=0, m_k=0) &= \frac{1}{\epsilon^2}. \qquad \text{(F.32)}\end{aligned}$$

The explicit form of the non-singular terms depend on the flavor and masses of the partons $j$ and $k$:

$$\begin{aligned}\mathcal{V}_{\tilde{q}}^{(NS)}(m_j>0, m_k>0) &= \frac{\gamma_{\tilde{q}}}{\mathbf{T}_{\tilde{q}}^2}\ln\frac{\mu^2}{Q_{jk}^2} - 2\ln\frac{(Q_{jk}-m_k)^2-m_j^2}{Q_{jk}^2} + \frac{4\,m_k(m_k-Q_{jk})}{2p_jp_k}\\ &\quad + \frac{\pi^2}{6} + \frac{1}{v_{jk}}\left[\ln\rho^2\ln(1+\rho^2) + 2Li_2(\rho^2)\right.\\ &\quad \left. - Li_2(1-\rho_j^2) - Li_2(1-\rho_k^2) - \frac{\pi^2}{6}\right] \qquad \text{(F.33)}\\ \mathcal{V}_{\tilde{q}}^{(NS)}(m_j>0, m_k=0) &= \frac{\gamma_{\tilde{q}}}{\mathbf{T}_{\tilde{q}}^2}\ln\frac{\mu^2}{Q_{jk}^2} - \frac{\pi^2}{6} - Li_2\left(\frac{s_{jk}}{Q_{jk}^2}\right) - 2\,ln\frac{s_{jk}}{Q_{jk}^2} \qquad \text{(F.34)}\end{aligned}$$

$$\mathcal{V}_g^{(NS)}(m_j=0,m_k>0) = \frac{\gamma_g}{\mathbf{T}_g^2}\left[\ln\frac{\mu^2}{Q_{jk}^2} - 2\,\ln\frac{Q_{jk}-m_k}{Q_{jk}} - \frac{2\,m_k}{Q_{jk}+m_k}\right] - \frac{\pi^2}{6} - Li_2\left(\frac{s_{jk}}{Q_{jk}^2}\right) + \left(\kappa-\frac{2}{3}\right)\left(2\frac{T_R}{Nc}n_f - 1\right)\frac{m_k^2}{s_{jk}}\ln\frac{2m_k}{Q_{jk}+m_k} \quad \text{(F.35)}$$

$$\mathcal{V}_g^{(NS)}(m_j=0,m_k=0) = \frac{\gamma_g}{\mathbf{T}_g^2}\ln\frac{\mu^2}{2p_jp_k} - \frac{\pi^2}{3}, \quad \text{(F.36)}$$

where $\kappa$ in (F.35) is again the free parameter already introduced in context with (F.11).

**Explicit subtraction formulae**

The subtraction cross section $d\sigma^A$ for the process (a) $e^+e^- \to \tilde{q}(1)\;\bar{\tilde{q}}(2)\;g(3)\;g(4)$ consists of the dipoles (F.1):

$$d\sigma_a^A = d\Phi^4\,(D_{13,2}+D_{13,4}+D_{14,2}+D_{14,3}+ D_{23,1}+D_{23,4}+D_{24,1}+D_{24,3}+D_{34,1}+D_{34,2}) \quad \text{(F.37)}$$

while the subtraction cross section for the process (b) $e^+e^- \to \tilde{q}(1)\;\bar{\tilde{q}}(2)\;q(3)\;\bar{q}(4)$ can be written as

$$d\sigma_b^A = d\Phi^4\,(D_{34,1}+D_{34,2})\,, \quad \text{(F.38)}$$

where the dipoles in process (a) are

$$D_{13,2} = \frac{1}{2p_1p_3}|M^{Born}(\tilde{p}_{13},\tilde{p}_2,p_4)|^2\left(1-\frac{N_C}{2C_f}\right)V_{\tilde{q}g,2} \quad \text{(F.39)}$$

$$D_{13,4} = \frac{1}{2p_1p_3}|M^{Born}(\tilde{p}_{13},p_2,\tilde{p}_4)|^2\,\frac{N_C}{2C_f}\,V_{\tilde{q}g,4} \quad \text{(F.40)}$$

$$D_{34,1} = \frac{1}{2p_3p_4}|T_{\mu\nu}^{Born}(\tilde{p}_1,p_2,\tilde{p}_{34})|^2\,\frac{1}{2}\,V_{gg,1}^{\mu\nu}, \quad \text{(F.41)}$$

and the other dipoles are permutations of the form $1 \leftrightarrow 2$ and $3 \leftrightarrow 4$. In process (b) we find the dipole

$$D_{34,1} = \frac{1}{2p_3p_4}|T_{\mu\nu}^{Born}(\tilde{p}_1,p_2,\tilde{p}_{34})|^2\,\frac{1}{2}\,V_{q\bar{q},1}^{\mu\nu}, \quad \text{(F.42)}$$

where the other dipole can be obtained by the permutation $1 \leftrightarrow 2$. To generate this dipoles we also need the corresponding three particle final-state Born matrix element $M^{Born}$. In particular we need this matrix element without performing any tensor contraction $T_{\mu\nu}^{Born}$, where $\mu$ and $\nu$ are the polarization indices of the virtual $Z^0$-boson respectively $\gamma$-boson and the

final-state gluon. The splitting functions $V_{ij,k}$ are explicitly given in (F.8)-(F.11).

The integrated insertion operator in case of the process $e^+e^- \to \tilde{q}(1)\,\bar{\tilde{q}}(2)\,g(3)$ is given by (F.20):

$$
\begin{aligned}
I_3 = & -\frac{\alpha_s}{2\pi}\frac{(4\pi)^\epsilon}{\Gamma(1-\epsilon)}\Bigg\{ \\
& \left(\frac{N_C}{2C_f}-1\right)\left[C_f\left(\frac{\mu^2}{s_{12}}\right)^\epsilon \mathcal{V}_1(s_{12})+\Gamma_1+\gamma_1+K_1\right] \\
& +\left(-\frac{N_C}{2C_f}\right)\left[C_f\left(\frac{\mu^2}{s_{13}}\right)^\epsilon \mathcal{V}_1(s_{13})+\Gamma_1+\gamma_1+K_1\right] \\
& +\left(\frac{N_C}{2C_f}-1\right)\left[C_f\left(\frac{\mu^2}{s_{12}}\right)^\epsilon \mathcal{V}_2(s_{12})+\Gamma_2+\gamma_2+K_2\right] \\
& +\left(-\frac{N_C}{2C_f}\right)\left[C_f\left(\frac{\mu^2}{s_{23}}\right)^\epsilon \mathcal{V}_2(s_{23})+\Gamma_2+\gamma_2+K_2\right] \\
& +\left(-\frac{1}{2}\right)\left[N_C\left(\frac{\mu^2}{s_{13}}\right)^\epsilon \mathcal{V}_3(s_{13})+\Gamma_3+\gamma_3+K_3\right] \\
& +\left(-\frac{1}{2}\right)\left[N_C\left(\frac{\mu^2}{s_{23}}\right)^\epsilon \mathcal{V}_3(s_{23})+\Gamma_3+\gamma_3+K_3\right]\Bigg\}
\end{aligned}
\tag{F.43}
$$

where the Born cross section factorizes completely from this insertion operator $I_3$ in (F.18). Expanding (F.43) in $\epsilon$ yields

$$
\begin{aligned}
I_3 \;=\; & C\left\{\frac{1}{\epsilon_{IR}^2}\;\left[\frac{\alpha_s}{2\pi}N_C\right]\right. \\
& \frac{1}{\epsilon_{IR}}\Big[\,-1/6\,\frac{\alpha_s}{2\pi}\Big(-3\,N_C\,\ln\frac{{m_{\tilde{q}}}^2}{s_{13}}-3\,N_C\,\ln\frac{\mu^2}{s_{13}} \\
& -11\,N_C-3\,N_C\,\ln\frac{{m_{\tilde{q}}}^2}{s_{23}}-3\,N_C\,\ln\frac{\mu^2}{s_{23}}+2\,n_f \\
& \left.+(3\,N_C-6\,C_f)\,\frac{1}{v_{12}}\,\ln\frac{1-v_{12}}{1+v_{12}}-12\,C_f\Big)\Big]+\mathcal{O}(\epsilon^0)\right\}
\end{aligned}
\tag{F.44}
$$

up to finite terms. The factor $C$ is defined by $C=(4\,\pi)^\epsilon\Gamma(1+\epsilon)$ and $v_{12}=\sqrt{1-4m_{\tilde{q}}^4/s_{12}^2}$. The singular parts cancel exactly the infrared divergences emerging in the virtual corrections.

# Appendix G

# Phase space

### Three-body phase space

In the process

$$e^+e^- \to \tilde{q}(p_1)\,\bar{\tilde{q}}(p_2)\,g(p_3) \tag{G.1}$$

with a squark $\tilde{q}$ an anti-squark $\bar{\tilde{q}}$ and a gluon $g$ with momenta $p_1$, $p_2$ and $p_3$ in the final-state we introduce the dimensionless variables

$$x_1 = \frac{2\,qp_1}{q^2} \qquad x_2 = \frac{2\,qp_2}{q^2} \tag{G.2}$$

where $q$ is the sum of all final-state momenta. The three-particle phase space factor can then be written as

$$\begin{aligned} P^{(3)} &= \frac{1}{(2\pi)^5}\int \frac{d^3p_1}{2p_{10}}\frac{d^3p_2}{2p_{20}}\frac{d^3p_3}{2p_{30}}\delta^4(q-p_1-p_2-p_3) \\ &= \frac{s}{32(2\pi)^5} d\alpha\, d\cos\beta\, d\gamma \int_z^1 dx_1 \int_{x_2-}^{x_2+} dx_2, \end{aligned} \tag{G.3}$$

where we introduce $s = q^2$, the dimensionless quantity $z = 2m_{\tilde{q}}/\sqrt{s}$ and the angles $\alpha$, $\beta$, and $\gamma$ describing the orientation of the final state coordinates. The boundaries of $x_2$ are given by

$$x_{2\pm} = \frac{1}{4(1-x_1)+z}\left[(2(1-x_1)(2-x_1)+z(2-x_1) \pm 2(1-x_1)\sqrt{x_1^2-z}\right] \tag{G.4}$$

This boundaries are determined by collinear configurations and are shown in figure G.1 as region $I$.

**Four-body phase space**

The final state particle momenta in the processes

$$\begin{aligned} e^+e^- &\to \tilde{q}(p_1)\,\bar{\tilde{q}}(p_2)\,g(p_3)\,g(p_4) \\ e^+e^- &\to \tilde{q}(p_1)\,\bar{\tilde{q}}(p_2)\,q(p_3)\,\bar{q}(p_4) \end{aligned}$$

with massless quarks $q$ respectively gluons $g$ can be written in the centre-of-mass system of the two massless particles as

$$\begin{aligned} p_1 &= p_{30}(1,0,0,\sqrt{1-\frac{m_{\tilde{q}}}{p_{10}}}) \\ p_2 &= p_{40}(1,0,\sin\alpha\sqrt{1-\frac{m_{\tilde{q}}}{p_{20}}},\cos\alpha\sqrt{1-\frac{m_{\tilde{q}}}{p_{20}}}) \\ p_3 &= p_{10}(1,\sin\theta\sin\phi,\sin\theta\cos\phi,\cos\theta) \\ p_4 &= p_{20}(1,-\sin\theta\sin\phi,-\sin\theta\cos\phi,-\cos\theta) \end{aligned}$$

To describe the un-oriented four-body phase space, we need five independent

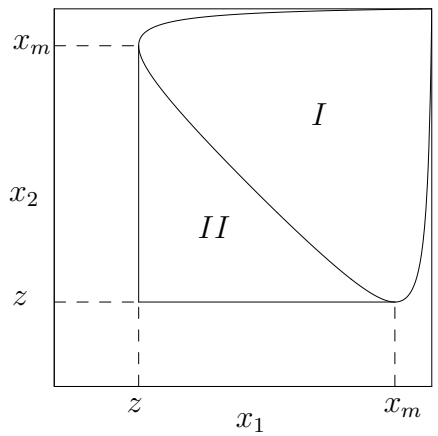


Figure G.1: *Dalitz-plot of the three particle phase space (region I) and the four particle phase space (region I and II).*

variables, which can be chosen:

$$x_1 = \frac{2\,qp_1}{q^2}, \qquad x_2 = \frac{2\,qp_2}{q^2}, \qquad y = \frac{(p_3+p_4)^2}{q^2}, \qquad \theta, \qquad \phi \tag{G.5}$$

where $q = p_1+p_2+p_3+p_4$. From this variables we can construct the variables emerging in the expressions for the momenta $p_1$ - $p_4$

$$p_{10} = \sqrt{\frac{q^2}{4y}}(1-y-x_2), \qquad p_{20} = \sqrt{\frac{q^2}{4y}}(1-y-x_1), \tag{G.6}$$

$$p_{30} = p_{40} = \sqrt{y\frac{q^2}{4}}, \tag{G.7}$$

$$\cos\alpha = \frac{p_{30}p_{40} + q^2/2(1-y) + m_{\tilde{q}}^2 - q^2(x_1+x_2)}{\sqrt{p_{10}^2 - m_{\tilde{q}}}\sqrt{p_{20}^2 - m_{\tilde{q}}}}. \tag{G.8}$$

The phase space factor becomes with this variables

$$P^{(4)} = \frac{1}{(2\pi)^8}\int \frac{d^3p_1}{2p_{10}}\frac{d^3p_2}{2p_{20}}\frac{d^3p_3}{2p_{30}}\frac{d^3p_4}{2p_{40}}\delta^4(q-p_1-p_2-p_3-p_4) \tag{G.9}$$

$$= \frac{s^2}{128(2\pi)^8} d\alpha\, d\cos\beta\, d\gamma \int_z^1 dx_1 \int_{x_2-}^{x_2+} dx_2 \int_{y-}^{y+} dy \int_1^{+1} d\cos\theta \int_0^{2\pi} d\phi,$$

where the angles $\alpha$, $\beta$, and $\gamma$ again describe the orientation of the final state coordinates and we introduce the boundaries of $y$

$$y_\pm = \frac{1}{4}\left[(2-x_1-x_2)^2 - (x_1^2 - m_{\tilde{q}}^2) - (x_2^2 - m_{\tilde{q}}^2) \pm 2\sqrt{x_1^2 - m_{\tilde{q}}^2}\sqrt{x_2^2 - m_{\tilde{q}}^2}\right]. \tag{G.10}$$

The boundaries of the variables $x_1$ and $x_2$ are shown in figure G.1 and the quantities $x_{2\pm}$ are defined in (G.4).

# Bibliography


[1] S. Coleman and J. Mandula, Phys. Rev. **159**, 1251 (1967).

[2] R. K. Kaul and P. Majumdar, Nucl. Phys. B **199**, 36 (1982).

[3] E. Gildener and S. Weinberg, Phys. Rev. D **13**, 3333 (1976).

[4] S. Weinberg, Phys. Rev. D **19**, 1277 (1979).

[5] L. Susskind, Phys. Rev. D **20**, 2619 (1979).

[6] P. Fayet and S. Ferrara, Phys. Rept. **32**, 249 (1977).

[7] H. P. Nilles, Phys. Rept. **110**, 1 (1984).

[8] H. E. Haber and G. L. Kane, Phys. Rept. **117**, 75 (1985).

[9] L. Girardello and M. T. Grisaru, Nucl. Phys. B **194**, 65 (1982).

[10] R. Brandelik *et al.* [TASSO Collaboration], Phys. Lett. B **86**, 243 (1979).

[11] D. P. Barber *et al.*, Phys. Rev. Lett. **43**, 830 (1979).

[12] C. Berger *et al.* [PLUTO Collaboration], Phys. Lett. B **86**, 418 (1979).

[13] R. K. Ellis, D. A. Ross and A. E. Terrano, Nucl. Phys. B **178**, 421 (1981).

[14] K. Fabricius, I. Schmitt, G. Kramer and G. Schierholz, Z. Phys. C **11**, 315 (1981).

[15] J. A. Vermaseren, K. J. Gaemers and S. J. Oldham, Nucl. Phys. B **187**, 301 (1981).

[16] Z. Kunszt, Phys. Lett. B **99**, 429 (1981).

[17] M. Weber, Ph. D. thesis, Hamburg, 2001.

[18] J. Wess and B. Zumino, Nucl. Phys. B **70**, 39 (1974).

[19] S. Dimopoulos, S. Raby and F. Wilczek, Phys. Rev. D **24**, 1681 (1981).

[20] P. Fayet, Phys. Lett. B **69**, 489 (1977).

[21] S. Dimopoulos and H. Georgi, Nucl. Phys. B **193**, 150 (1981).

[22] N. Sakai, Z. Phys. C **11**, 153 (1981).

[23] R. Haag, J. T. Lopuszanski and M. Sohnius, Nucl. Phys. B **88**, 257 (1975).

[24] J. E. Kim and H. P. Nilles, Phys. Lett. B **138**, 150 (1984).

[25] S. Weinberg, Phys. Rev. D **26**, 287 (1982).

[26] H. Goldberg, Phys. Rev. Lett. **50**, 1419 (1983).

[27] J. R. Ellis, J. S. Hagelin, D. V. Nanopoulos, K. Olive and M. Srednicki, Nucl. Phys. B **238**, 453 (1984).

[28] L. J. Hall and L. Randall, Phys. Rev. Lett. **65**, 2939 (1990).

[29] S. Dimopoulos and D. W. Sutter, Nucl. Phys. B **452**, 496 (1995).

[30] H. E. Haber and G. L. Kane, Phys. Rept. **117**, 75 (1985).

[31] H. Georgi and S. L. Glashow, Phys. Rev. Lett. **32**, 438 (1974).

[32] S. P. Martin, hep-ph/9709356.

[33] D. E. Groom *et al.* [Particle Data Group Collaboration], Eur. Phys. J. C **15**, 1 (2000).

[34] J. L. Feng, M. E. Peskin, H. Murayama and X. Tata, Phys. Rev. D **52**, 1418 (1995).

[35] M. M. Nojiri, K. Fujii and T. Tsukamoto, Phys. Rev. D **54**, 6756 (1996).

[36] W. Beenakker, R. Hopker, M. Spira and P. M. Zerwas, Nucl. Phys. B **492**, 51 (1997) [arXiv:hep-ph/9610490].

[37] TESLA Technical Design Report, Part III, Physics at an $e^+e^-$ Linear Collider, R. Heuer, D.J. Miller, F. Richard and P.M. Zerwas (eds.), DESY 2001–011.

[38] The CLIC Study Team, A 3 TeV $e^+e^-$ linear collider based on CLIC technology, CERN 2000–008.

[39] J. R. Ellis, M. K. Gaillard and G. G. Ross, Nucl. Phys. B **111**, 253 (1976) [Erratum-ibid. B **130**, 516 (1976)].

[40] G. Kramer, G. Schierholz and J. Willrodt, Phys. Lett. B **79**, 249 (1978) [Erratum-ibid. B **80**, 433 (1978)].

[41] E. Laermann, K. H. Streng and P. M. Zerwas, Z. Phys. C **3**, 289 (1980) [Erratum-ibid. C **52**, 352 (1980)].

[42] H. D. Dahmen, D. H. Schiller and D. Wahner, Nucl. Phys. B **227**, 291 (1983).

[43] D. H. Schiller and D. Wahner, Nucl. Phys. B **259**, 597 (1985).

[44] A. Arhrib, M. Capdequi-Peyranere and A. Djouadi, Phys. Rev. D **52**, 1404 (1995) [arXiv:hep-ph/9412382].

[45] G. 't Hooft and M. Veltman, Nucl. Phys. B **44**, 189 (1972).

[46] W. A. Bardeen, A. J. Buras, D. W. Duke and T. Muta, Phys. Rev. D **18**, 3998 (1978).

[47] F. Jegerlehner, Eur. Phys. J. C **18**, 673 (2001).

[48] G. Passarino and M. Veltman, Nucl. Phys. B **160**, 151 (1979).

[49] G. J. van Oldenborgh and J. A. Vermaseren, Z. Phys. C **46**, 425 (1990).

[50] A. Denner, Fortsch. Phys. **41**, 307 (1993).

[51] G. 't Hooft, Nucl. Phys. B **61**, 455 (1973).

[52] J. C. Collins and A. J. Macfarlane, Phys. Rev. D **10**, 1201 (1974).

[53] W. J. Marciano and A. Sirlin, Nucl. Phys. B **88**, 86 (1975).

[54] F. Bloch and A. Nordsieck, Phys. Rev. **52**, 54 (1937).

[55] T. Kinoshita, J. Math. Phys. **3**, 650 (1962).

[56] T. D. Lee and M. Nauenberg, Phys. Rev. **133**, B1549 (1964).

[57] A. Bassetto, M. Ciafaloni and G. Marchesini, Phys. Rept. **100**, 201 (1983).

[58] S. Catani and M. H. Seymour, Phys. Lett. B **378**, 287 (1996).

[59] S. Catani, S. Dittmaier, M. H. Seymour, Z. Trocsanyi, (2001). [hep-ph/0201036].

[60] Vermaseren, Symbolic manipulation with FORM, Amsterdam 1991.

[61] T. Hahn and M. Perez-Victoria, Comput. Phys. Commun. **118**, 153 (1999) Package download and further informations online: http://www.feynarts.de/looptools.

[62] G. P. Lepage, CLNS-80/447.

[63] Z. Bern, L. J. Dixon and D. A. Kosower, Phys. Lett. B **302**, 299 (1993) [Erratum-ibid. B **318**, 649 (1993)].

[64] A. Brandenburg and P. Uwer, Nucl. Phys. B **515**, 279 (1998).

[65] S. P. Martin and M. T. Vaughn, Phys. Lett. B **318**, 331 (1993).

[66] W. Siegel, Phys. Lett. B **84**, 193 (1979).

[67] D. M. Capper, D. R. Jones and P. van Nieuwenhuizen, Nucl. Phys. B **167**, 479 (1980).

[68] W. Siegel, Phys. Lett. B **94**, 37 (1980).

[69] E. C. Stueckelberg and A. Petermann, Helv. Phys. Acta **26**, 499 (1953).

[70] M. Gell-Mann and F. E. Low, Phys. Rev. **95**, 1300 (1954).

[71] A. Denner, H. Eck, O. Hahn and J. Kublbeck, Nucl. Phys. B **387**, 467 (1992).

[72] G. 't Hooft and M. Veltman, Nucl. Phys. B **153**, 365 (1979).

# Acknowledgments

I would especially like to thank my supervisor, P. M. Zerwas, for his guidance and support throughout my three years in his group. I am very grateful for the privilege and opportunity of working with him.
Special thanks are given to Arnd Brandenburg for his collaboration. From the frequent discussions with him over physical questions as well as technical problems I learned very much.
To Stefan Dittmaier I am very grateful for his support, in particular in context with the subtraction formalism.
Many thanks to Marcus Weber for the great collaboration and for reading the manuscript.
I am grateful to Margarete Mühlleitner, Benedikt Plümper, Ayres Freitas, and Andreas von Manteuffel for their encouragement, support and friendship during the last three years, and for making the physics department such a pleasant place to work.
Many special thanks go of course to the soccer team for the nice traditional soccer matches.
Most importantly, I would like to thank my parents for their encouragement and support over the years.
My love and thanks go to Meriem Rezgaoui, who follows me with tender and loving care during all the time.